RHEOLOGICAL RESPONSES OF POLYMER MATERIALS

WITH DIFFERENT ARCHITECTURES

By

MIAO HU, M.S.

A DISSERTATION

IN

CHEMICAL ENGINEERING

Submitted to the Graduate Faculty
of Texas Tech University in
Partial Fulfillments of
the Requirements for
the Degree of

DOCTORAL OF PHILOSOPHY

Approved

Gregory B. McKenna
Chairman of committee

Ronald Hedden

Brandon Weeks

Edward L.Quitevis

Peggy Gordon Miller
Dean of graduate school

August, 2011

Acknowledgments

I would like to express my great and sincere gratitude to my advisor Professor Gregory B. McKenna for his supervision and guidance during my graduate studies at Texas Tech University. It is my honor to have the opportunity of working under his supervision. Prof. McKenna opened a new door for me in the field of polymer rheology and I learned a lot from him. His support and encouragement helped me to accomplish my Ph.D. studies here in Texas Tech University.

Thanks Dr. Robert H. Grubbs, Dr. Julia A. Kornfield in Caltech for their support and great help in this project. Also I'd like to thank their students Dr. Yan Xia, Dr A.J. Boydston, Dr Irina Gorodetskaya, and Mr. Chris Daeffler for their time and great effort to preparing samples for this study.

I would also like to thank my qualifying and doctoral defense committee members, Prof. Sindee L. Simon, Prof. Ronald Hedden, Prof. Brandon Weeks, and Prof. Edward L.Quitevis. Thank you for your time to review my dissertation and give valuable suggestions.

Thanks Dr. Paul O'Connell, Dr. Nabila Shamim and our group members for their help and support with my work.

Research supported by the U.S. Department of Energy, Office of Basic Energy Sciences, Division of Materials Sciences and Engineering under Award #DE-FG02-05 ER46218.

This dissertation is dedicated to my beloved Jinhua Wang and my parents for their continuous patience and love.

Table of Contents

Acknowledgments iii
Abstract vii
List of Figures ix
List of Tables xv
List of Symbols and Nomenclature xvi
Chapter I: Introduction 1
Chapter II: Influence of molecular structure on polymer rheology 3
2.1 Linear polymer and reptation model 3
2.2 Branched polymers and the hierarchical models 5
2.2.1 Star polymers 6
2.2.2 Dendritic polymer 7
2.2.3 Comb and H-shape polymer 8
2.2.4 Hierarchical model 10
2.3 Macrocyclic polymer 13
2.3.1 Solution properties of macrocyclic polymers 13
2.3.2 Glass transition behavior of macrocyclic materials 16
2.3.3 Viscoelastic properties of macrocyclic materials 17
2.3.3.1 Temperature dependence of viscosity 17
2.3.3.2 Plateau modulus (G_N^0) 18
2.3.3.3 Zero shear viscosity (η_0) and molecular weight relationship 20
2.3.4 Molecular model for macrocyclic materials 23
2.3.5 Synthesis of macrocyclic materials 26
2.3.5.1 Traditional methods for synthesis macrocyclic polymers 28
2.3.5.2 Ring expansion metathesis polymerization (REMP) method 34
Chapter III: Experiments and data analysis 38
3.1 Materials 38
3.2 GPC-MALLS analysis 40
3.3 Rheological measurements 41
3.4 Data analysis 42
3.4.1 Estimation of plateau modulus (G_N^0) and entanglement molecular weight (M_e) 42

3.4.2 van Gurp-Palmen plot 44
3.4.3 Estimate the glass transition temperature (T_g) and fragility (m) 46
3.4.4 Retardation spectrum 47
Chapter IV: Viscoelastic properties of polymer rings with different structure or composition 49
4.1 Polyoctenamer (PCO) rings 49
4.1.1 The molecular information for linear and cyclic PCO 49
4.1.2 Dilute solution properties of linear and cyclic PCO 54
4.1.3 Viscoelastic properties of linear and cyclic PCO 55
4.1.3.1 Influence of chemical hydrogenation to the chemical structure 55
4.1.3.2 Dynamic responses of linear and cyclic PCOs 57
4.1.3.3 The rubbery plateau modulus (G_N^0) of linear and cyclic PCOs 61
4.1.3.4 The zero shear viscosity for linear and cyclic PCOs 63
4.1.4 Conclusion 65
4.2 Poly(ammonium) rings 66
4.2.1 Examine the purity of the cyclic sample 66
4.3.2 The rheological responses of linear and cyclic poly(ammonium) 68
4.3.2.1 Zero shear viscosity of the linear and cyclic sample 69
4.3.2.2 Dynamic responses of linear and cyclic poly(ammonium) 71
4.4.3 Summary 73
4.3 Dendronized rings 74
4.3.1 Synthesis of dendronized ring 74
4.3.2 Viscoelastic properties of dendronized ring 76
4.3.3 Compare the viscoelastic responses of linear and cyclic dendronized polymer 78
4.3.4 Conclusion for dendronized polymers 81
4.4 The Wedge rings 81
4.4.1 Molecular information of wedge polymers 81
4.4.2 Viscoelastic properties of linear and cyclic wedge polymer 83
4.4.3 Summary 88
4.5 Relaxation behavior of ring/linear mixture 88
4.5.1 Rheological polydispersity 89
4.5.2 Retardation spectrum of ring/linear mixture 92
4.6 Conclusions and future work 104

Chapter V: Brush polymers with different side chain structures 106
5.1 The rheological responses of densely branched brush polymer 106
5.1.1 Synthesis and molecular information of the densely branched brush sample 108
5.1.2 Results and discussion. 109
5.1.2.1 Intrinsic viscosity. 109
5.1.2.2 Dynamic responses of the brush polymers. 112
5.1.2.3 Sequential relaxation. 117
5.1.2.4 Temperature dependence of the dynamic responses. 118
5.1.2.5 Segmental regime. 120
5.1.2.6 Arm regime. 121
5.1.2.7 Terminal regime. 123
5.1.3 Summary and Conclusions 127
5.2 The rheological responses of linear wedge polymer 129
5.2.1 Polymer Synthesis 131
5.2.2 Result and discussion 132
5.2.2.1 Chain conformation in solution. 132
5.2.2.2 Dynamic responses of wedge polymer. 132
5.2.2.3 Zero shear viscosity of the wedge polymer. 135
5.2.3 Conclusion 136
5.3 The influence of side chain structure to the viscoelastic properties of brush polymer 137
5.4 Summary and Future work 139
Chapter VI Future work 141
Reference: 143

Abstract

Polymer rheology is a sensitive method to determine the change in the molecular chemical structure, size, architecture, and composition for polymer materials. In this dissertation, we focus on the influence of the molecular architecture and composition to the rheological responses of some polymer with unique architecture.

The first part of the work is to characterize the macrocyclic polymer materials prepared by the Ring Expansion Metathesis Polymerization (REMP) method. In this work, we tried different methods to get pure ring samples, examine their viscoelastic properties and compare the results with theoretical predictions. Four kinds of polymer rings (polyoctenamer, polyammonium, dendronized and wedge ring) were synthesized using two catalysts UC5 and UC6. However, limited by the reaction mechanism of the catalyst, we still can't get 100% pure ring polymer with current reaction system. It is found that for monomers with simple structures, the samples prepared by the two catalysts contain at least 20% of linear chain contamination. Even we change the structure of the monomer and the use the macromonomer to increase the steric hindrance to help generate ring samples. The samples still contain certain amount of linear chain contamination. The relaxation behaviors of these ring/linear mixtures and some literature reported ring samples were analyzed by the retardation spectrum. It is found that polymer rings may reptate like the linear chains. Their relaxation time scales following what is predicted by the reptation model. Linear chain contamination will increase the viscosity, radius of gyration and plateau modulus of the polymer ring samples. With linear chain contamination, the "threading effect" will slow down the relaxation of polymer rings. But

when the amount of linear chain contamination is high, the mixtures still relax following the reptation model.

In the second part, the rheological responses of a new kind of branched polymer with well defined side chain structure and branching space were studied. The branched polymer was prepared by the Ring Opening Metathesis Polymerization (ROMP) of norbornane based macromonomers linked with different length or composition of side groups. Due to the spacing effect of the side chains, these branched polymers are hard to get entangled. For PLA brush polymers, with increasing side chain length, similar double relaxation behaviors were found as those long chain branched polymers. The brush polymers relax following the sequence of the segmental relaxation first, then the side chain (arm) relaxation and the terminal (whole chain) relaxation. With such high molecular weight, the samples are still not well entangled. The plateau found for the relaxation of the backbone is not the rubbery plateau and is actually the inverse value of the steady state recoverable compliance. For wedge polymer with enough high backbone DP, the samples can get entangled and reptate as a common linear chain. But influenced by the huge side chain structure, the polymer exhibits a much lower rubbery and glassy modulus. The large volume fraction of side chain strongly influenced the glassy behaviors of the brush polymer. The PLA brush, wedge and dendronized polymer have the same backbone, but their glass transition behaviors are strongly affected by the steric hindrance introduced by the side chain structures.

List of Figures

Figure 2.1 Illustration of reptation model for an entangled linear molecule in melt …..... 4

Figure 2.2 Illustration for the constrain release ……..…4

Figure 2.3 Scheme for the structure of dendritic polymers …….…… .7

Figure 2.4 Scheme for the structure for H-shape (a) and comb (b) polymers ……8

Figure 2.5 PS linear combs with equal backbone (Mb=275 kg/mol) and branch degree (~30), branch lengths increase (0, 6.5k, 11.7k, 25.7k, 47k and 98k g/mol) …….. 9

Figure 2.6 The intrinsic viscosity change with molecular weight for cyclic and linear polystyrene in (a) good solvent and (b) in θ-solvent. ……..…… 15

Figure 2.7 Glass transition temperatures (T_g) of cyclic (round) and linear (square) PDMS change with their number-average of skeletal bonds n. The two lines are theoretical prediction by Di Marzio and Guttman……..……17

Figure 2.8 The reduced viscosity change with temperature for both cyclic (dotted points) and linear polystyrene (line)…….……18

Figure 2.9 Double logarithmic plot of recoverable compliance versus reduced time for cyclic polystyrene (M_w = 390,000 g/mol) compared with that of a linear polystyrene fraction (M_w = 600,000) ……19

Figure 2.10 Comparison of the dynamic moduli of linear (line) and cyclic (symbol) polybutadiene at 26.2 ^oC. ……..19

Figure 2.11 Stress relaxation moduli G(t) of two polystyrene rings (open triangles and open squares) and with their linear counterparts (respectively filled triangles and filled squares) at reference temperature of 170^oC. …….……20

Figure 2.12 Plots of the zero-shear viscosities as a function of molecular weight for linear (open symbols) and cyclic (filled symbols) PDMS at 298 K. ……..……21

Figure 2.13 Zero-shear viscosity as a function of molecular weight for linear (line) and cyclic (symbols) polystyrene at 169.5^oC.…….……..22

Figure 2.14 Zero shear viscosities as a function of molecular weight for linear (line) and cyclic polybutadiene (solid triangles are rings contaminated with 20-25% linear, the open triangle is polybutadiene ring) at 26.2^oC. …….23

Figure 2.15 The lattice model for linear (L) and branched (B) polymers (solid lines) in a gel with fixed obstacles. ……24

Figure 2.16 (a) "lattice tree" model for polymer rings, (b) simplified "lattice tree" in gel…….……..24

Figure 2.17 Possible structure for linear or macrocyclic polymers ……..……27

Figure 2.18 Cyclization methods ……..28

Figure 2.19 AFM image for linear and cyclic poly(styrenesulfonate)s ……..……..29

Figure 2.20 Reduced viscosity vs. concentration of cyclic molecules in the mixture of cyclic and linear PS molecules. The broken line and solid line are reduced viscosity for pure linear molecules. ……...……30

Figure 2.21 The modulus (G(t)) of linear and cyclic PS mixture change with increasing linear chain fractions ……...……..31

Figure 2.22 SEC chromatograms of cyclic PS (solid line) and corresponding linear precursor (dashed line) ……..32

Figure 2.23 LCCC chromatograms of cyclic PSs and corresponding linear precursors at the chromatographic critical condition of linear PS. ……...…….33

Figure 2.24 Synthesis of cyclic polymers using ring expansion metathesis polymerization (REMP)……..……35

Figure 2.25 Conversion of monomer with time for different REMP catalyst ……..36

Figure 3.1 Molecular structure of the REMP catalyst……...……39

Figure 3.2 The monomer and synthesis route for polymer rings with different structures……...…….40

Figure 3.3 Master curve of the storage moduli for a monodisperse long chain polymer……..43

Figure 3.4 Master curve of the storage and loss moduli for a polydisperse polymer. ……44

Figure 3.5 Van Gurp-Palmen plot of polystyrene with different molecular weight(a) and polymers with different chemical composition or polydispersity ……46

Figure 4,1 The GPC-MALLS curve for cyclic (a,b,c) and linear (d,e) PCO samples…….……52

Figure 4.2 the radius of gyration of linear and cyclic PCO samples in THF at room temperature……55

Figure 4.3 The damping factor (tan(δ)) vs angular frequency for hydrogenated and unhydrogenated PCO samples……57
Figure 4.4 The measured (black) and the creep data converted (green) dynamic responses of linear and cyclic PCO at 80^{o}C……58

Figure 4.5 Compare the dynamic responses of linear and cyclic PCOs with near molecular weight……60

Figure 4.6 The van Gurp-Palmen plot for linear (green), cyclic PCO from UC6 (black) and cyclic PCO from UC5 with different molecular weight……62

Figure 4.7 Plot of the zero shear viscosity (η_0) against weight average molecular weight (M_w) for linear and cyclic PCOs from different catalyst……65

Figure 4.8 Catalyst decomposition in REMP reaction……67

Figure 4.9 The structure of the crown ether and ammonium composite……67

Figure 4.10 The zero shear viscosity vs molecular weight for linear and cyclic poly(ammonium) samples at the reference temperature of 40^{o}C……70

Figure 4.11 Compare the dynamic responses of linear and cyclic poly(ammonium) samples with near molecular weight……71

Figure 4.12 van Gurp-Palmen plot of the linear and cyclic poly(ammonium) at the reference temperature of 40^{o}C……73

Figure 4.13 The structure of the dendronized macromonomer……74

Figure 4.14 Visualized AFM image of the dendronized polymer rings……75

Figure 4.15 The dynamic master curve for the dendronized polymer ring sample at the reference temperature of 80^{o}C……76

Figure 4.16 The recoverable compliance of dendronized polymer ring……77

Figure 4.17 van Gurp-Palmen plot of the linear and cyclic dendronized polymer……79

Figure 4.18 The shift factors of linear and cyclic dendronized polymer……80

Figure 4.19 The radius of gyration of linear and cyclic wedge polymer in THF……83

Figure 4.20 The dynamic mater curve of the linear and cyclic wedge polymer at the reference temperature of 80^{o}C…….....……..84

Figure 4.21 The shift factor for linear and cyclic wedge polymer…….....……..85

Figure 4.22 van Gurp-Palmen plot of linear and cyclic wedge polymer…….....86

Figure 4.23 Compare the dynamic responses of linear and cyclic wedge polymer with near DP…….....87

Figure 4.24 The zero shear viscosity of linear and cyclic wedge polymer vs molecular weight…….....……88

Figure 4.25 The relation between polydispersity (M_w/M_n) and normalized modulus at fixed phase angle ($\delta=60^{o}$)…….....……90

Figure 4.26 Retardation spectrum for Rouse model…….....……93

Figure 4.27 The retardation spectrum of Lattice animal model…….....……..93

Figure 4.28The retardation spectrum of 6% PS solution …….....……94

Figure 4.29 The retardation spectrum of polyisobutylene …….....……95

Figure 4.30 The retardation spectrum of McKenna's 380k PS ring…….....……..96

Figure 4.31 The retardation spectrum of Roovers' PBd ring…….....……..98

Figure 4.32 The retardation spectrum of Kapnistos' 198k PS ring…….....……99

Figure 4.33 The retardation spectrum of cyclic PCO prepared by different catalyst…….....……..99

Figure 4.34 The retardation spectrum of the cyclic poly(ammonium)s samples…….....……100

Figure 4.35 The retardation spectrum of dendronized ring…….....……101

Figure 4.36 The retardation spectrum of wedge ring sample…….....……..102

Figure 4.37 The retardation spectrum of cyclic PS and it mixture with known amount of linear chain…….....……103

Figure 5.1. Scheme of the synthesis of polynorbornene-*g*- polylactide brush polymers and schematic of the resulting brush polymer…….....……108

Figure 5.2. Intrinsic viscosity versus molecular weight for brush polymers with fixed side chain molecular weight but increasing DP (In THF at room temperature ≈25^{o}C) …….....110

Figure 5.3. Plot of $(M^2/|\eta|)^{1/3}$ vs $M^{1/2}$ for the three groups of brush samples of different side chain length. (In THF at room temperature≈25^{o}C)…….....…….111

Figure 5.4. Comparison of the dynamic responses of the investigated brush polymers with fixed DP (200, 400 and 800). (Vertical shift of C=0, 1 and 2 used to separate the respective the curves) …….....……..113

Figure 5.5. van Gurp-Palmen plot for brush polymers with (a) fixed side chain molecular weight and (b) fixed backbone DP…….....……116

Figure 5.6. Sequential relaxation of the brush polymers. (Vertical shift of C=0, 1 and 2 used to separate the respective the curves)…….....…….118

Figure 5.7. Temperature shift factors for brush polymers with different side chain molecular weight (1.4k, 4.4k and 8.7k Da) at the reference temperature of 80^{o}C…….....……..119

Figure 5.8. Expanded plot of the arm regime and segmental regime for the brush polymers with fixed DP. (Vertical shift of C=0, 1 and 2 used to separate the respective DP curves) …….....……..121

Figure 5.9. Double logarithmic representation of the retardation spectra ($L(\tau)$) for brush polymers with fixed 200 DP backbone and different side chain molecular weights ……...……....……123

Figure 5.10. Expanded plot of the terminal regime for the relaxation of the brush polymer with fixed side chains. (Vertical shift of C=0, 1 and 2 used to separate the curves)…….....…….124

Figure 5.11. Double logarithmic representation of steady state recoverable compliance (J_s) vs. DP for the three groups of brush polymers studied…….....……126

Figure 5.12. Double logarithmic representation of zero shear viscosity (η_0) at Tg+30^{o}C vs. weight average molecular weight (M_w) for the three groups of brush polymer samples with different side chain lengths…….....……..127

Figure 5.13. Scheme of the synthesis of wedge polymers…….....……..131

Figure 5.14. The radius of gyration (R_g) change for wedge polymer with different molecular weight in THF at room temperature (≈25^{o}C)…….....……..132

Figure 5.15 The dynamic master curve for wedge polymer with different backbone DP at the reference temperature of 80^{o}C…….....…….133

Figure 5.16. The shift factors for wedge polymer with different backbone DP at the reference temperature of 80^{o}C…….....…….134

Figure 5.17. The zero shear viscosity for the wedge polymer at the reference temperature of 80^{o}C…….....….136

Figure 5.18 The retardation spectrum of Linear wedge polymer…….....…..136

Figure 5.19 The van Gurp-Palmen plot of linear brush polymer with different side chain structure…….....…….138

Figure 5.20 The shift factors for linear polymers with different side chain structures with the same reference temperature 80^{o}C…….....……..139

List of Tables

Table 4.1 Molecular information for linear and cyclic PCO from GPC-MALLS……..…51

Table 4.2 The plateau modulus (G_N^0) and entanglement molecular weight (M_e) for linear and cyclic PCOs…….....…….61

Table 4.3 Compare the cyclic/linear ratio of two catalysts…….....….68

Table 4.4 Molecular information for linear and cyclic poly(ammonium) samples…..…..69

Table 4.5 The parameters estimated from the dynamic master curve and shift factors of linear and cyclic dendronized polymers…….....….80

Table 4.6 The molecular weight of linear and cyclic wedge polymers…….....……82

Table 4.7 Compare the polydispersity values estimated by van Gurp-Palmen plot for linear and cyclic samples with that estimated by GPC…….....……91

Table 5.1 Sample molecular weight and characterization data…….....….109

Table 5.2 WLF fitting parameters, fragility, apparent activation energy and glass transition temperature determined from the dynamic modulus data for the brush polymers…….....…….119

Table 5.3 Estimated backbone plateau modulus (G'_b) and steady state recoverable compliance (J_s) for the brush polymers at 80^{o}C …….....……125

Table 5.4. Molecular weight and characterization data for linear wedge polymer…….....…131

Table 5.5 Compare the glass transition temperature and fragility of linear polymer with different side chain structure…….....…139

List of Symbols and Nomenclature

g – radius of gyration branching index

$<R_g^2>$ - mean square radius of gyration

g' – viscosity branching index

$|\eta|$ - intrinsic viscosity

N_a - the number of monomer units in each arm

N_e - the entanglement number of monomer units

τ_{rep} – reptation time

q- number of branches

D – diffusion coefficient

a- tube diameter

ξ - the arm coordinates

S_a - the arm length

L - the primitive path length of the arm

D_{eff} - the effective curvilinear diffusion coefficient of the free end of the retracting arm

U_{eff} - the effective potential for the arm retraction

p - the branching point friction

Φ - the volume fraction

T_g – glass transition temperature

M_w – weight average molecular weight

η_0 - zero shear viscosity

SEC - size exclusion chromatography

G' – storage modulus

G"- loss modulus

G_N^0 – plateau modulus

M_e – entangled molecular weight

δ – phase angle

ω – angular frequency

a_T – shift factors for time temperature supposition

m – fragility

E_g – apparent activation engery

$L(\tau)$ – retardation spectrum

$H(\tau)$ – relaxation spectrum

J(t) – creep compliance

PDI – polydispersity index

GPC – gel permeation chromatography

MALLS – multi-angle laser light scattering

PCO – polyoctenamer

PBD – polybutadiene

PLA – poly(lactide acid)

DP – degree of polymerization

Chapter I:
Introduction

Rheology is an important method in polymer materials analysis. The rheological response is sensitive to the changes in chemical nature, molecular structure, molecular weight and molecular weight distribution, material composition or concentration and other interactions between polymer chains. In this dissertation we would examine the rheological responses of several series of polymers materials with different molecular structures and compositions, find the possible factors which may influence their viscoelastic responses and compare the results with theoretical predictions.

The dissertation focuses on the influence of polymer architecture on the rheological responses for polymer with two unique structures, macrocyclic polymer and densely grafted polymer. For macrocyclic polymer or polymer rings, because of the nature of its structure, the molecule should not reptate in the conventional sense because there is no chain end to follow. Study the rheological responses of this kind of polymers would provide some fundamental results and help to improve our understanding in the polymer chain dynamic. In this work, several series of macrocyclic polymers and the corresponding linear polymers with the same chemical nature were synthesized by our collaborators in Caltech. The rheological responses of these polymers were studied by both dynamic test at different temperature, steady flow and creep experiment. The master curves covered from the glassy to the flow region were constructed by time temperature supposition for some samples. The zero shear viscosities were determined from the steady flow experiments to obtain the viscosity vs molecular weight relationship for both linear and cyclic samples. By comparing the viscosity and plateau modulus for

linear and cyclic polymers, the relaxation behaviors for macrocyclic polymer can be obtained and some critical factors which may influence the results were analyzed.

Branched polymer has been excessively studied in polymer rheology. Due to the steric hindrance, it's hard to obtain brush polymers with both large degree of polymerization and densely or regularly spaced branches. In this work we obtained several groups of densely branched polymer with the same backbone but with different lengths and structures for the side chains. The unique conformations for these densely branched polymers and their influences to the relaxation behavior were analyzed. The dynamic master curves were constructed by shifting the dynamic rheological responses at different temperature to one reference temperature. The zero shear viscosities were estimated by steady shear experiment and the steady state recoverable compliance values for different polymers were estimated by creep experiments. The viscoelastic properties and glassy behaviors of brush polymer with different side chain structures were compared together to examine the determined influence of the side chain structure.

Chapter II:
Influence of molecular structure on polymer rheology

Polymer materials are widely used in everyday life. The rheological properties of polymer materials strongly influenced their application and processing behaviors. It has been proved that even for polymer materials synthesized with the same monomer, due to their structure differences, their mechanical properties, glass transition temperature and melting temperature won't be the same.[1] Over the past several decades, much knowledge has been obtained on the influence of polymer structure to their rheological behaviors. [2] Study the viscoelastic behaviors for polymer materials with new architecture is always a hotspot in both academic and industrial field. [3] And these studies will help to better understand the relaxation behavior for both linear and nonlinear polymer materials and validate the application of reptation model to different polymer structures. [2]

2.1 Linear polymer and reptation model

Polymer materials with the simple linear structure are widely used. For entangled linear polymers, their diffusion and relaxation behaviors can be well described by the reptation model. The reptation model was first proposed by de Gennes [4] in 1971 and further developed by Doi and Edwards [5]. The idea for reptation model is that a linear polymer chain is trapped into a three dimensional tube. The diameter of the tube is the contour length of the polymer chain. Upon external strain, it will move like a snake within the tube following its head. Figure 2.1 illustrate the chain motion of reptation model. This model neglects the movement of the surrounding chains and the interaction between other chains and the chain ends of the examined polymer chain. [6] The results

predicted from this reptation model do not match well with experimental observations. The predicted reptation time should scale following the 3.0 power of the molecular weight, while the experimental data suggest the exponent of 3.4 for mostly narrow dispersed linear polymers. [7] Similarly the diffusion coefficient for entangled linear chains is found to be scaled as -2.3 rather than -2 as predicted by the reptation model. [7]

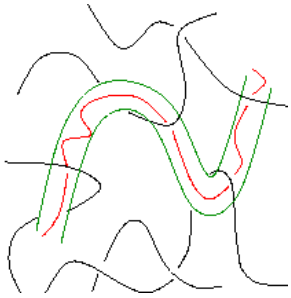

Figure 2.1 Illustration of reptation model for an entangled linear molecule in melt

Over the past two decades, two effects were exclusively studied and were applied to modify the reptation model. They are "constrain release" [8] and "contour length fluctuation"[9]. The scheme for the "constrain release" is shown in Figure 2.2. In the reptation model, the tube is formed by constrains from the surrounding chains, when those chains reptate along their own tube, the shape of the tube will change constantly due to the environment change.

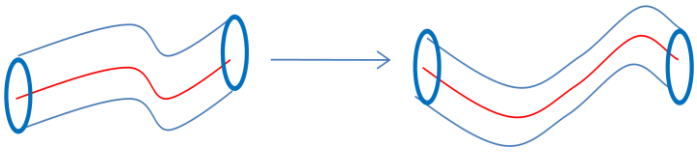

Figure 2.2 Illustration for the constrain release

Similarly in reptation model, the surrounding chains are flexible. They will stretch and retract upon external stress or strain change. These fast fluctuations will change the shape of the tube and help the chain relax faster which caused the 3.4 power law. This effect is called "contour length fluctuation". When the chain molecular weight is enough high, this effect will not be that significant and lead to a weaker exponent of 3.0 for molecular weight vs zero shear viscosity. [10] With take into account of these effects, the modified reptation model by McLeish and his coworkers has been proved to be a successful model in predicting the relaxation behaviors for linear polymer chains over a large range of molecular weight.

2.2 Branched polymers and the hierarchical models

The rheological responses for branched polymer have drawn much attention over the past several decades and due to the sensitivity of the rheological measurement, polymer rheology has become an important method to detecting the branching structure. [11] The existence of the side chain will inhibit the relaxation of the backbone and the traditional reptation model need to be further modified to predict the relaxation behavior for branch polymers. Many factors may affect the viscoelastic properties for the branched polymers, like the branch chain structure and length, branching density and distribution.[2, 3] Briefly the branched polymer can be classified as star polymer, H-shaped polymer, comb polymer and dendritic polymer.

For the solution properties of branched polymers, it is found that they tend to take a more compact conformation comparing with linear polymers with the same molecular

weight.[1-5, 12] The parameter radius of gyration branching index or viscosity branching index are introduced, [12]

$$g = \frac{<R_g^2>_b}{<R_g^2>_l} \quad \text{radius of gyration branching index} \quad (2.1)$$

or $$g' = \frac{|\eta|_b}{|\eta|_l} \quad \text{viscosity branching index} \quad (2.2)$$

,the radius of gyration and intrinsic viscosity for branched and linear polymers should be in the same solvent. Several factors may influence the branching index values, like the molecular structure, branching structure and molecular weight, etc.

2.2.1 Star polymers

The star polymers have only one branching point and the two longest arms can be regard as the backbone. They can not reptate, but the polymers will relax and diffuse through the "arm retraction" mechanism. [5, 7, 13-15] To relax, the arms will first retract back to the center and then stretch out to the next position. The molecular weight dependence of the zero shear viscosity scale differently than the normal 3.4 power law for the linear polymers. The zero shear viscosity will be determined by the molecular weight of the arms as shown in equation 2.3. [7, 14]

$$\eta \approx (\frac{N_a}{N_e})^{\frac{3}{2}} \exp(\frac{\gamma'}{2}\frac{N_a}{N_e}) \quad (2.3)$$

,where γ' is a dimensionless constant, N_a is the number of monomer units in each arm, N_e is the entanglement number of monomer units. From the equation it can be seen that the viscosity of the star polymers follow an exponential growth with the number of entanglement in each arm (N_a/N_e), but independent of the number of the arms. Comparing with linear polymers of the same molecular weight, the zero shear viscosity for the star polymers is lower than that of the linear chains. [14] The rheological response

for star polymers have been exclusively studied by many group, [14-20] basically the star polymer will follow the hierarchical relaxation mechanism and the relaxed side chains will act as a solvent to the whole molecular.

2.2.2 Dendritic polymer

Dendritic polymer or dendrimer is a special kind branched polymer.[21] As shown in Figure 2.3, the core part is branched structure. The new branches grow on the previous branch and form a new layer. This process can be repeated three-dimensionally until a regular, tree-like structure is created. With this growing mechanism, the density of the outer layer is usually higher than the inner layers and they polymer form a hard shell with soft core inside. [21, 22] The special structure bring dendritic polymer a very special rheological properties, that is, it prefer to show Newtonian flow behavior even at high molecular weight.[22, 23] The dendritic structure contains a lot of chain end, which will alter the glass transition behavior of the polymers. By altering the nature of the chain end and their interactions, people can easily get different dendritic polymers covering a wide range of glass transition temperature.[24] However for dendritic polymer with simple structure with two to three layers, they still follow the hierarchical relaxation mechanism and double or triple relaxation behavior can still be observed. [18]

Figure 2.3 Scheme for the structure of dendritic polymers

2.2.3 Comb and H-shape polymer

Comb and H-shape polymers are another big group of branched polymers and H-shape is the simplest form of comb polymer with the branches attached at the two end of the backbone. Unlike what is shown in Figure 2.4, the branched for the comb polymers are not strictly located on one side of the backbone. They can distributed three dimensionally surround the backbone, as what we would discussed later, the properties and interactions between the brushes can greatly affect the properties of the comb polymers.

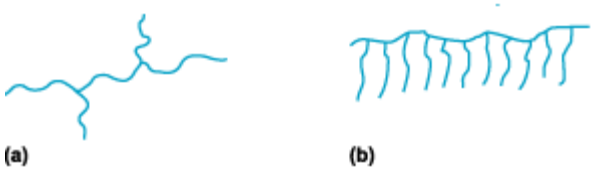

Figure 2.4 Scheme for the structure for H-shape (a) and comb (b) polymers

In the rheological study for star polymer, side chain length and their retraction behavior play an important role in the total relaxation mechanism of the whole polymer. Compared to the star polymer, comb polymer has an extend backbone. It can be expected that the relaxation of the side chains by “arm retraction” will suppress the relaxation of the backbone. Figure 2.5 is the rheological responses for PS comb polymers with different branching length. With increasing the side chain length, there are two rubbery plateaus were found in the dynamic responses. The first one at higher frequency is associated with the relaxation behavior of the longer side chains and the second one at lower frequency is related with the relaxation of the backbone. This phenomenon is

called double relaxation and is matched well with the hierarchical relaxation mechanism for the brush polymers. [15, 19, 20, 25-34]As marked by the red arrow, the plateau modulus for the PS backbone decrease with increasing side chain length and the relaxation time of the backbone also get longer.

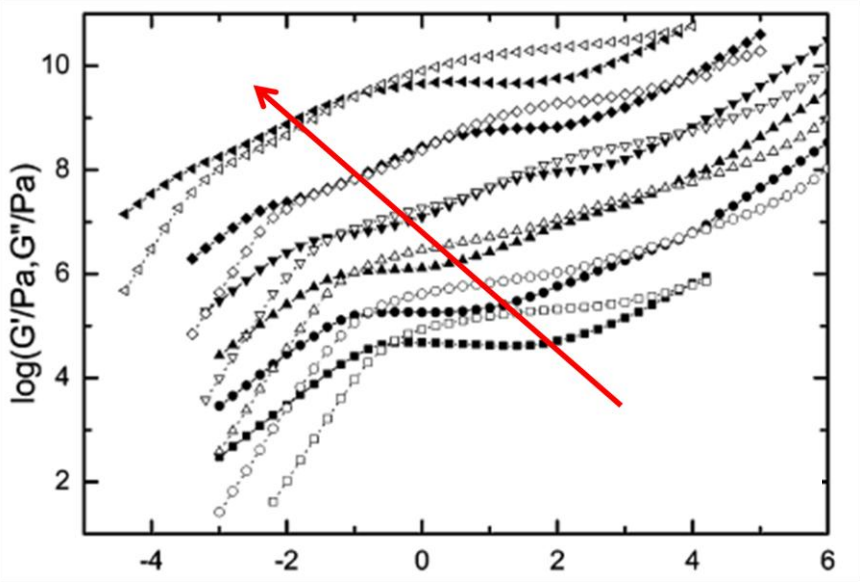

Figure 2.5 PS linear combs with equal backbone (Mb=275 kg/mol) and branch degree (~30), branch lengths increase (0, 6.5k, 11.7k, 25.7k, 47k and 98k g/mol) (After Kapnistos et. al.[25])

The relaxed side chain will act as a solvent to dilate the tube of the backbone. The reptation time for the comb polymer when the backbone and the branches are composed by the same polymer can be expressed as, [7]

$$\tau_{rep} \approx \frac{L_{bb}^2}{D_c} \approx \frac{L_{bb}^2}{(\frac{a^2}{(q-2)\tau_{arm}})} \approx \tau_{arm}(q-2)(\frac{N_{bb}}{N_e}) \qquad (2.4)$$

, where a is the tube diameter, τ_{arm} is the arm retraction time, q is the number of branches and (q-2) is the total number of branches along the backbone, D_c is the diffusion coefficient of the backbone, Ne is the number of monomers to form entanglements, L_{bb} is

the total length of the backbone, and N_{bb} is the total number of monomers on the backbone. From the expression, it can be found that the relaxation time not only depend on the relaxation of the branches but also related with the relaxation of the branching points and the backbone.

2.2.4 Hierarchical model

To describe the relaxation behavior of branched polymers, the hierarchical model is widely used,[2, 11, 19, 35] and has been applied to various branched polymers with different structures such as H-shaped [32], star [17-19] and comb[25, 28, 36]. The basic idea of this model is that polymers relax in sequence: the grafted branches relax first, followed by the branching points, and the backbone subsequently reptates in a dilated tube. [15, 19] The relaxed branches act as a solvent for the unrelaxed backbone, [18] and due to the dilution effects of the side chains, with decreasing volume fraction of the unrelaxed backbone, the modulus will also decrease following the power law of $\alpha+1$, where α is the dilution parameter. [11, 15]

When the branched polymer is subject to a small strain change, the branch arm end will react first at time much shorter than the Rouse time of the arm, which can be express as,[11, 19]

$$\tau_{early}(\xi) = \frac{9}{16}\pi^3\tau_e S_a^4\xi^4 \qquad (2.5)$$

, where ξ is the arm coordinates, S_a is the arm length. Later the arm will retract at longer relaxation time, [11, 19]

$$\tau_{late} = \frac{L^2}{D_{eff}}\left(\frac{2\pi}{U''_{eff}(0)}\right)^{1/2}\int_0^{\xi} d\xi' \exp\left[U_{eff}(\xi')\right] \qquad (2.6)$$

,where L is the primitive path length of the arm and D_{eff} is the effective curvilinear diffusion coefficient of the free end of the retracting arm, U_{eff} is the effective potential for the arm retraction, which is related with volume fraction of the unrelaxed chain.

After the arm gets fully relaxed, then unless the branching points are linked with some part which will inhibit its relaxation, the branching points will start to move. The collapsed arms will bring some friction to the branching point and the curvilinear friction constant can be express with the Einstein relaxation, [31]

$$\zeta_a = \frac{2k_bT\tau_a}{p^2a^{*2}} \quad (2.7)$$

, where p^2 is the branching point friction, a^2 is the diameter of the dilated tube, τ_a is the relaxation time for the arm. In hierarchical model the p^2 is usually found to be 1/12.[32]

The length of the side chains may not be uniform. The shorter side chains should relax faster than longer side chains. The relaxed side chains will collapse onto the branching point and should not be counted into the unrelaxed volume fraction. The unrelaxed side chains will form new branching structure with the backbone and called the "compound arms". [11] These relaxed side chains will bring external friction to the relaxation of the longer side chains which connect with the short chains at the same branching point. This effect will increase the time for the arms to retract and relax,[11] and the diffusion coefficient of the side chain will get smaller depending on the friction of the branching point. [37]

When only two arms are not relaxed, they two together with the backbone can be regard as one linear chain, then this linear chain will reptate. The reptation time for this linear chain is estimated by Larson et. al., [35]

$$\tau_d = \frac{1}{\pi^2 k_B T}\zeta_{tot}a^2\Phi^a_{tube}(\tau_{rep})[S_{a,1}(1-\xi_{a,1}) + S_{a,2}(1-\xi_{a,2})]^2 \quad (2.8)$$

, where τ_{rep} is the reptation time for this linear chain to reptate in an undilated tube with diameter of a; $\Phi_{tube}^{\alpha}(\tau_{rep})$ is the diameter of the tube for the linear chain to reptate at time τ_{rep}; and ζ_{tot} is the total friction of the chain. There is still much discussion on the actual tube diameter of these linear chains. [35, 37] By changing the expression of τ_{rep},, in different model the linear chain may reptate in the tube of different diameter. In hierarchical model the partly dilated tube is used with $\tau_{rep} = a^2\zeta_{tot}/2k_BT$.

Constrain release [8] commonly exists in the relaxation of linear polymers. However for brush polymer, due to the relaxation of the side chains, at a certain time when all the side chains are relaxed, the volume fraction for the unrelaxed chains will get a fast drop. The tube diameter can't change as quickly as the unrelaxed volume fraction, thus as discussed by Milner et. al.[20] the relaxed brush chain will reptate follow a "constrain release Rouse" motion in a wider "supertube".

Another important theory in hierarchical model is the dynamic dilution theory, [15] which means the relaxed side chains will act as solvent and reduced the plateau modulus of the backbone chain. The scaling equation for the modulus change with the unrelaxed volume fraction of the branched polymers is,

$$G(\Phi) = G_N^0\Phi^{\alpha+1} \qquad (2.9)$$

α is the dilution exponent, which may related with some entanglement behavior. Φ is the volume fraction of the unrelaxed part. Based on different assumption and experiment results, [15, 16, 19, 29, 38] the exact value for α could be either 1 by Ball and McLeish[15] or 4/3 by Milner and McLeish [19]. α=1 can fit well with the situation where the linear chain reptation dominate the terminal relaxation, like comb polymer or polydispersed linear

chains. [29, 39] When α=4/3, the arm retraction should dominate the terminal relaxation, like the star polymer or star-linear blend. [16, 18, 19, 37, 38]

2.3 Macrocyclic polymer

Macrocyclic polymers (cyclic polymer) or polymers rings are an important kind of polymers with very interesting properties. [40] Due to the molecular nature, macrocyclic polymers have no chain end and each unit along the polymer chain are chemical or physical equivalent. [41] This topological constraint make the polymer rings tend to form a more compact molecule structure comparing with linear polymers with similar molecular weight. [42-45] Much work has been done to study the viscosity,[46-49] conformation [50-54] and viscoelastic [48, 55-58] properties of macrocyclic polymers and some conclusions have been widely accepted. These widely accepted conclusions are listed in the following section.

2.3.1 Solution properties of macrocyclic polymers

Unlike linear polymers, the chain end of an ideal linear chain can "random walk" without any restrictions. [7] For macrocyclic polymers, the two chain ends are forced to connect together, which will result into a more compacted conformation. [40] Assuming the Kuhn length of a polymer chain is l and the number of polymer unit is n. Than for ideal linear chains, the radius of gyration should be,

$$R_{g,l}^2 = \frac{nl^2}{6} \qquad (2.10)$$

While for macrocyclic polymer, due to the two chain ends need to connect together, the radius of gyration should be,

$$R_{g,r}^2 = \frac{nl^2}{12} \qquad (2.11)$$

Comparing the two equations, it can be found that in θ solvent the radius of gyration of macrocyclic polymer should be half of the linear polymer with the same molecular weight ($g=R_{g,r}^2/R_{g,l}^2=0.5$). In good solvent, the macrocyclic polymer is expected to swell more and the ratio is estimated to be 0.54. [40] Neutron scattering experiments done by Huggins [51], Hadziioannou [59] and Roover[49] on cyclic Polydimethylsiloxane (PDMS) and polystyrene (PS) in θ solution found similar results as predicted. The radius of gyration will affect the hydrodynamic radius R_h and the intrinsic viscosity, as stated in Semlyen's book, [40] the ratios are expected to be,

$$g_h = \frac{<R_h^2>_r}{<R_h^2>_l} \approx 0.85 \qquad (2.12)$$

$$g' = \frac{|\eta|_r}{|\eta|_l} = 0.662 \qquad (2.12)$$

Experimental data for the g_h is reported by Roover (g_h=0.86) [49] and Hadziioannou (g_h=0.89) [59]. For the g' ratio in θ condition, the model work done by Bloomfield and Zimm [60] (g'=0.658) or Fukatsu and Kurata [61] (g'=0.645) give similar predictions. Geiser and Hocker [62] studied the intrinsic viscosity change with molecular weight for a series of low molecular weight cyclic polystyrene in θ condition and the g' ratio is reported to be between 0.64 and 0.68. McKenna et. al. [47, 48] studied the intrinsic viscosity for a much wider molecular weight range of cyclic polystyrene materials in both good and θ solvent. As shown in Figure 2.6, in both conditions the intrinsic viscosity of most cyclic polymers are lower than that of linear polymer with the same molecular weight. At higher molecular weight range, especially in good solvent condition, the intrinsic viscosity for the cyclic is much lower than the linear polymers, and this phenomenon is attributed to the existence of knotted or catenated rings. [48]

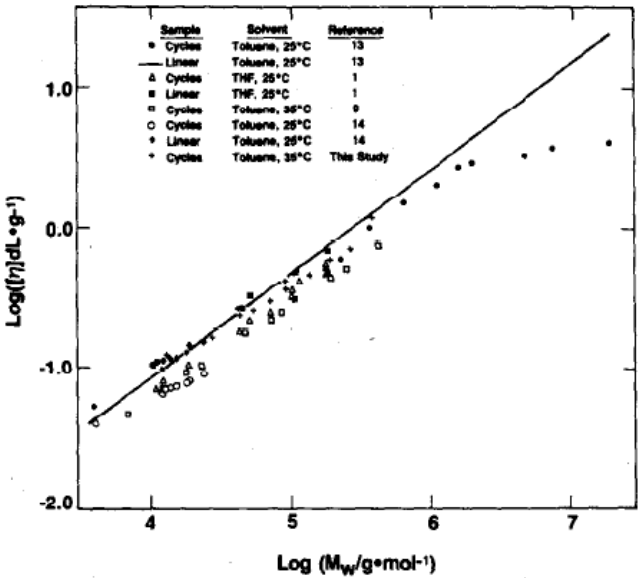

(a)

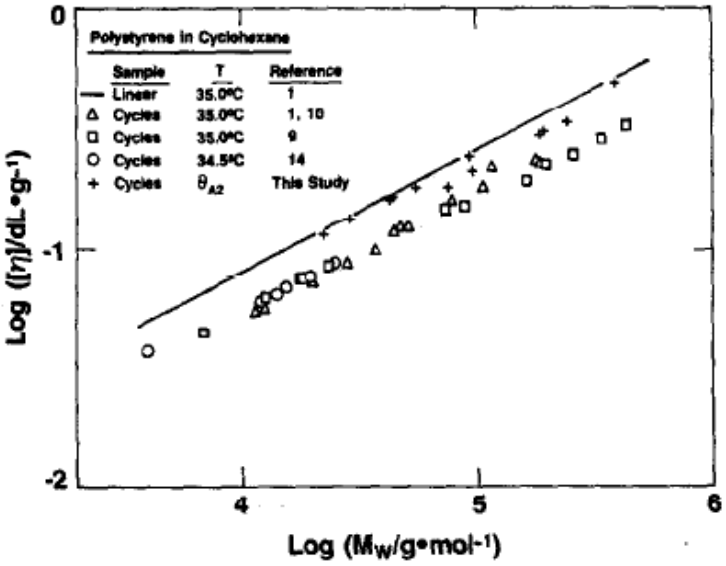

(b)

Figure 2.6 The intrinsic viscosity change with molecular weight for cyclic and linear polystyrene in (a) good solvent and (b) in θ-solvent. (After McKenna et al. [48])

2.3.2 Glass transition behavior of macrocyclic materials

The unique architecture of macrocyclic polymers makes them lack of chain end, which result into the macrocyclic polymers tend to take a more compact conformation in solutions. Comparing with other segments in polymer chains, chain ends have more flexibly and may plasticize the polymer chain. Based on this assumption, Kanig and Ueberreiter [63] proposed the equation to describe the molecular weight dependence of glass transition temperature (T_g) change with molecular weight.

$$T_g = [\frac{1}{T_g^{\infty}} + \frac{K}{M_w}]^{-1} \qquad (2.13)$$

K is constant and varies between polymers, T_g^{∞} is the glass transition temperature of linear polymer at extremely high molecular weight and M_w is the polymer molecular weight. For macrocyclic polymer, they lack the mobility introduced by the chain ends, thus their T_g is expected to the same as T_g^{∞}. Santangelo et. al. [64] found that the glass transition temperature of a low molecular weight polystyrene is much higher than its linear competitor and near the value of T_g^{∞}. The segmental relaxation behaviors of the polymer rings are found to be similar as high molecular weight linear chains.

Semlyen et.al.[65] examined the glass transition temperature of a series of PDMS linear and rings. As shown in Figure 2.7, unlike linear polymers, the glass transition temperatures of macrocyclic polymers are found to decrease with increasing molecular weight.

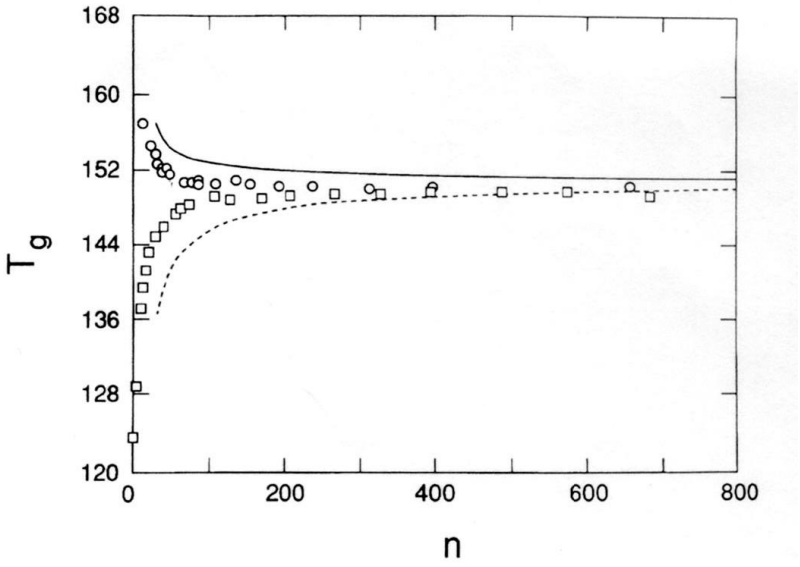

Figure 2.7 Glass transition temperatures (T_g) of cyclic (round) and linear (square) PDMS change with their number-average of skeletal bonds n. The two lines are theoretical prediction by Di Marzio and Guttman.[66] (After Clarson S. J. et.al. [65])

2.3.3 Viscoelastic properties of macrocyclic materials

The segmental relaxation behaviors for macrocyclic polymers are found to be different from linear polymer with the same molecular weight. If compare the relaxation behaviors of the polymer chain with linear and macrocyclic architecture, what are the similarities and differences between the two kind of polymers?

2.3.3.1 Temperature dependence of viscosity

Mckenna et. al.[47] investigate the zero shear viscosity change with temperature for a series of polystyrene rings with different molecular weight. As shown in Figure 2.8, the reduced viscosity (η_0/β_η) vs molecular weight (M_w) plot shows no differences between the two kinds of polymers. The differences between the VFT fitting parameters for the cyclic and linear polystyrene samples are within the experimental error. Similar results

were found by Dodgson et. al. [58], in their work on the flow activation energy (E_a) of PDMS, the E_a for both linear and cyclic are near to each other at higher molecular weight.

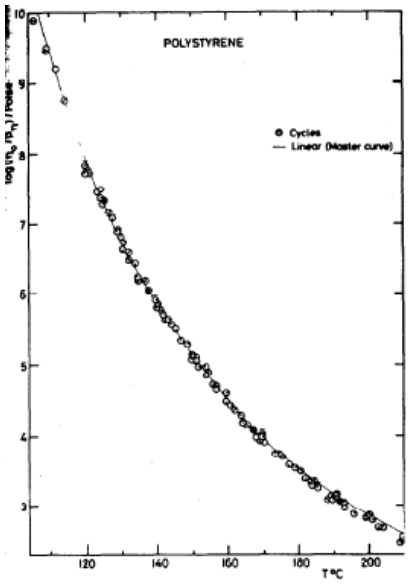

Figure 2.8 The reduced viscosity change with temperature for both cyclic (dotted points) and linear polystyrene (line)

2.3.3.2 Plateau modulus (G_N^0)

For entangled linear polymers, in their dynamic mater curves, there is always a well defined rubbery plateau. However for macrocyclic polymer there is much debate on the ratio of $G_N^0{}_l$ for linear and $G_N^0{}_r$ for macrocyclic [48, 56] and even the existence of the rubbery plateau [57]. As shown in Figure 2.9, McKenna et.al. reported the $G_N^0{}_r$ is half of the $G_N^0{}_l$ for linear polystyrene in their work to creep the cyclic PS and get the steady state recoverable compliance($J_N^0 = 1/G_N^0$). Roovers did the dynamic test on the cyclic polybutadiene (PBd) and found the value should be 1/5 (Figure 2.10). However, some recent work done by Kapnistos et. al. [57], they didn't find the rubbery plateau in their stress relaxation experiment for cyclic polystyrene fractionate by the liquid chromatography at the critical condition (LCCC) (Figure 2.11).

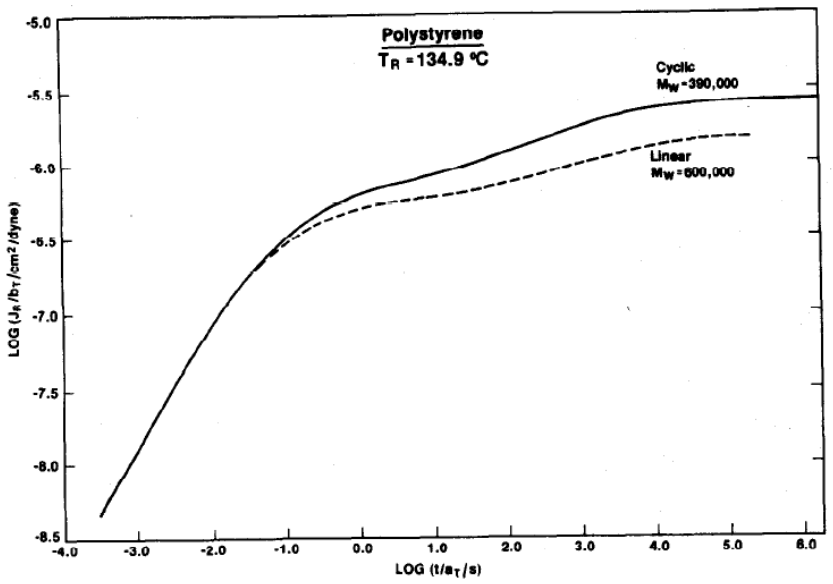

Figure 2.9 Double logarithmic plot of recoverable compliance versus reduced time for cyclic polystyrene (Mw = 390,000 g/mol) compared with that of a linear polystyrene fraction (Mw = 600,000) (After McKenna et al.[48])

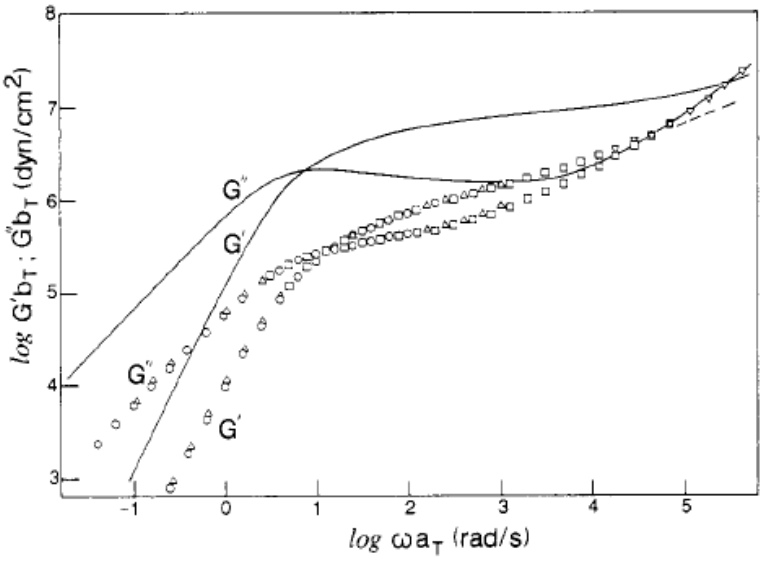

Figure 2.10 Comparison of the dynamic moduli of linear (line) and cyclic (symbol) polybutadiene at 26.2 °C. (After Roovers et al.[56])

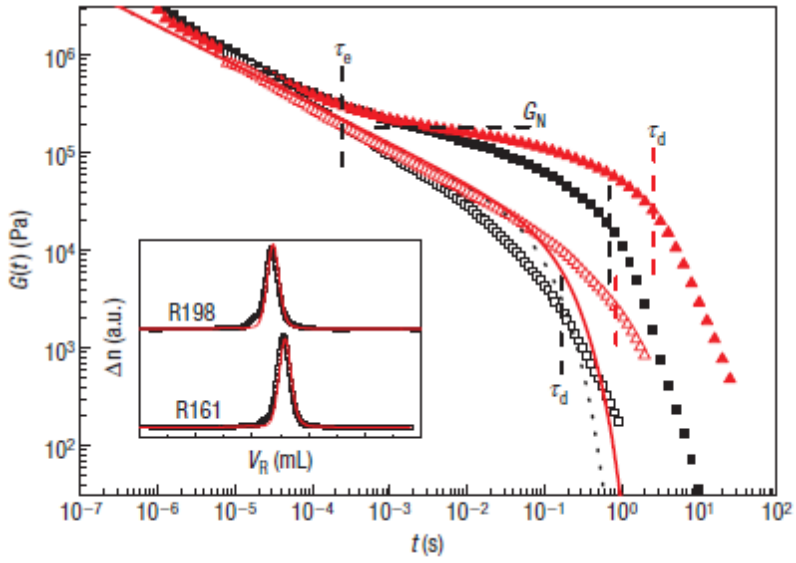

Figure 2.11 Stress relaxation modules G(t) of two polystyrene rings (open triangles and open squares) and with their linear counterparts (respectively filled triangles and filled squares) at reference temperature of 170°C. (After Kapnistos et.al.[57])

2.3.3.3 Zero shear viscosity (η_0) and molecular weight relationship

In dilute solution, due to the structure constrains in unperturbed condition the intrinsic viscosity of macrocyclic polymers is about 2/3 of the intrinsic viscosity of linear polymers with the same molecular weight. [40] In polymer melt, the polymer chain dissolved in itself and the intra-molecular interactions environment is similar as in θ condition. [5, 7]Then if the macrocyclic polymers retain their conformation in solution, the viscosity of macrocyclic polymer should be lower than the linear polymers. Dodgson [58] examined the zero shear viscosity of some low molecular weight PDMS rings. As shown in Figure 2.12, the zero shear viscosity of cyclic PDMS are lower than the linear ones except for some low molecular weight samples, which can be corrected by taking into account of the difference in glass transition temperature for rings and linear.

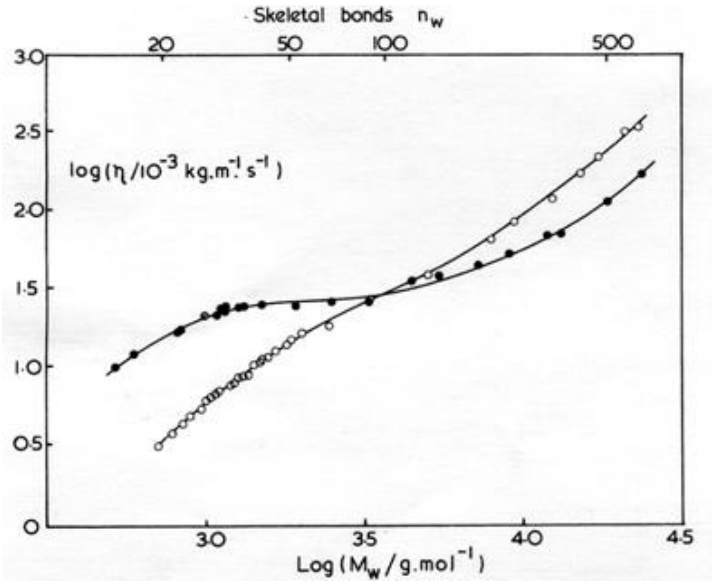

Figure 2.12 Plots of the zero-shear viscosities as a function of molecular weight for linear (open symbols) and cyclic (filled symbols) PDMS at 298 K. (After Dodgson et al.[58])

A shown in Figure 2.13, McKenna et. al. [47, 48] found similar phenomenon as Dodgson did. When the molecular weight of cyclic PS is lower than a critical value (M_c), the zero shear viscosity of cyclic polymer is about half of the linear ones. The scaling parameters for linear and cyclic are the same within this molecular weight range. However, when the molecular weight is above M_c, than the zero shear viscosity of cyclic PS increases faster than the linear samples and the viscosity line for cyclic PS approaches the viscosity line for linear PS. If estimated the number of entanglements using McKenna's plateau modulus data for the cyclic PS, than up to 9 entanglements, the zero shear viscosity of cyclic PS is lower than the linear PS.

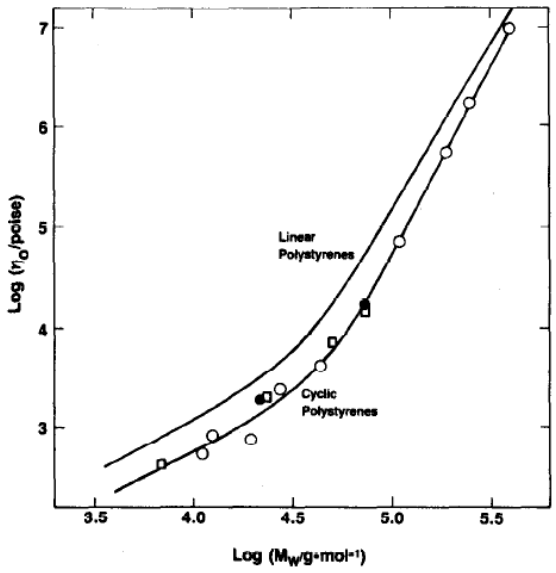

Figure 2.13 Zero-shear viscosity as a function of molecular weight for linear (line) and cyclic (symbols) polystyrene at 169.5^{o}C. (After McKenna et al. [48])

Roovers [56] studied the viscoelastic responses of some cyclic polybutadiene (PBd) and found that the only pure cyclic sample exhibited a much lower zero shear viscosity than the linear ones. As shown in Figure 2.14, the zero shear viscosity of cyclic PBd is about 1/10 of the zero shear viscosity of the linear PBd with the same molecular weight. For Roovers's rings if use the plateau modulus estimated in the paper, then the number of entanglements is around 7. If polymer rings can get entangled, then this PBd sample should be long enough to get entangled. However, the viscoelastic results of Roovers' PBd ring are much different from what McKenna et. al. found for cyclic PS.

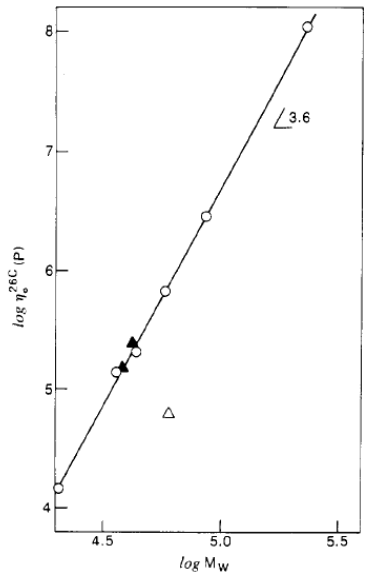

Figure 2.14 Zero shear viscosities as a function of molecular weight for linear (line) and cyclic polybutadiene (solid triangles are rings contaminated with 20-25% linear, the open triangle is polybutadiene ring) at 26.2°C. (After J. Roovers.[56])

2.3.4 Molecular model for macrocyclic materials

Reptation theory has been successful applied to predict the viscoelastic behavior of linear and branched polymers, [1-9, 19, 20, 25-34, 39, 42, 67] however for the macrocyclic polymers, since they have no chain ends, will they reptate and how would they reptate is still a big theoretical challenge. [13, 42] To simplify the movement of linear polymers in melt, de Gennes [68] first proposed the "lattice model" idea, in which the constrains like entanglements applied by the environments are treated as fixed obstacles and the polymer chain will diffuse along the tube. As shown in the scheme drawn by Rubinstein (Figure 2.15), the dash line is the primary path of the linear chain and the loops along the dashed lines are unentangled loops. The unentangled loops are expected to follow the Rouse-type relaxation ($\tau_e \sim M_e^2$) and the linear polymer will relax with the reptation time ($\tau \sim M^3$). [1, 68] For branched polymers, their relaxation behavior would be more complicated. As the loops form by the branches cannot pass the branch points along the primary path, but they

will retract back to the branch point and then stretch out to the next equilibrium configuration. This process will slow down the relaxation of the primary path.

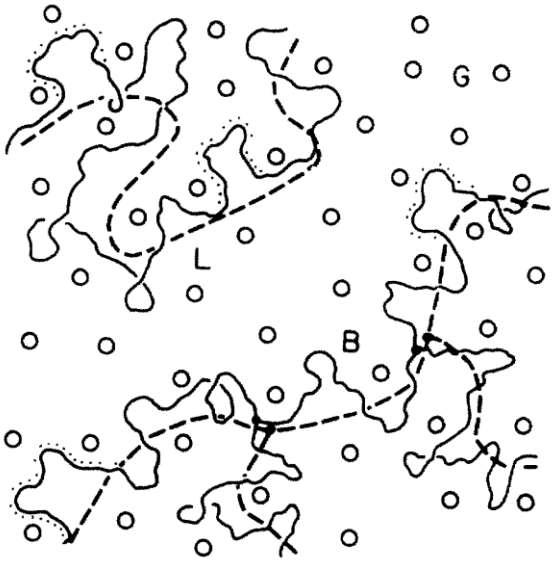

Figure 2.15 The lattice model for linear (L) and branched (B) polymers (solid lines) in a gel with fixed obstacles. (After M. Rubinstein [67])

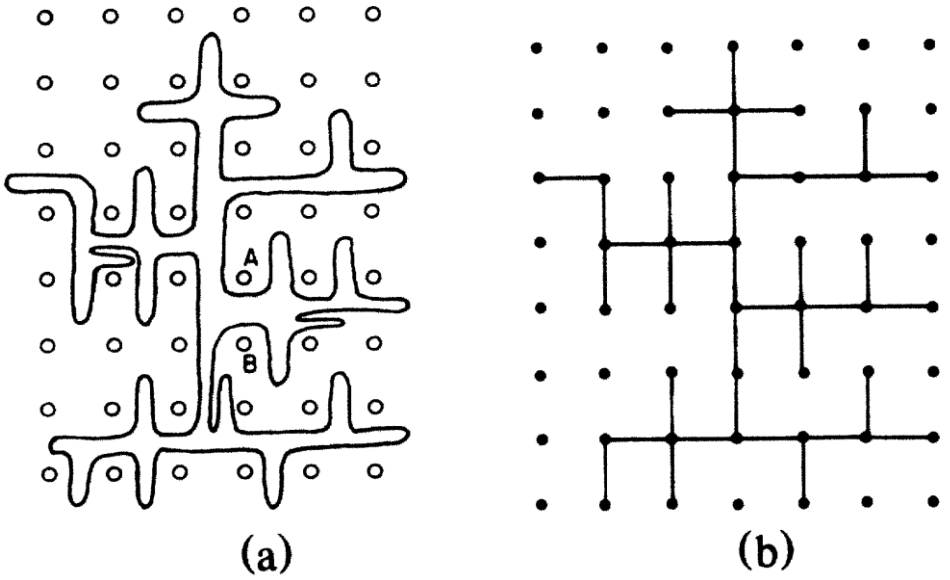

Figure 2.16 (a) "lattice tree" model for polymer rings, (b) simplified "lattice tree" in gel(After M. Rubinstein [67])

"Lattice tree" model based on the "lattice model" and the "lattice animal" idea proposed by Khokhlov and Nechaev [69] was first derived by Rubinstein. [67, 70] As shown in Figure 2.16b, in this model, the polymer rings are treated as branched polymers except the branched point is not fixed. The macrocyclic polymer is treated as a trunk which represents the main path, and then there are branches or leaves which represent different size of loops. Similar as in "lattice model", these branches or leaves are not entangled and the relaxation time scales as Rouse chains. The longest relaxation time for the polymer rings are, [57]

$$\tau \approx (\frac{N}{N_e})^{5/2}\tau_e \qquad (2.14)$$

, where N_e is the average number of monomers between entanglements, and τ_e is the relaxation time of an entanglement segment. Base on this, the relaxation modulus can be express as, [57]

$$G(t) = G_N(\frac{t}{\tau_e})^{-\frac{5}{2}}\exp(-\frac{t}{\tau_{ring}}) \qquad (2.15)$$

, where G_N is the plateau modulus and for this equation t should be large than τ_e. As shown in Figure 2.11, the theoretical prediction agrees well with Kapnistos's experimental data. [57] However, experimental work done by Takano suggested that the PS rings examined in Kapnistos's paper have a high possibility of being knotted rings. [71]

The "lattice tree" model simplifies the movement of polymer rings in melt state, but does not agree well with most experimental data. [40, 47, 48] To fully understand the relaxation behavior of polymer rings, as suggested by Rubinstein two other effect should be considered. [70] Firstly, similar as for linear polymers, constrains applied by the surroundings will change as the trunk diffuse along the primary path. Along the trunk there will be different relaxation time for different section of branches or leaves. [72]

Secondly, the "lattice tree" only considers the diffusion of a single polymer ring. In melt state, it is highly possible that with enough large ring size, two neighbored rings may penetrate with each other. This strong topological interaction will slow down the dynamic diffusion of the polymer rings and the relaxation time will not scale as expected in equation 2.14 and will depend more on molecular weight.

Recently the computer simulation work done by Kremer[73, 74] based on the theory of primitive path analysis[75, 76] suggested that for noncatenated rings due to the entropy barrier, the rings should not interpenetrated with each other. Unlike what has shown in Figure 2.16, there should be no topological constrains within the rings and the ring should take a collapsed conformation. Similar assumption was made by Beaucage based on their experimental work, that large molecular weight ring may collapse.[77] With this assumption, the collapsed rings should only take the Rouse motion and the zero shear viscosity (η_0) of the macrocyclic polymer should scale as 1 with molecular weight. The zero shear viscosity of the rings would be much lower than linear chain as the molecular weight get higher because for linear chains their zero shear viscosity would scale follow the 3.4 power law. Kremer's assumption on the collapsed ring conformation is questioned by other's recent work with computer simulation. Tsolou et. al. [44] found the ring should get entangled found deviation from Kremer's predictions at high molecular weight range.

2.3.5 Synthesis of macrocyclic materials

There is much inconsistency in the result for the viscoelastic properties of polymer rings. Some of them are attributed to the quality of the rings. Since 1946, when Scott synthesized the first PDMS rings, [78] synthesis of cyclic polymer has been an active

field for polymer chemists. [41] Different approaches have been applied to synthesize different polymer rings or polymer rings with different structure (Figure 2.17). [41]

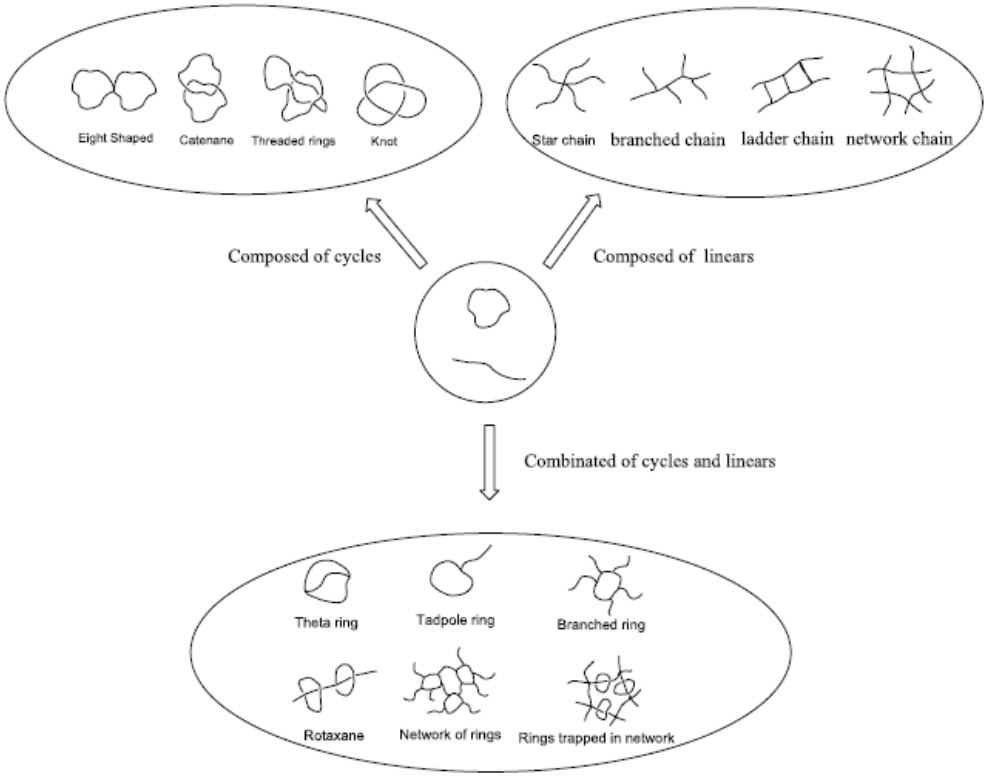

Figure 2.17 Possible structure for linear or macrocyclic polymers (after Endo [41])

Brown and Slusarczuk [79] synthesized the first polymer PDMS. Semlyen et. al. separated the pure PDMS rings with gel permeation chromatography (GPC) and did some systematic studies on the viscosity, radius of gyration, refraction index and other properties of the macrocyclic PDMS. [40, 50, 51, 53, 58, 65, 80] Even though the molecular weight ranges of the cyclic PDMS are comparably low; their results provided some guidelines for the following research work. Geiser et.al. [62] synthesized the some linear PS by anionic polymerization and linked the two ends together using some bifunctional terminating agent. The intrinsic viscosity of these PS rings followed well with theoretical

expectations. Similar methods were applied to get PS rings and the properties of PS rings are studied by Roovers [49, 55, 81] and McKenna [46-48] . Polybutadiene (PBd) rings are synthesized and well examined by Roovers. [56, 82] Other ring polymers like polyisoprene [83], cyclic ether [40], etc. are synthesized following various routes in the past several decades.

2.3.5.1 Traditional methods for synthesis macrocyclic polymers

Basically the cyclization process for synthesizing polymer rings can be classified into two categories. One is the ring chain equilibrium (Figure 2.18a) method which is often seen in polycondensation or ring opening polymerization methods. Another one is the most commonly used end to end cyclization. The cyclization process may happen between two linear chains with different "living" ends (Figure 2.18b) or one linear chain linked by a bifunctional agent (Figure 2.18c). [41]

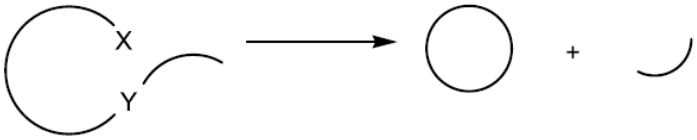

(a) ring chain equilibrium

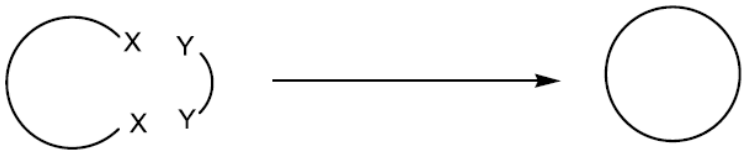

(b)bimolecular process

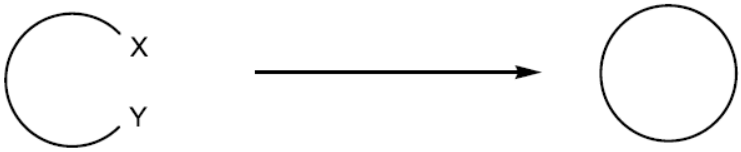

(c) unimolecular process

Figure 2.18 Cyclization methods (After Endo[41])

The traditional way of synthesizing polymer ring requires to prepare the linear polymers first and then links the chain ends into macrocyclic polymers.[41] As the properties of linear polymers have been well studied, [7] the molecular weights of polymer rings made from some linear precursors can be easily determined. The properties of macrocyclic or linear polymers with the same molecular weight are compared with different characterization methods. However, the chemical process to cyclization the linear chains is an equilibrium process. There will be some unreacted linear chain in the cyclic polymers. [40, 41, 54, 84, 85] The linear chains are very hard to separate from the rings. Figure 2.19 shows the atomic force microscopy (AFM) for both linear and cyclic poly(styrenesulfonate)s separated by liquid chromatography at the critical condition (LCCC) from the linear/cyclic mixture after the end to end cyclization. [85]

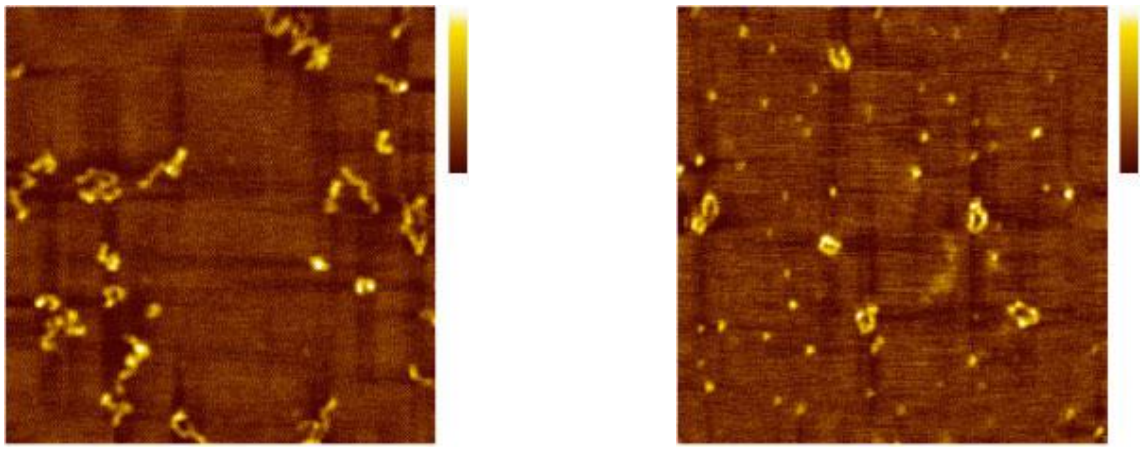

(a) (b)

Figure 2.19 AFM image for linear and cyclic poly(styrenesulfonate)s (after Kawaguchi et. al.[85])

Linear chain contamination will greatly alter the viscoelastic properties of the polymer rings. With a small amount of linear chain contamination in cyclic polymers, as shown in Figure 2.20, the viscosity of the mixture will increase dramatically.[46] Similar results were found by Roovers in the mixture of linear and cyclic Polybutadiene or polystyrene. [56] Further work done by Kapnitos suggested that adding 20% of linear in the cyclic polymers will make the mixture behavior like the linear chains (Figure 2.21). [57]

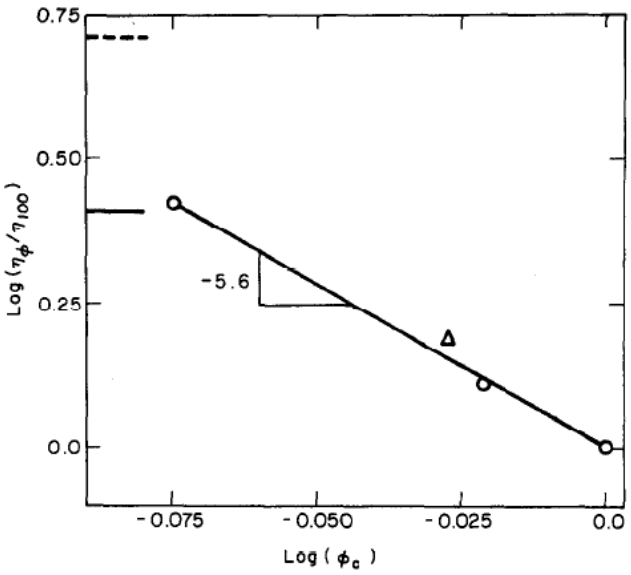

Figure 2.20 Reduced viscosity vs. concentration of cyclic molecules in the mixture of cyclic and linear PS molecules. The broken line and solid line are reduced viscosity for pure linear molecules. Φc is the volume fraction of the polymer rings (After McKenna et al.[46])

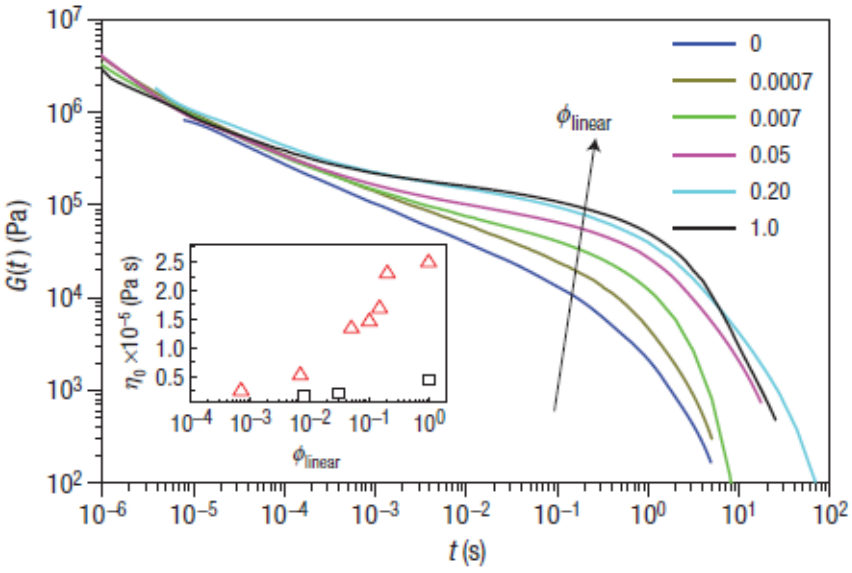

Figure 2.21 The modulus (G(t)) of linear and cyclic PS mixture change with increasing linear chain fractions (after Kapnistos et.al. [57])

McKenna et. al. [46] attribute the phenomenon to the existence of "threading effect", in which the linear chain will penetrate into the cyclic chains and form the structure like rotaxane as shown in Figure 2.17. Computer simulation found the size of the polymer rings will be greatly expanded by the linear chains, and the radius of gyration value will scale the same way as viscosity did in experimental work. [86] Other simulation work further confirms the idea of "threading effect" in the ring/linear mixture. [87-89]

The existence of linear chain contamination is expected to have great influences to the measured properties of polymer rings. To get pure rings, two separation methods have been applied. The first one is called fractional precipitation. [47, 81, 82, 90] This method is to apply the differences between the phase separation behavior of linear and cyclic polymers to separate the rings from linear in dilution solutions. [40] In 1970s, size exclusion chromatography (SEC) was applied to separate the polymer rings and linear chains. As discussed before, the hydrodynamic radius (R_h) of polymer rings is 0.85 smaller than that

of linear chains. As shown in Figure 2.22, the SEC retention time for the linear and cyclic polymers are different, but the differences are not large enough to completely separate the two species. [91, 92]

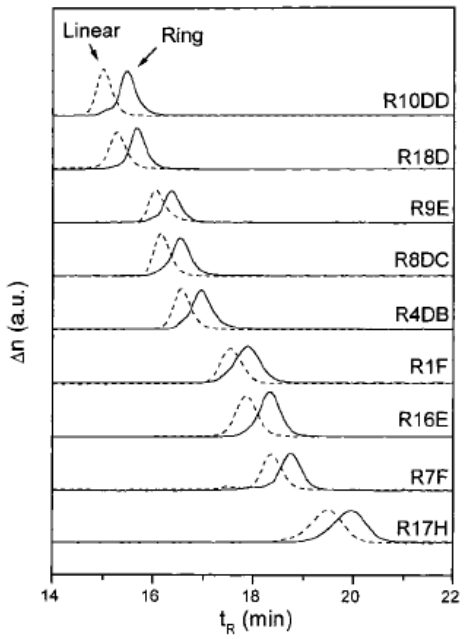

Figure 2.22 SEC chromatograms of cyclic PS (solid line) and corresponding linear precursor (dashed line) (After Lee et. al.[92])

Later it was found that a more efficient way to separate the linear and cyclic polymers was proposed and called as liquid chromatography at critical condition (LCCC). [91, 92]This method is based on Gorbunov and Skvortsov's theoretical work, [93] and the critical condition is defined as the elution time for the linear polymer is the same as the retention time of the solvent. At this critical condition, the elution peaks of linear and cyclic polymers can be well separated (Figure 2.23).

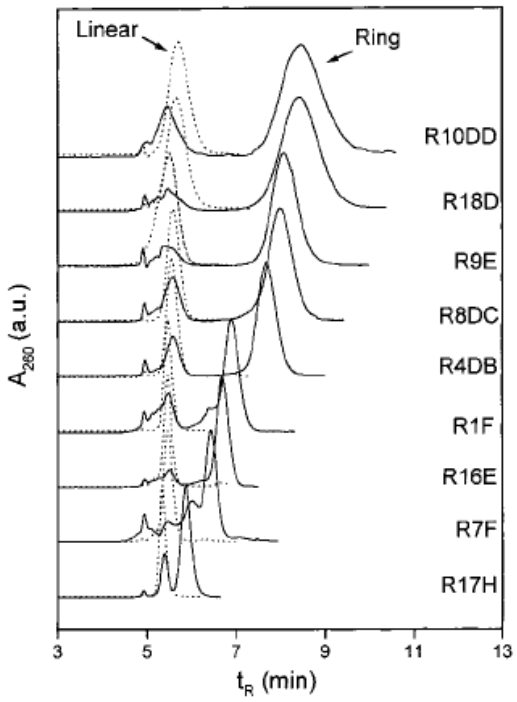

Figure 2.23 LCCC chromatograms of cyclic PSs and corresponding linear precursors at the chromatographic critical condition of linear PS. (After Lee et. al.[92])

Another important problem in synthesizing the macrocyclic polymer is the forming of knotted rings (see Figure 2.17) during the ring closure process. As suggested by computer simulation work, when the molecular weight of the linear chain is higher than 10^5g/mol, nearly 40% of the synthesized rings are knotted rings. [94] These knotted joints will add more constrains to the chain dynamic and the size of knotted rings will be smaller than knot-free rings. [71, 95] If closing two neighbored linear chains together, another interesting ring structure may formed and called as catenated rings (Figure 2.17). Similar as knotted rings, the conformations of catenated rings should be smaller than pure rings of the same molecular weight. The intrinsic viscosities of knotted and catenated rings are smaller than pure rings. As shown in Figure 2.6, at high molecular weight range the slopes of measurement intrinsic viscosities vs molecular weight are smaller than those

at low molecular weight range. This phenomenon should be the symbol of the existence of knotted or cantenated rings. [47]

In summary, linear chain contamination and forming knotted or cantenated rings are two hard to avoid problems during the synthesis of polymer rings using the ring closure methods. A simple way to check the purity of the rings is to check the intrinsic viscosity and compare with their linear competitors. If the g' values is much higher than 2/3, then the rings may get contaminated by linear chains; while if the g' value is much lower, the rings may contain knotted or cantenated structures.

2.3.5.2 Ring expansion metathesis polymerization (REMP) method

In 2002, a new route to synthesize the macrocyclic polymers was developed by Bielawski et. al. [96, 97] in Prof. Grubbs group based on the metathesis polymerization mechanism. The method was first called as "ring opening metathesis polymerization (ROMP)". Later to avoid confusion with normal ring opening polymerization, in which the ring structure on the monomer was opened to form linear polymer structure, the method was named as "ring expansion metathesis polymerization (REMP)".[98-100] As shown in Figure 2.24, the monomer is cyclooctene, an eight-units ring with a single double bond and the special catalyst itself has a ring structure on it. During the reaction, the C=C double bonds on the monomer will couple with the Ru=C bond in the catalyst and form a square like structure. This structure is not stable, it can be split evenly and allow the monomer insert into the ring structure in the catalyst. With repeatable reaction of the monomers with the catalyst, the size of the ring in the catalyst gets expanded and a large polymer ring is formed.

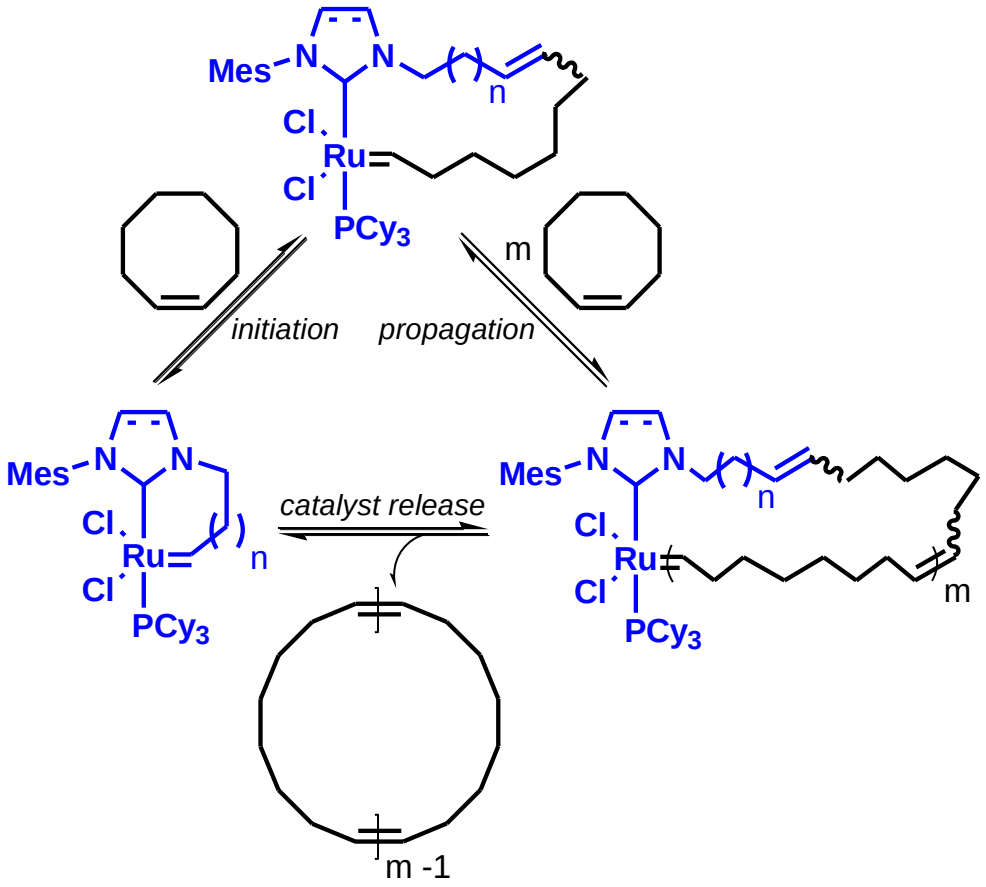

Figure 2.24 Synthesis of cyclic polymers using ring expansion metathesis polymerization (REMP).

The reaction speed for the REMP is fast. Depending on the unit structure of the ring in the catalyst, high conversion of monomer can be achieved within several hours (Figure 2.25). As the monomer conversion is high, the molecular weight of the rings can be simply calculated by the molar mass of monomer multipled by the monomer molecular weight and divided by the molar of catalyst. The molecular weight of the achieved polymer rings is much higher than those from ring closure method which is limited by the possibility of forming knotted rings. However, it is hard to syntheses the ring catalyst and the structure of the ring catalyst is similar as the catalyst used to get the

linear polymers. If there is some linear catalyst contamination, it will break the large rings into linear chains. Thus the catalyst need to be further purified before use.

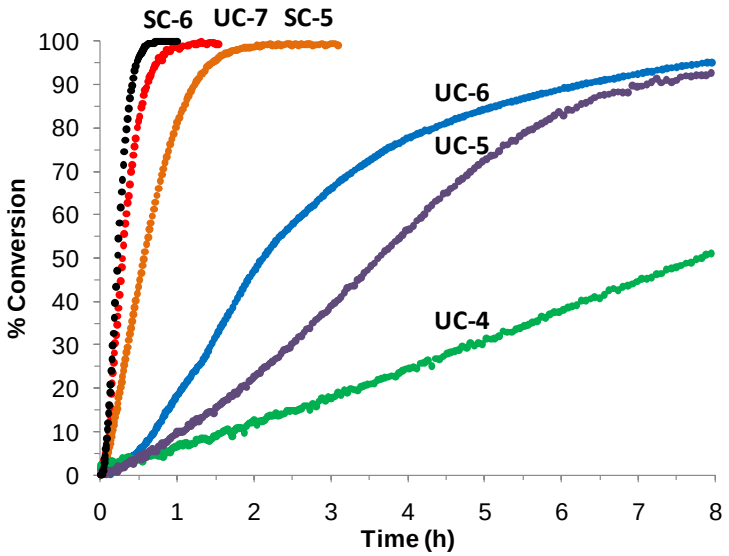

Figure 2.25 Conversion of monomer with time for different REMP catalyst

In first part of this work, the linear viscoelastic properties of several series of high molecular weight cyclic polymers with different structures were studied and compare with their linear competitors. Complex viscosity, flow activation energy, and plateau modulus were obtained from dynamic experiments. Zero-shear rate viscosities were obtained from steady-shear experiments and were used to obtain the viscosity-M_w relationship for this series of samples. To prepare pure macrocyclic polymers, monomers with different unique structures were applied. These monomers were also used to prepare some linear materials to compare with the corresponding polymer rings. The linear polymers with different side chain structures and compositions exhibit unique viscoelastic properties. The second part of this work is to study the influence of side

chain structure and composition to the relaxation behaviors of brush polymer. The experimental data for these brush polymers are compared with theoretical predictions.

Chapter III:
Experiments and data analysis

3.1 Materials

Cyclic polymers with different structure and chemical compositions were synthesized in Prof. Grubbs' lab at the California Institute of Technology (Caltech) using the ring expansion metathesis polymerization (REMP) method as shown in Figure 2.24. The reaction kinetics of a series of catalysts with different ring structures was studied and two catalysts (UC5 and UC6) were used to synthesize the ring polymers in this study. The structures of the ring catalyst are shown in Figure 3.1. Figure 3.2 shows the route for the synthesis of different ring polymers from different monomers and the final product of the ring polymer are name as polyoctenamer (PCO), polyammonium, dendronized and wedge rings. As shown in Figure 3.2, the monomers used to synthesize the ring polymers are all contain some ring structures. The linear samples with the same chemical composition were prepared by the ring opening metathesis polymerization (ROMP) method using the linear catalyst which contains a linear structure connected with Ru=C structure.[101] The polymerization of linear and ring sample was carried out in solution. After reacted for several hours, the reaction system would get "gel up". The polymer materials were filtered out using a filter paper and wash excessively to remove any residual monomers. Then the excess solvent can be removed by putting the polymer gel in vacuum for one week. Some of the samples were further purified by fractional precipitation. The polymers samples were dissolved into dilute solutions. By gradually decreased the temperature, polymer materials with different molecular weight or architecture would come out according to their differences in solubility. Fractions of

samples were collected at different temperature and GPC was used to determine their actual molecular weight. Limited by the amount of catalyst or monomers and other difficulty in preparing samples, in all cases the amount of linear and cyclic samples available for testing was quite limited (~0.3 g).

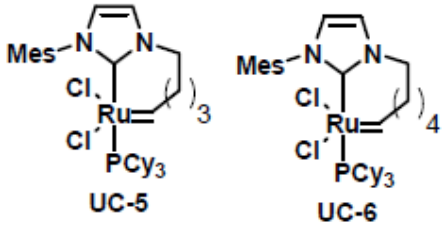

Figure 3.1 Molecular structure of the REMP catalyst

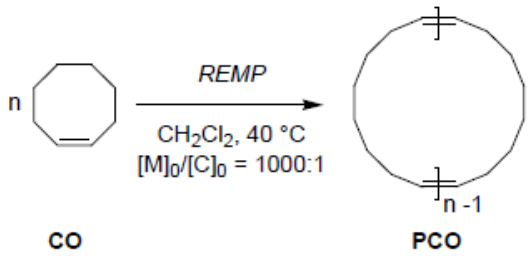

(a) Polyoctenamer (PCO) rings

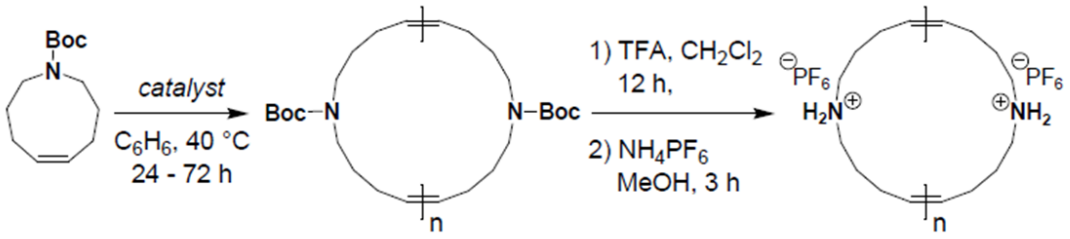

(b) Poly(ammonium) rings

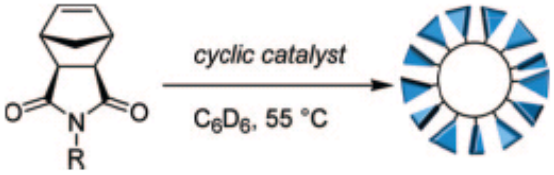

(c) Dendronized rings

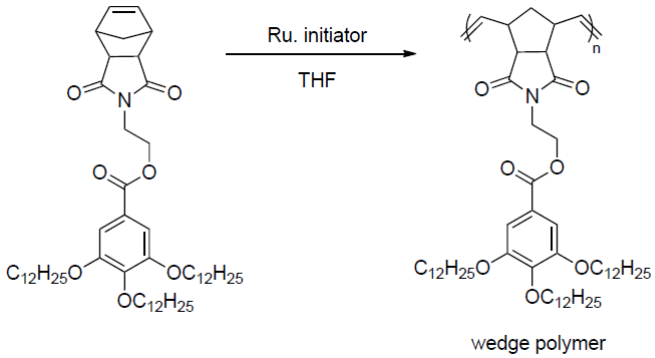

(d) Wedge polymers

Figure 3.2 The monomer and synthesis route for polymer rings with different structures

3.2 GPC-MALLS analysis

The molecular weight of the synthesized samples can be estimated from the ratio of the monomer to the initiator. Detailed information about the polymers like the molecular weight (M_w), intrinsic viscosity ($|\eta|$) and radius of gyration (R_g) can be determined by the GPC. Gel permeation chromatography (GPC) was carried out in THF on two PLgel 10 μm mixed-B LS columns (Polymer Laboratories) connected in series with a DAWN EOS multiangle laser light scattering (MALLS) detector, an Optilab DSP differential refractometer, and a ViscoStar viscometer (all from Wyatt Technology). In this work, no calibration standards were used. As there is little information available for these new polymers, the refraction index (d*n*/d*c*) values for the polymer materials were obtained inline by assuming 100% mass elution from the columns. dn/dc value is an important parameter in determining the Mw for polymer materials using GPC method. Literature [102, 103]study show that for linear polymers in low molecular weight range, the dn/dc values are influenced by the sample molecular weight and follows the equation,

$$\frac{dn}{dc} = \left(\frac{dn}{dc}\right)_m + \frac{K}{M_n} \qquad (3.1)$$

The dn/dc values are influenced by the segmental density change which is strongly affected by the existence of chain ends. For high molecular weight linear chains or polymer rings, the influence of chain ends is minor and the dn/dc value is expected to be a constant. However, the measured dn/dc values in our experiment are different for linear and cyclic samples. To get the accurate the molecular weight information, the dn/dc value for linear chains is used to estimate the molecular weight of polymer rings. [50]

3.3 Rheological measurements

Limited by the amount of samples, the rheological measurements were carried out using an ARG2 (TA instrument) or MCR-501 rheometer (Anton Paar Inc.) with 8mm parallel plate and approximately 1mm gap under nitrogen flow. To avoid any degradation or oxidation during the sample preparation, about 0.03g sample powder was pressed into hard pellet at room temperature. Then the sample pellet was melted on the rheometer and reshape into the desired shape profile. For most samples, the experimental temperature range would cover from the glassy to the flow region of the samples. Only for the PCO samples, limited by their crystallized nature, their viscoelastic properties can only be examined in their melting state. The measured frequency range is 0.01-100 rad/s. The machine compliance was corrected by disabling the software auto correction function and the raw data were corrected using the measured machine compliance value following Hutcheson and McKenna's method. [104] The dynamic responses at different temperature were shifted and constructed the master curve of $G'(\alpha_T\omega)$ and $G''(\alpha_T\omega)$ vs $\alpha_T\omega$ at different reference temperature. The shift factors for both linear and macrocyclic polymers were fitted with the WLF equation. The C_1 and C_2 at this reference temperature

were estimated from the curve fitting and were used to back calculate the isochronal temperature dependence of the G'(ω) and G"(ω) with reference frequency of 0.01Hz. The glass transition temperature for each sample was estimated as the corresponding temperature at the peak of the tan(δ) in the glass transition region. For some samples, the creep experiment was performed with 8mm parallel plate. The experiment was carried out until the sample achieved steady state. The viscosity was measured individually and the steady state recoverable compliance was determined by subtracting viscosity divided by time from the creep compliance .[1]

3.4 Data analysis

3.4.1 Estimation of plateau modulus (G_N^0) and entanglement molecular weight (M_e)

The plateau modulus (G_N^0) is an important parameter in evaluating the viscoelastic properties of polymer materials. According to the tube model,[5] the average molecular weight between entanglements or entanglement molecular weight (M_e) can be directly related with the plateau modulus (G_N^0) with equation,

$$G_N^0 = \frac{4}{5}\frac{\rho RT}{M_e} \qquad (3.2)$$

The number of entanglement per molecule $Z=M/M_e$. The chain relaxation time of the whole molecule can be estimated from the Z and τ_e, where τ_e, is the relaxation time of chain segments between entanglement. For one polymer, the τ_e, or M_e are fixed values, thus the relaxation time will scale with the increase of molecular weight. As entanglement molecular weight is so important in determining the viscoelastic responses of polymer materials, and it can be directly related with plateau modulus, determining the plateau modulus in experiment becomes an important procedure in viscoelastic analysis.

Limited by the condition of the samples or the method to determine the plateau modulus, the experiment values of plateau modulus have around 20% error comparing from model prediction. [105] From dynamic experiment, for mono dispersed samples, as shown in Figure 3.3, the plateau modulus can be directly read from the plateau region in the storage modulus (G') curve.

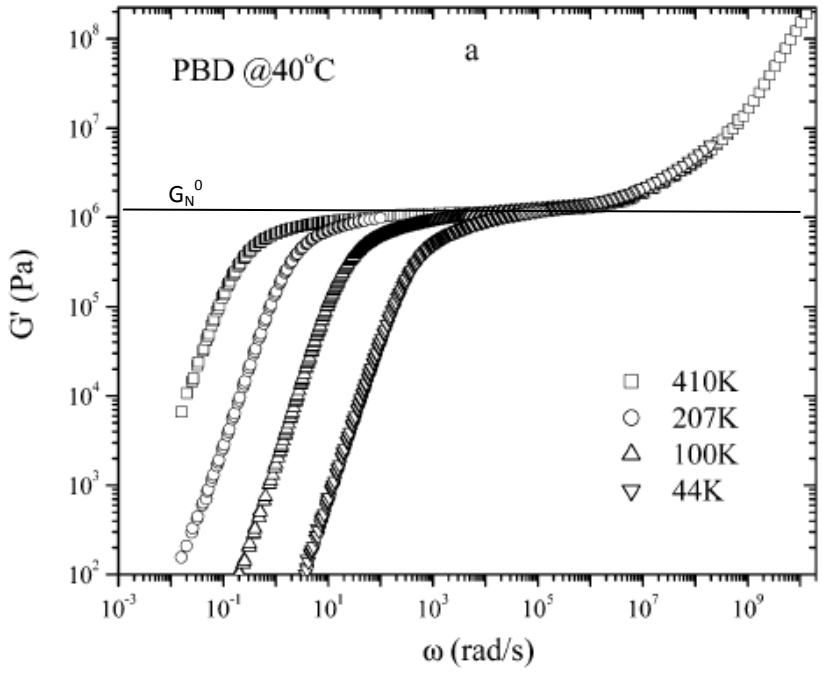

Figure 3.3 Master curve of the storage moduli for a monodisperse long chain polymer. (after Wang et. al.[106])

For polydispersed samples, as shown in Figure 3.4, it is hard to determine a clear plateau to find the plateau modulus in the dynamic curve. Thus several alternative methods may be applied. If a complete dynamic curve can be obtained, then the plateau modulus can be estimated by integrating the loss modulus over the terminal and rubbery region, [1, 107]

$$G_{N,exp}^0 = \frac{2}{\pi}\int_{-\infty}^{+\infty} G''(\omega) d\ln\omega \qquad (3.3)$$

Based on the assumption that the loss peak over the lnω should be symmetric, the above equation can be simplified to another form, [108, 109]

$$G^0_{N,exp} = \frac{4}{\pi}\int_{-\infty}^{\omega_{max}} G"(\omega) d ln\omega \qquad (3.4)$$

Other more empirical methods include finding the plateau modulus at the minimum of tanδ (Figure 3.4). [110] Other method including estimating the plateau modulus by multiplying the corresponding G" value at the maximum of loss modulus (G") with 4.83.

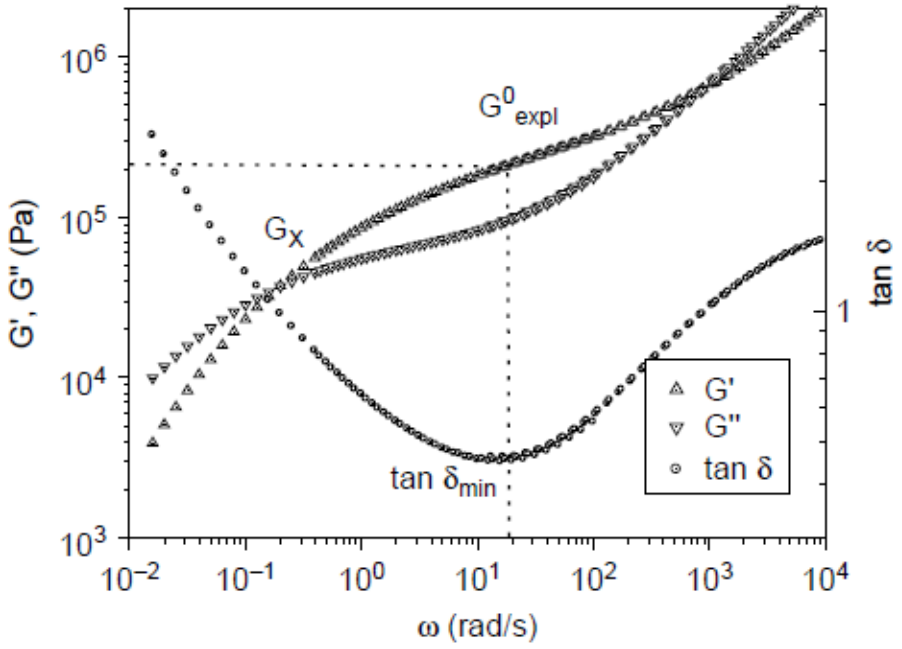

Figure 3.4 Master curve of the storage and loss moduli for a polydisperse polymer. (after Liu et. al. [105])

3.4.2 van Gurp-Palmen plot

Another method to find the plateau modulus is to use the van Gurp-Palmen plot. [105, 111, 112] In this method, the absolute value of the complex modulus |G*| is plotted against the phase angle δ= $\tan^{-1}$(G'/G") or tan(δ). As shown in Figure 3.5a, at the minimum of δ the corresponding |G*| is the plateau modulus of the samples. The shape of the van Gurp-

Palmen plot is very sensitive to the molecular weight distribution, composition and molecular architecture [111, 112]. As shown in Figure 3.5b, in van Gurp-Palmen plot, polymers with different chemical compositions can be overlapped with each other simply by normalizing their complex modulus by their plateau modulus. At the same phase angle (δ), the corresponding complex modulus (|G*|) value will change linearly with their composition or polydispersity change. With these unique features, van Gurp-Palmen plot has gained much popularity in rheology.

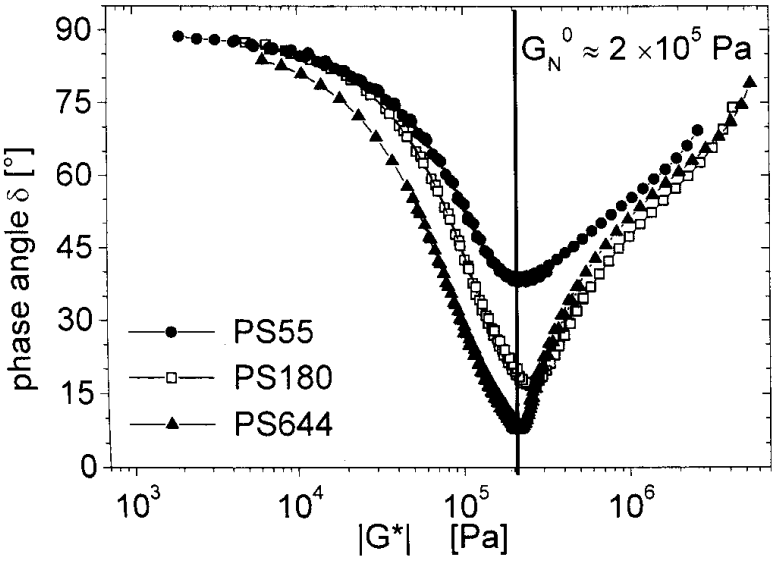

(a)

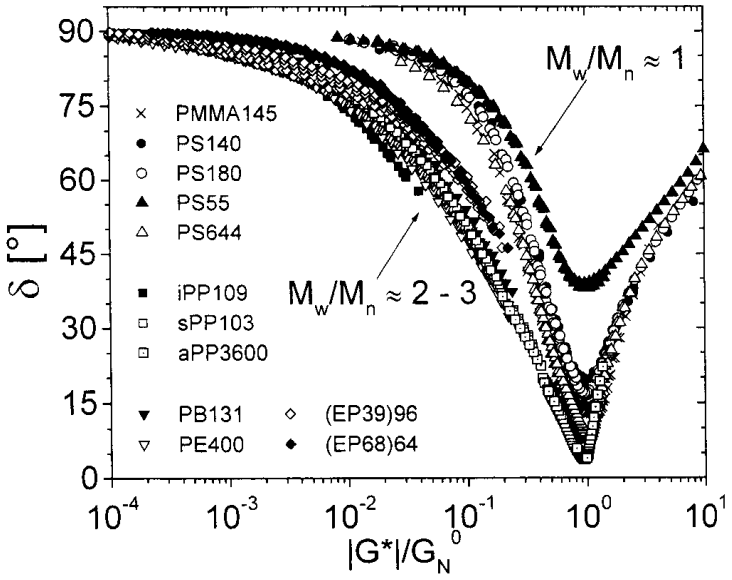

(b)

Figure 3.5 Van Gurp-Palmen plot of polystyrene with different molecular weight(a) and polymers with different chemical composition or polydispersity (after Trinkle et. al. [111])

3.4.3 Estimate the glass transition temperature (T_g) and fragility (m)

As discussed before, the shift factors with reference temperature at 80°C, which curve is in the middle of the rubbery region, were fitted with the WLF equation.[113]

$$\log(a_T) = \frac{-C_1(T-T_{ref})}{C_2+T-T_{ref}} \qquad (3.5)$$

The C_1 and C_2 at this reference temperature (T_{ref}) were estimated from the curve fitting. According to the principle of time (frequency)-temperature superposition, the temperature dependence of the G' (ω) and G"(ω) (G' (ω) and G"(ω) vs T) at the frequency of ω=0.01Hz (τ=1/ω) was converted from the dynamic master curve (G' (ω) and G"(ω) vs ω) with the WLF equation and used to determine the glass transition temperature (T_g) for the relaxation time of 100 seconds. T_g was estimated from the peak of the tan(δ) curve in the dynamic modulus thermal spectrum. We fit the shift factors with the WLF equation at the reference temperature set to T_g to estimate the C_1^g and C_2^g.

The fragility (m) [114-116] and apparent activation energy (E_g) of the brush samples were estimated with equations, [117, 118]

$$m = \frac{C_1^g T_g}{C_2^g} \quad (3.6)$$

$$E_g = ln10R\frac{C_1^g}{C_2^g}T_g^2 \quad (3.7)$$

3.4.4 Retardation spectrum

According to Plazek, [119, 120] retardation spectrum (L(τ)) is a very useful tool to examine the relaxation behavior of polymer chains. Retardation spectrum can be calculated from the stress relaxation modulus, dynamic results or creep data. According to Ferry, the relaxation spectrum (H(τ)) can be estimated from the relaxation modulus with equation,

$$H(\tau) = -M(m)G(t)dlog(G(t)/dlog(t)|_{t=\tau} \quad (3.8)$$

The retardation spectrum (L(τ)) can be obtained from H(τ) and G(t) with equation,

$$L(\tau) = \frac{H(\tau)}{\{G(t)+H(\tau)\left[\frac{\pi}{2}\left(csc\frac{m\pi}{2}-sec\frac{m\pi}{2}\right)-\Gamma(m)+1.37\right]\}^2+\pi^2H^2} \quad (3.9)$$

To calculate the retardation spectrum (L(τ)) from the dynamic data, the relaxation spectrum(H(τ)) was first estimated from the storage modulus (G') with the equation, [1]

, for m<1,

$$H(\tau) = AG'dlogG'/dlog\omega|_{1/\omega=\tau} \quad (3.10)$$

$$A = \frac{\sin(m\pi/2)}{m\pi/2} \quad (3.11)$$

,for 1<m<2,

$$H(\tau) = A'\,G'(2 - dlogG'/dlog\omega)|_{1/\omega=\tau} \quad (3.12)$$

$$A = \frac{\sin(m\pi/2)}{\pi(1-m/2)} \quad (3.13)$$

Then L(τ) was calculated from the H(τ) and the dynamic data with equation,

$$L(\tau) = \frac{H(\tau)}{[G'(1/\tau) - G''(1/\tau) + 1.37H(\tau)]^2 + \pi^2 H^2(\tau)} \qquad (3.14)$$

The retardation spectrum ($L(\tau)$) can also be directly estimated from the creep data, [1]

$$L(\tau) = M(-m)\left[J(t) - \frac{t}{\eta_0}\right] dlog\left[J(t) - \frac{t}{\eta_0}\right] / dlog(t)|_{t=\tau} \qquad (3.15)$$

As our creep experiment are perform at the temperature much higher than the glass transition temperature (T_g). Limited by the instrument response time, the creep data did not give much information about the glassy responses. If we want to get the retardation spectrum ($L(\tau)$) curves covering the whole range, we need to combine the results from both the dynamic and the creep methods.

Chapter IV:
Viscoelastic properties of polymer rings with different structure or composition

4.1 Polyoctenamer (PCO) rings

Our first attempt to study the viscoelastic properties of macrocyclic polymers was to examine the rheological responses of linear and cyclic polyoctenamer (PCO) samples. Octenamer monomer is an eight unit ring with one double bond on it. The double bond can react with the double bond linked with the Ru in the metathesis catalyst and insert into the ring of the REMP catalyst. Two series of cyclic PCO samples using two catalysts (UC5 and UC6) were synthesized following the REMP method and the linear PCO samples were prepared by the ROMP method.

4.1.1 The molecular information for linear and cyclic PCO

The molecular weights of the linear and cyclic PCO samples were determined by the GPC-MALLS by setting the dn/dc value to be 0.1 ml/g. The molecular weight, intrinsic viscosity and radius of gyration of linear and cyclic PCOs are listed in Table 4.1. As shown in the table, the polydispersity index (PDI) for the most of the samples are less than 1.5. For macrocyclic samples, with decreasing molecular weight the PDI value increase. This is because of the reaction kinetic of the REMP reaction. The catalyst used for the REMP reaction have a very high reaction speed, with a small amount of catalyst, the monomer can reach a very high conversion ratio at a short time. To get low molecular weight samples, excess catalyst is needed. The role of the excess catalyst is to react with the double bonds on the macrocyclic polymers and break the large rings into small ones. As the “cleave” reaction is random and it is hard to control the size of the small rings, the

PDI for the low molecular weight rings would be larger than that of high molecular weight rings. [98, 99]

If compare the PDI for the macrocyclic polymers made from catalyst UC6 and UC5, the PDI of samples made from catalyst UC5 is narrower than those made from catalyst UC6. As shown in Figure 2.24, reaction kinetic study shows that catalyst UC5 has a slower reaction speed, which will help to better control the molecular weight and PDI. [98, 99] Fractional precipitation can help to further purify the linear and cyclic samples and narrow their polydispersity. Limited by the amount of raw materials, only some of the samples are further purified. The PDI for these further purified samples are around 1.1. The solution and viscoelastic properties of these further purified samples were compared with those unpurified ones.

Table 4.1 Molecular information for linear and cyclic PCO from GPC-MALLS

	M_n (kg/mol)	M_w (kg/mol)	PDI	M_{p1}[a] (kg/mol)	M_{p2}[a] (kg/mol)	$\|\eta\|$ (ml/g)	$\|\eta\|_a$[b] (ml/g)	R_g (nm)	R_{ga}[b] (nm)
Cyclic PCO prepared by catalyst UC6									
CPCO2	228	307	1.3	279	95.4	278	230	34.9	36.7
CPCO4	80	129	1.6	117	22.6	142	101	20.8	24.7
CPCO6fxn1[c]	59	68	1.2	63.4		102		14.8	
CPCO6	60	90	1.5	91	50.1	113	46.5	16.3	12.6
CPCO8	187	302	1.6	300	62.8	267	174	36.6	40
C72	187.1	223.6	1.2	220				32.2	
Cyclic PCO samples prepared by catalyst UC5									
B241	197	242	1.3	256				39	
B292	157	210	1.3	227	74			34.6	40.3
B283	56	118	2.1	113	15.8			26.1	35
B288	153	232	1.5	247	55			34.3	41.8
C87	398.6	490	1.2	465				45.4	45.6
C89	119.4	167.3	1.4	153					
C94	365.5	482.4	1.3	539	165			50.1	53.9
Linear PCO samples									
1031	32	54	1.7	50		62.9		12.5	
213	131	172	1.3	146		185		22.7	
917	149	200	1.4	175.7				20	
1019	38	116	3.1	112		128	54.3	19.4	21.1
128	91	125	1.4	107		157.6		18.8	
330fxn2 [c]	165	184	1.1	165		218		23.9	
128fxn1 [c]	131	146	1.1	129				22.6	
B99fxn1 [c]	375	410	1.1	352				42.1	

* a- M_{p1} and M_{p2} represent the sample molecular weight determined at the first and second peak of the GPC curve; b- the $|\eta|$ and R_g are determined by including both peaks in the GPC curves; c- these samples were prepared by the fractional precipitation.

Figure 4.1 shows the GPC curves for cyclic PCO and linear PCO samples. If compare the fractionated cyclic samples (Figure 4.1b) with those unfractionated cyclic samples (Figure 4.1a,c), The GPC curves for those fractionated samples are much narrower. For some unknown reasons, the unfractionated cyclic samples contain some low molecular weight factions which come out of the tube at longer retention time. To further study the influence of these low molecular weight fractions to the material, the molecular weight at each peak point (M_{p1} and M_{p2}) were estimated from the GPC curve.

The molecular weight, intrinsic viscosity (|η|) and mean square of radius of gyration (R_g) were determined using the peak range between the two black lines. If changing the range of the peak to be analyzed, the |η| and (R_g) values would be affected. The molecular weight results for the first and second peak M_{p1} and M_{p2}, the intrinsic viscosity (|η|) and radius of gyration (R_g) values with and without including the low molecular weight fractions are shown in Table 4.1. As shown in the table, if we include the low molecular weight portion into the calculation of the intrinsic viscosity (|η|) of the polymers, the |η| would be lowered. If compare the molecular weight of the low molecular weight portion prepared by the two catalysts, for samples with near molecular weight, the molecular weight of the low molecular portion from catalyst UC6 is higher than that from catalyst UC5.

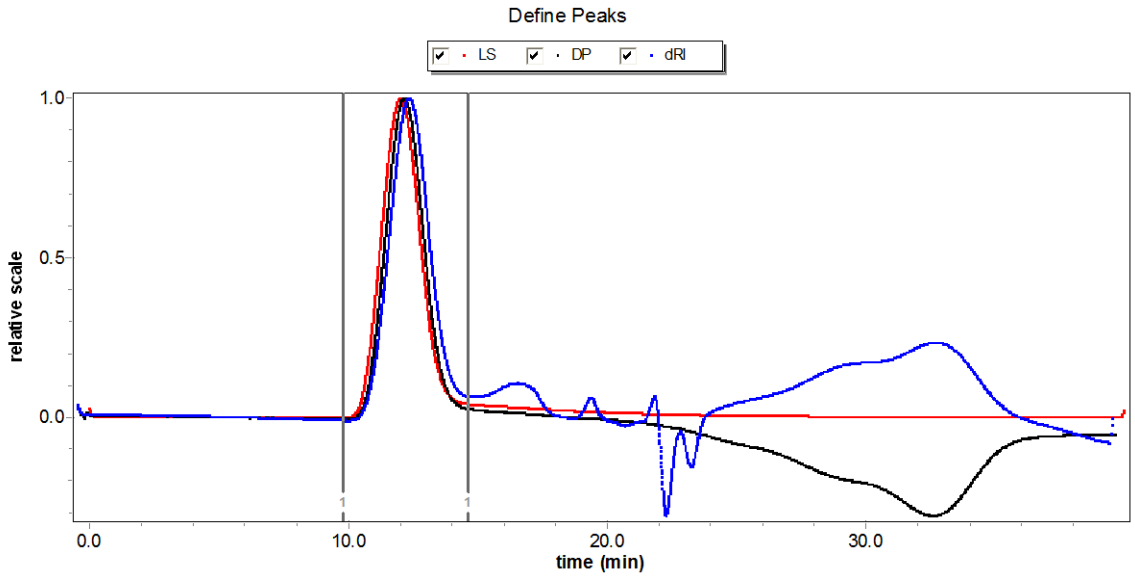

(a) cyclic PCO from catalyst UC6 (CPCO2 Mw=307kg/mol)

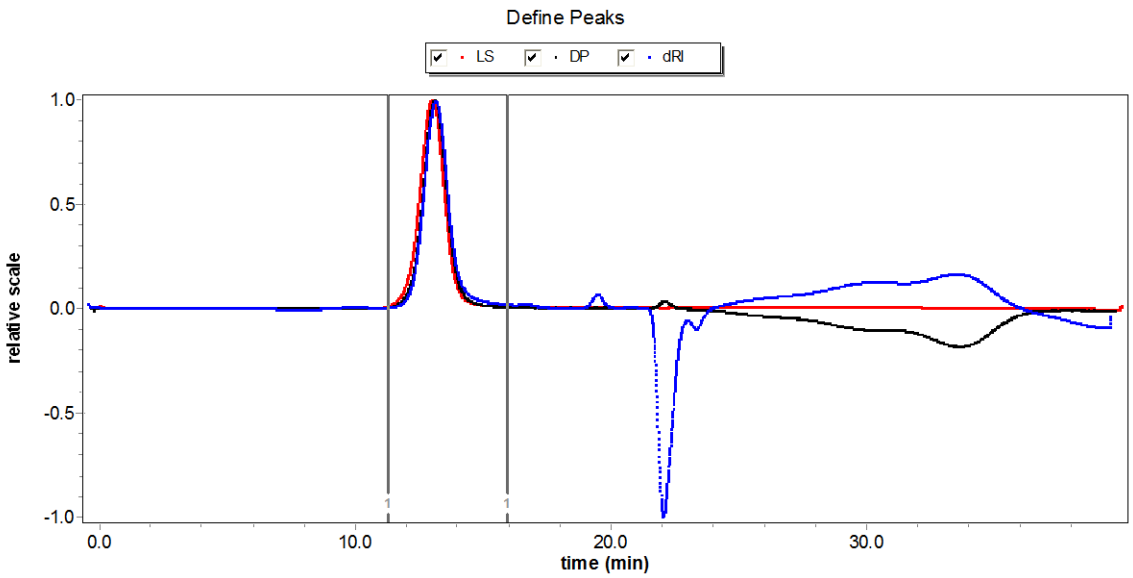

(b) fractionated cyclic PCO (CPCO6fxn1 Mw=68kg/mol)

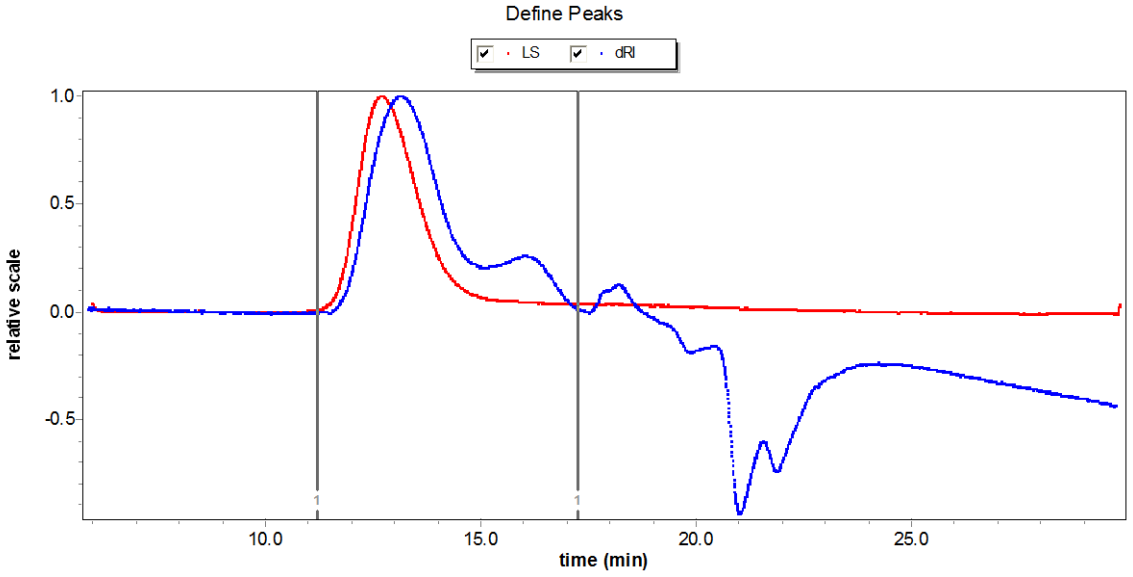

(c) cyclic PCO from catalyst UC5 (B288 Mw=232kg/mol)

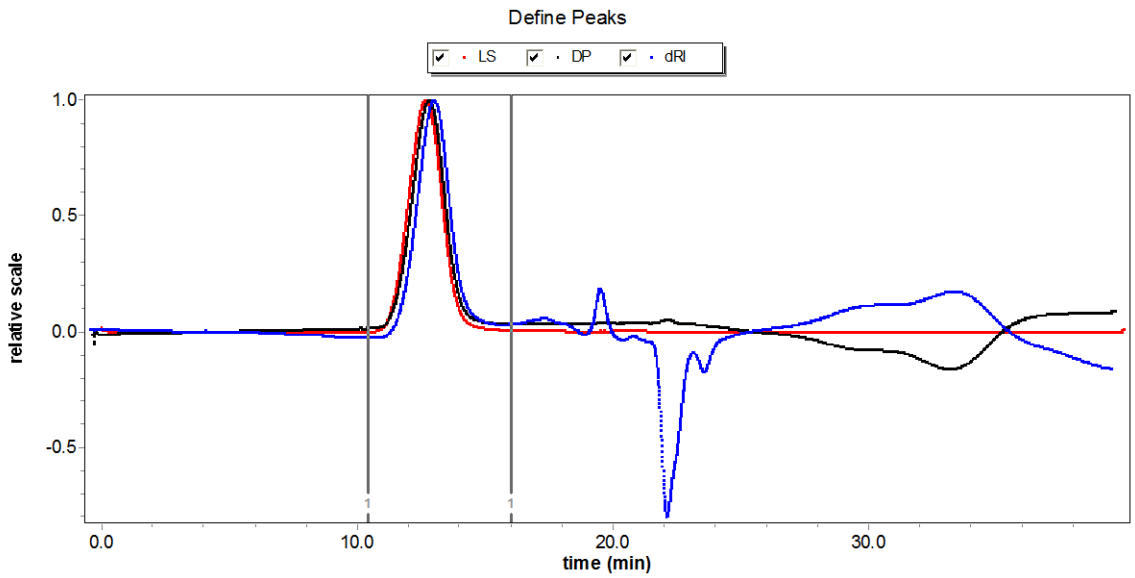

(d)Linear PCO (LPCO 218 Mw=153kg/mol)

Figure 4,1 The GPC-MALLS curve for cyclic (a,b,c) and linear (d,e) PCO samples

4.1.2 Dilute solution properties of linear and cyclic PCO

Figure 4.2 show the radius of gyration (R_g) of both linear and cyclic PCO in THF solution at room temperature. In this plot it can be found that the R_g values for the cyclic PCOs are all higher than the linear samples with the same molecular weight. Literature expectation and previous experiment results indicated that the R_g of the cyclic samples should be half of the linear sample with the same molecular weight. [40, 50] The much larger R_g values for the PCO rings could because of the linear contamination, which would cause the "thread effect" and increase the intrinsic viscosity the mixture.[47] The R_g results for the linear and cyclic PCOs indicated that the macrocyclic samples prepared by the REMP method were not pure rings. If there is linear chain contamination, from the reaction kinetic study, the high molecular weight rings should be cleaner than those of low molecular weight ones. [98, 99] Experimental data shows that the cyclic catalyst UC5 is easier to control which should help to get good rings. [98] However, in this work, the R_g of PCO samples prepared by the catalyst UC6 is more near to the R_g values of linear PCOs,

while for the cyclic PCOs made from catalyst UC5, the R_g is much higher. If we checks the individual data, for cyclic PCOs prepared by catalyst UC6, the R_g of the higher molecular weight samples deviate more from the linear samples than those low molecular weight ones. While for samples from UC5, the R_g of high molecular weight samples are more close to the linear ones. The origin of this interesting phenomenon needs further investigation.

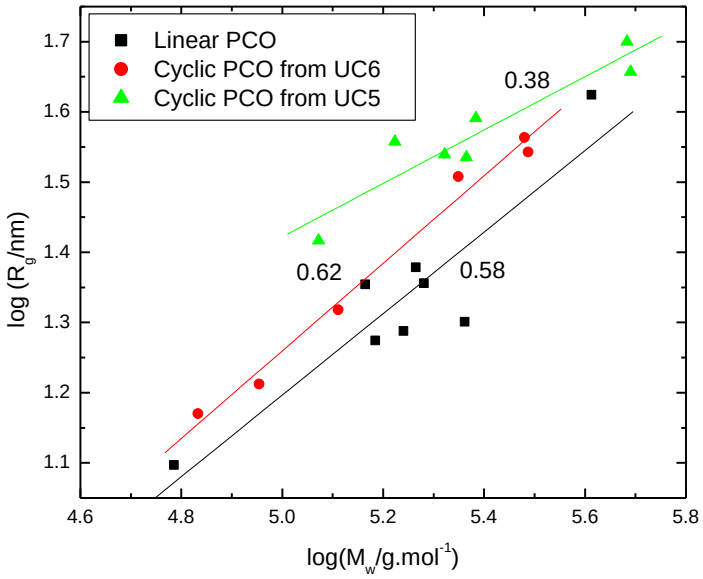

Figure 4.2 the radius of gyration of linear and cyclic PCO samples in THF at room temperature

4.1.3 Viscoelastic properties of linear and cyclic PCO

4.1.3.1 Influence of chemical hydrogenation to the chemical structure

The original idea of this project is to study the viscoelastic properties of macrocyclic polyethylene (PE). The chemical structure of PCO samples is similar to PE except there are some unsaturated double bonds on the PCO samples. The cyclic PE can be prepared by hydrogenating the cyclic PCO samples. Usually there are two ways to hydrogenate the unsaturated bonds. One is the catalyzed way, in which unsaturated bonds are

hydrogenated by Pd catalyst absorbed on activated carbon in a high pressure chamber full of hydrogen gas. [121] This way may take a long time and it's hard to get rid of the carbon contamination from the final product. The other way is a chemical way, which can be performed at normal pressure with simple devices.[101, 122-124] In this method diamide (NH_2-NH_2) is generated, and then it will react with the unsaturated double bonds and hydrogenate them. The cyclic PE can be prepared from the chemical hydrogenation of the cyclic PCO. However when we compared the viscoelastic responses of the PCO sample and its hydrogenation products from the two methods, it was found that the chemical hydrogenation did not work as well as it is expected.

Hydrogenation of an unsaturated polymer can affect some of its physical properties, but it will not greatly affect the molecular structure, which determined the relaxation behavior of a polymer molecule. Thus, the damping factor or tan(δ) for PCO samples before and after the hydrogenation should be similar around the same physical state range. This curve can be used to evaluate whether the molecular structure of chain changed or not. The graph below is the damping factor vs angular frequency for the linear PCO and its hydrogenation products around their flow region. For a linear polymer with narrow PDI, after the crossover its tan (δ) value should keep increasing with the decreasing of frequency. However as shown in Figure 4.3, there is a minor shoulder in the tan(δ) curve. It is assumed that in the polymerization of linear PCO some extra structures may be generated during the "Secondary metathesis".[125] Thus in its tan δ curve, the small shoulder indicate the contamination of other molecular structures. For the PE sample prepared by hydrogenated with Pd catalyst at high pressure, its tan(δ) curve is similar as that for the original PCO sample. However, for the PE prepared by the chemical

hydrogenation, the tan(δ) curve is quite different from that of the original PCO which means some extra structures like branching is formed during the hydrogenation process. Limited by the experimental conditions for hydrogenating the PCO at high pressure, in this study the linear and cyclic PCO samples are carefully examined in well protected nitrogen environment. Their rheological responses are compared with the viscoelastic properties of large PCO rings.

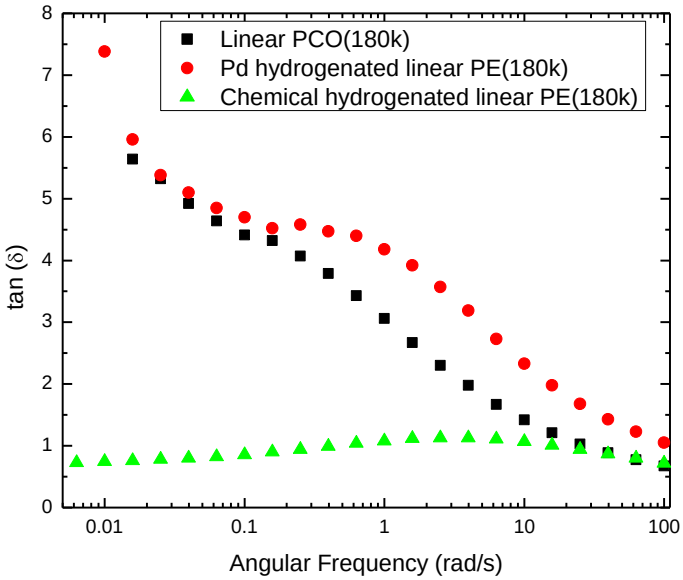

Figure 4.3 The damping factor (tan(δ)) vs angular frequency for hydrogenated and unhydrogenated PCO samples

4.1.3.2 Dynamic responses of linear and cyclic PCOs

The dynamic responses of linear and cyclic PCOs prepared by different catalyst are shown in Figure 4.4. The PCO samples are semi crystallized polymers. The melting temperature is around 67°C. [126] Thus in the dynamic test, the temperature is set as 80°C. As shown in the figures, at this temperature most of the PCO samples are in their flow state. Only for the high molecular weight samples, they show part of the rubbery region in their dynamic responses. If the samples are pure samples, after the crossover of the

storage modulus (G') and loss modulus (G") curve, the slope on the double log plot of G' and G" vs angular frequency should be 1 and 2. [1] From the dynamic curve, the high molecular weight sample CPCO2 looks quite "clean". However, in Figure 4.4 for most of the linear and cyclic samples, after the crossover most of the samples didn't exhibit the terminal flow behavior as expected. Especially for those low molecular weight samples, obviously there are some long time relaxation exist after the crossover point. Fractionating the samples can help but cannot totally remove these contaminations (compare Figure 4.4 (b) and (c), or Figure 4.4 (e) and (f)).

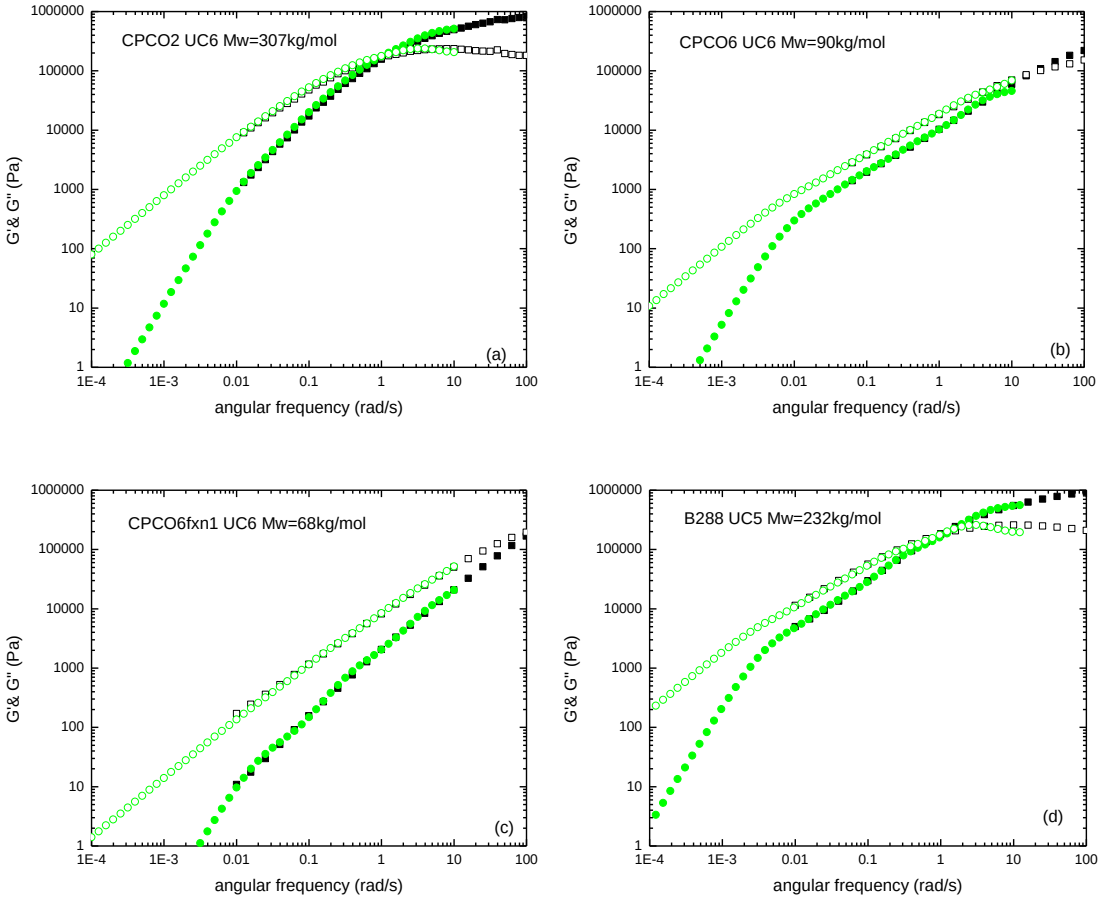

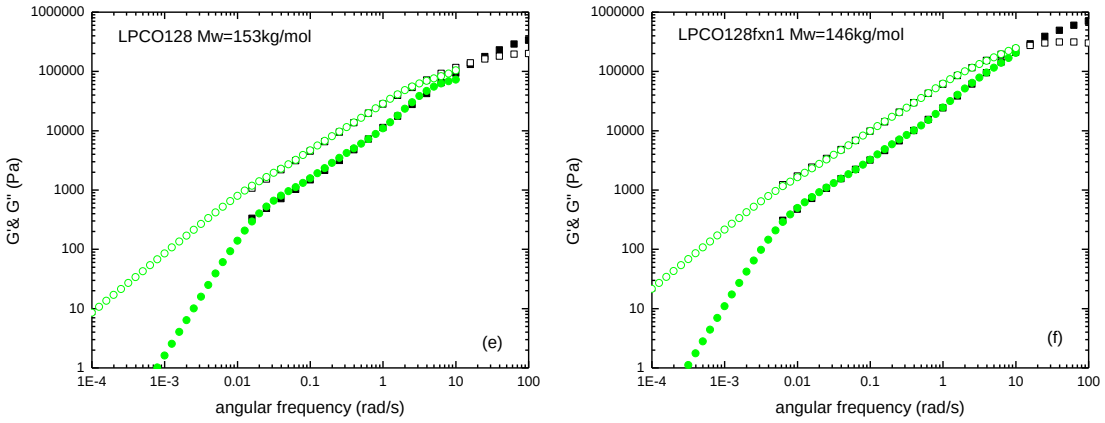

Figure 4.4 The measured (black) and the creep data converted (green) dynamic responses of linear and cyclic PCO at 80°C. ((a) and (b) are cyclic PCO prepared by catalyst UC6, (c) is the fractionated sample of (b), (d) is cyclic PCO prepared by catalyst UC5, (e) and (f) are linear PCOs and (f) is fractionated from (e))

Figure 4.5 compares the dynamic response of cyclic and linear PCOs with the near molecular weight. The rubbery plateau modulus (G_N^0) can be estimated from the G' plot of the highest molecular weight samples for each kind (Figure 4.5a). As shown in the plot, the rubbery plateau modulus of linear sample is higher than the cyclic samples. The result is similar as what has been found before.[48, 56] For those low molecular weight samples (Figure 4.5b and c), the values of G' and G" for cyclic PCOs from catalyst UC5 are higher than the linear and cyclic samples from UC6. The cyclic samples from catalyst UC5 should contain some structure which gives a much higher modulus and need more time to relax. Thus it can be expected that the zero shear viscosity of cyclic PCOs from UC5 should be higher than the linear PCOs and the cyclic PCOs from catalyst UC6.

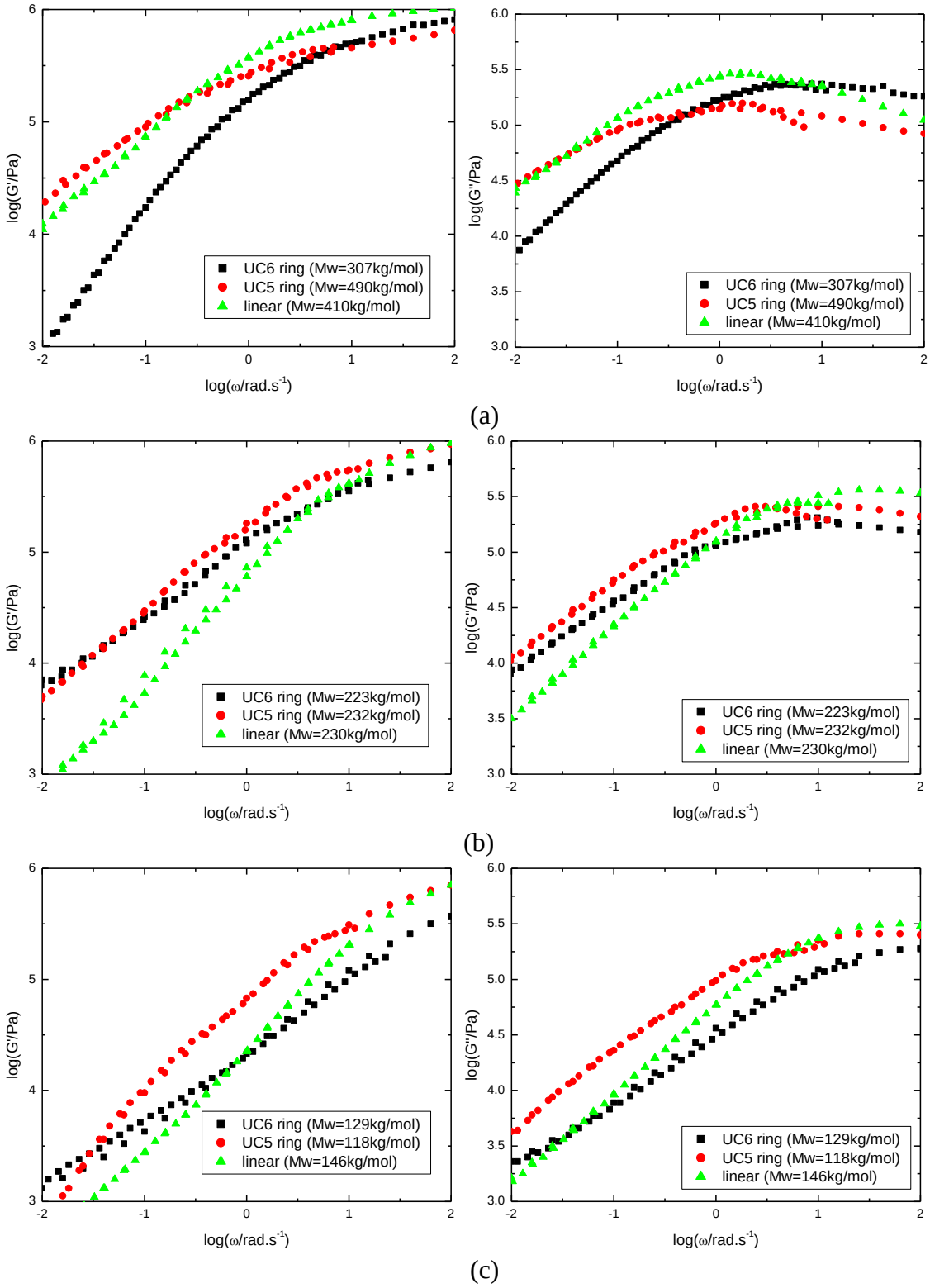

Figure 4.5 Compare the dynamic responses of linear and cyclic PCOs with near molecular weight.

4.1.3.3 The rubbery plateau modulus (G_N^0) of linear and cyclic PCOs

There are various ways to determine the rubbery plateau modulus from the dynamic data. However for our experiment, limited by the temperature range, most of the dynamic curves only cover part of the rubbery region. Only for those high molecular weight samples, they showed some sign of reaching the maximum in the loss modulus curve. The plateau moduli of the linear and cyclic PCOs are estimated with the equation (3.4) using the dynamic data of those high molecular samples. The calculated average values of the plateau modulus are listed in Table 4.2. The density of PCO is around 0.91g/ml. With equation (3.2), the entanglement molecular weight of the PCO are estimated and listed in Table 4.2. Similar as what has been found by McKenna [48]and Roovers [56], the plateau modulus for the cyclic polymers are lower than that of linear PCOs. The ratio is about 0.75 which is higher than what has been found in previous work.

Table 4.2 The plateau modulus (G_N^0) and entanglement molecular weight (M_e) for linear and cyclic PCOs

	Linear PCO	Cyclic PCO from UC6	Cyclic PCO from UC5
Plateau modulus (G_N^0) (Pa)	$1.15*10^6$	$0.81*10^6$	$0.7*10^6$
Entanglement molecular weight (M_e) (kg/mol)	2320	3300	3820

van Gurp-Palmen plot is a very useful way to determine and compare the rubbery plateau modulus of polymer materials. Figure 4.6 shows the van Gurp-Palmen plot of three random choose linear and cyclic PCOs with different molecular weight. If extrapolate the curve to lower tan(δ) values, the plateau modulus of the cyclic PCOs are lower than that of the linear chains. The plateau modulus estimated with the van Gurp-Palmen plot for those high molecular weight samples matches well with our integrated

results using equation (3.4). However, if examine the detailed distribution of the three curves with different molecular weight for each group of samples, the extrapolated plateau modulus and the curve shapes are different. As shown in Table 4.1, most of the linear and cyclic samples have a comparable narrow polydispersity. Theoretically for materials with the same chemical structure their curves in the van Gurp-Palmen plot should overlap with each other. However for our data, the linear PCOs can match with each other well. While for the cyclic PCOs prepared by different catalyst, the shape of their low molecular weight and high molecular weight curves are quite different. As the van Gurp-Palmen plot is very sensitive to the structure or composition change, it can be assumed that either the structure or the composition change during the polymerization process to gain low molecular weight cyclic samples.

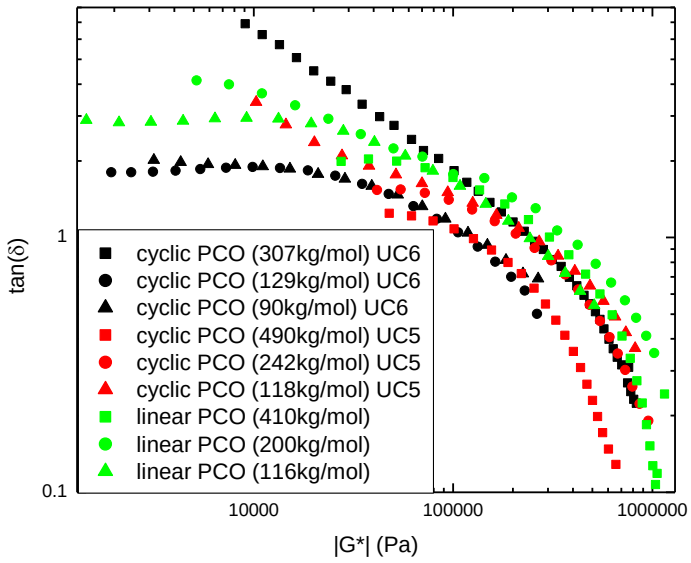

Figure 4.6 The van Gurp-Palmen plot for linear (green), cyclic PCO from UC6 (black) and cyclic PCO from UC5 with different molecular weight.

4.1.3.4 The zero shear viscosity for linear and cyclic PCOs

Figure 4.7 are the zero shear viscosity (η_0) of linear and cyclic PCOs with different molecular weight. Similar as what has been found previously section on the radius of gyration, the zero shear viscosity for the cyclic polymers are higher than their linear competitors and the cyclic polymers prepared by catalyst UC5 gave an even higher viscosity. The results are quite different from theoretical predictions [67, 70, 73, 74] and previous experiment results [40, 47, 56].

The viscosities of the linear chains increase following the 3.4 power law. While the cyclic chains only follow the 2 or 2.7 power law of zero shear viscosity vs molecular weight, the value is near to the predicted value of 2.5 based on the "lattice animal" model. The zero shear viscosity for the large molecular weight cyclic samples can be fitted together with the linear samples by one. However as the molecular weight get lower; the data start to deviate from the linear line. As discussed before, the catalyst can fast initiate the polymerization process and get high molecular weight cyclic samples. To get low molecular weight samples, extra catalyst is needed to chop the large ring into small rings. Thus the low molecular weight samples should have a much wider polydispersity than those of high molecular one. If something happened during the polymerization process, the rings with large molecular weight should be purer than those of low molecular ones. The differences between the two catalysts are their reaction speed. As shown in Figure 2.25, catalyst UC6 reacts faster than UC5. Thus the high molecular weight samples obtained with catalyst UC6 should be better. Using catalyst UC5, the reaction should be easier to control and the property of low molecular weight rings should be better. As listed in Table 4.1, the polydispersity of cyclic polymer for catalyst UC6 and UC5 fit well with the predictions. Then the question is why the better low molecular weight rings

(rings from UC5) gives an even higher viscosity than those bad rings (ring from UC6) of similar molecular weight. Similarly the viscosity of better high molecular rings (rings from UC6) is just near and slightly lower than the linear PCOs, while the high molecular weight rings from UC5 fall onto the prediction line for linear PCOs. One possible explanation for this phenomenon is there might be linear chain contamination is the samples. As discussed before, with the existence of a small amount of linear chains, due to the threading effect, the viscosity of the rings will increase following the 5.6 power law.[46] When the amount of linear chain reaches 20%, there should be no differences between the linear chain and the linear/ring mixture. [57] Based on these literature results, one assumption can be made. It is high possible that we got linear chain contamination in our cyclic samples especially for the low molecular rings. The viscosity for the low molecular rings from UC5 is higher may because they have comparable small amount of contamination and the threading effect is still very strong. While the high molecular weight rings from UC6 (CPCO2 M_w=208kg/mol), it should be the best ring we got in this work for PCO samples. The zero shear viscosity of this sample is about 0.4 of the linear chains with near molecular weight. The value is higher than what Roovers has found in this work with Polybutadiene. [56]

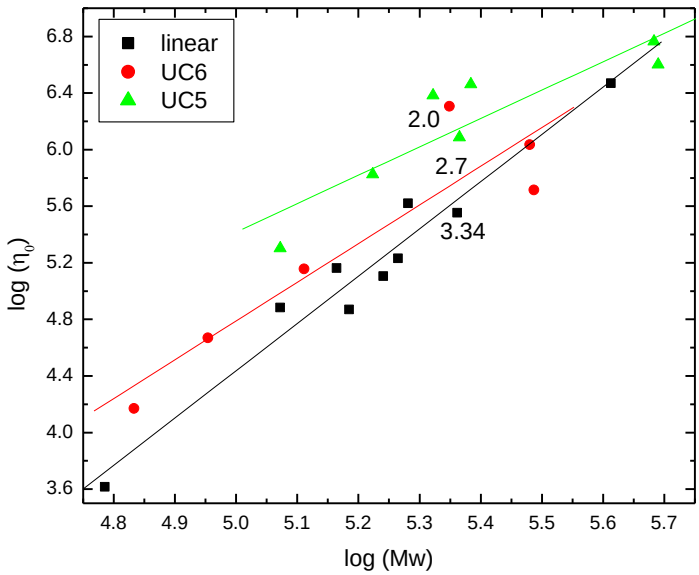

Figure 4.7 Plot of the zero shear viscosity (η_0) against weight average molecular weight (M_w) for linear and cyclic PCOs from different catalyst

4.1.4 Conclusion

In summary, two series of cyclic polyoctenamer (PCO) samples were synthesized using the REMP method with two catalysts with different structures. For some unknown reasons, the radius of gyration (R_g) values for the cyclic PCOs are higher than the linear ones. Limited by the crystallization nature of PCO, the dynamic curves only cover the flow and part of the rubbery region. For most samples, after the crossover of storage (G') and loss (G") modulus curve, the samples didn't get into the terminal flow region as expected for pure samples. Most of the cyclic samples exhibit the existence of some long time relaxation mechanism. Based on the analysis with the zero shear viscosity, it can be assumed that the cyclic samples may get contaminated with linear chains. The viscosity of the best cyclic sample is around 0.4 of the linear ones.

4.2 Poly(ammonium) rings

To study the exact composition of the ring material synthesized via the REMP method and try to get purified ring, another series of cyclic polymer, cyclic poly(ammonium), were studied. Similar as the cyclic polyoctenamer samples, there is no linear poly(ammonium) available. To compare the viscoelastic response of linear and cyclic poly(ammonium), linear poly(ammonium)s were synthesized. The poly(ammonium) samples will not crystallize, thus a more complete dynamic master curve can be constructed via the time temperature superposition (TTS). The plateau modulus can be estimated more accurately at the minimum point of tan(δ) in the van Gurp-Palmen plot.

4.2.1 Examine the purity of the cyclic sample

Following the discussion in previous section on cyclic PCOs, the cyclic samples may get contaminated by the linear chains. Based on the reaction mechanism, if there is any linear chain contamination, the double bond on the linear chain will react with the ring on the catalyst and break the ring into linear chain. This reaction will generate a large amount of linear chains in the final product. In previous study on the PCOs, the catalysts are further purified to remove the possible contamination of the linear catalyst. But the viscosity of cyclic PCO samples still show the sign of much linear chain contamination. Then there should be other reason which leads to the linear chain contamination. Our collaborator AJ Boydston did more studies on the reaction mechanism of the REMP reaction. [98] Two possible source of the linear chain contamination were found. One is the catalyst incorporation and decomposition. As shown in Figure 2.24, the cyclic monomers insert into the ring in the catalyst to form

large polymer rings. When the reaction is complete, the catalyst should be release from the polymer to form stable rings. However, if the catalyst is hard to release from the polymer ring, with longer reaction time the polymer ring will break up into linear chains (Figure 4.8). Reaction kinetics study has shown that the REMP catalyst with smaller ring release quicker than the ones with large rings. For the two catalyst used in the CPCO study, catalyst UC5 should be better to avoid the side reaction which will generate linear chain contamination.

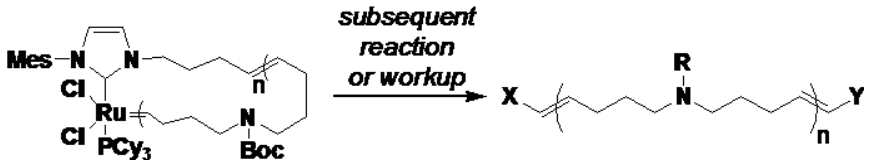

Figure 4.8 Catalyst decomposition in REMP reaction

Another source of linear chain contamination is the olefin isomerization to form other structures. The reaction is initiated by the metal-hydrides of the catalyst. This reaction will consume the catalyst and lower the reaction speed. To examine the exact ratio of linear to cyclic after the REMP reaction, a new method to separate the linear and cyclic polymer was proposed. The crown ether can reacted with the ammonium group to form catenated structure with the help of Ru metathesis catalyst (Figure 4.9). [127]

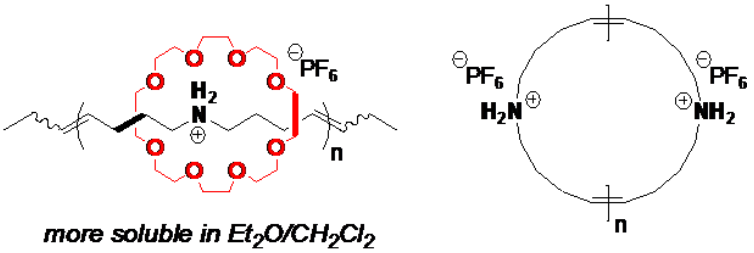

Figure 4.9 The structure of the crown ether and ammonium composite.

With this method, it can be found that with the same monomer conversion ratio, the polymer rings prepared by catalyst UC6 contain a larger amount of linear chain than those by catalyst UC5 (Table 4.3). Even for the "better" polymer ring prepared by catalyst UC5, it still contains about 20% of linear chain contamination, which is large enough to change the rheological properties of the macrocyclic polymer materials.

Table 4.3 Compare the cyclic/linear ratio of two catalysts

Catalyst	Time (h)	M_w (kDa)	PDI	Cyclic/Linear
UC-5	23	485	1.21	80:20
UC-6	16	237	1.28	45:55

Further study shows that for the catalyst UC5 around 90% of monomer conversion can be achieved in 23h. If we double the reaction time, the amount of linear chain contamination will be raised to around 30%. While at shorter time or lower monomer conversation, even if the molecular weight of the polymer ring hasn't reached the desired value, the linear chain contamination can be lowered to less than 10%. However, no matter how hard we try to alter the reaction condition or catalyst structure, for the poly(ammonium) system, we can't get 100% pure rings.

4.3.2 The rheological responses of linear and cyclic poly(ammonium)

The cyclic poly(ammonium) samples contain linear chain contamination. To double check whether the linear chain contamination is the only reason leading the results for cyclic PCO materials. The rheological responses of the linear and cyclic poly(ammonium) are examined. In this study we only examine the macrocyclic polymer materials prepared by catalyst UC5. Table 4.4 is the list of linear and cyclic poly(ammonium) samples prepared in this study.

Table 4.4 Molecular information for linear and cyclic poly(ammonium) samples

	Mw (kg/mol)	PDI
Linear		
2AB89	236.0	1.13
2AB90	188.4	1.09
2AB110	143.0	1.66
2AB122A	54.8	1.13
2AB122B	48.7	1.24
2AB122C	33.3	1.16
Cyclic		
2AB112	134.0	1.08

In this system, we only got one cyclic poly(ammonium) sample. Sample 2AB122A, 2AB122B and 2AB122C are further purified linear samples to ensure each ammonium group is properly hydrogenated.

4.3.2.1 Zero shear viscosity of the linear and cyclic sample

Figure 4.10 present the zero shear viscosity of the linear and cyclic poly(ammonium) samples with different molecular weight. Similar results as shown in Figure 2.9 were found. The zero shear viscosity of the cyclic poly(ammonium) sample is near the viscosity value of the linear chains. Previous results have shown that macrocyclic polymer prepared by catalyst UC5 can be well controlled to contain less than 20% of linear chain contamination. While other study has shown that due to the "threading effect", the viscosity of the linear and ring mixture will increase dramatically, [46] and with up to 20% linear chain contamination, the mixture should behave like the linear chains. [57] In the cyclic poly(ammonium) system, it is known that there might be

around 20% contamination, thus the zero shear viscosity of this linear/ring mixture is expected to be the same as the linear chains.

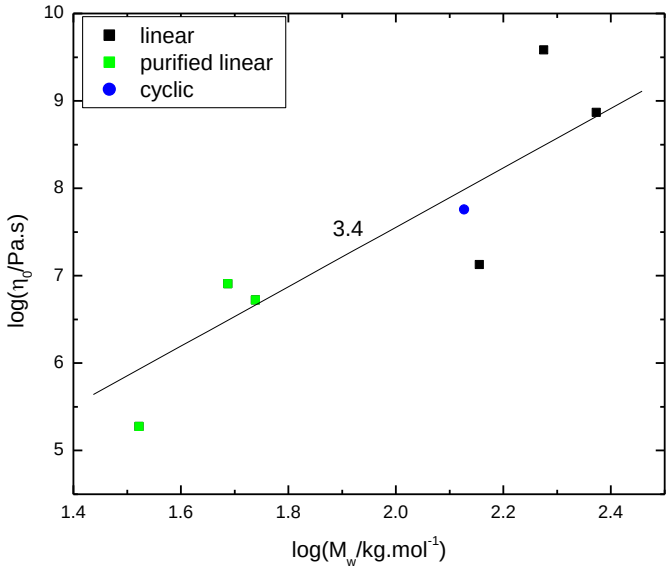

Figure 4.10 The zero shear viscosity vs molecular weight for linear and cyclic poly(ammonium) samples at the reference temperature of 40^{o}C

Compare with our previous study on the cyclic PCO system, cyclic PCOs prepared by catalyst UC6 should contain around 40% linear chain. Thus as shown in Figure 4.7, there are little differences between the linear and cyclic PCO samples prepared by the catalyst UC6. While for the cyclic samples prepared by catalyst UC5, their viscosity values are higher than the linear chains. It is known that for cyclic samples prepared by catalyst UC5, it should contain around 20% linear chain contamination. And high molecular weight samples should contain less linear chain than the low molecular weight samples. Thus the deviation from the zero shear viscosity vs molecular weight line for linear PCO samples should well represent the ratio of linear/cyclic change in the cyclic samples prepared by catalyst UC5.

4.3.2.2 Dynamic responses of linear and cyclic poly(ammonium)

Figure 4.11 compares the dynamic responses of linear and cyclic poly(ammonium) samples with the near molecular weight. Similar as what we found in the cyclic PCO system. The storage and loss modulus of the cyclic samples with linear chain contamination are all higher than linear samples with near molecular weight. The cyclic samples with linear chain contamination need more time to relax then the linear samples.

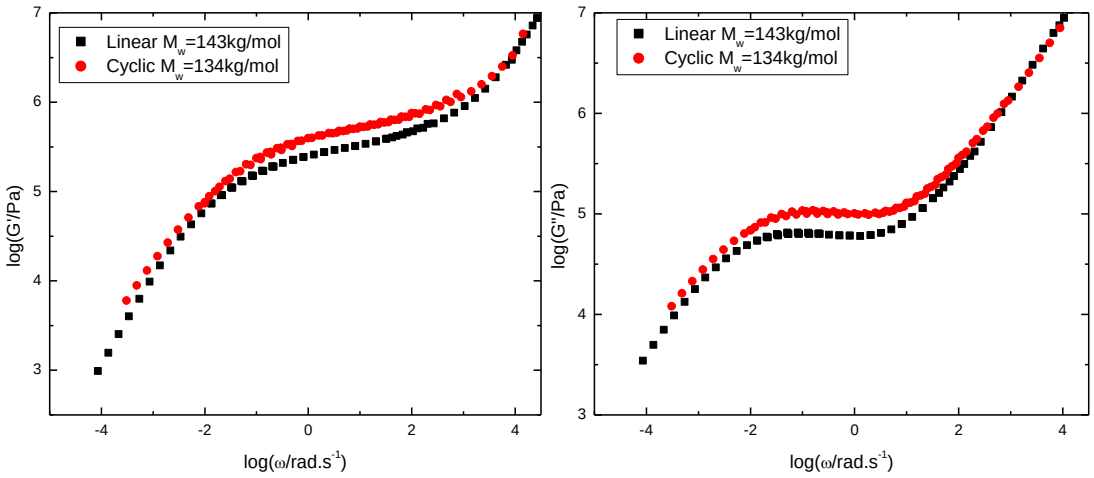

Figure 4.11 Compare the dynamic responses of linear and cyclic poly(ammonium) samples with near molecular weight.

In previous study on the cyclic PCOs, limited by material nature of the PCO samples, we could not get the whole rubbery region of the samples. The plateau modulus values of the linear and cyclic PCO samples are estimated by integrating limited range of the dynamic data. For poly(ammonium) samples, the sample will not crystallize. The dynamic master curve covering the rubbery to the flow state can be created by the time temperature superposition of the dynamic curves at different temperature. The plateau modulus of the linear and cyclic poly(ammonium) samples can be directly estimated using the van Gurp-Palmen plot. Figure 4.12 is the van Gurp-Palmen plot of the linear

and cyclic poly(ammonium) at the same reference temperature. It can be found that the plateau modulus of the only ring is about $4.86*10^5$Pa, which is higher than the plateau modulus of unpurified linear samples. Even if the linear samples are further purified, their plateau modulus (G_N^0) is roughly the same as the cyclic poly(ammonium). It is known that $G_N^0=\rho RT/M_e$. [1] A higher plateau modulus means a lower entanglement molecular weight (M_e), which means with the same molecular weight, the rings will get more entangled. Estimated from the plateau modulus (G_N^0) and polymer molecular weight, the number of entanglement for the cyclic poly(ammonium) is around 26. These poly(ammonium) rings contain linear chains. If consider the nature of "threading effect", linear chains go through a ring and form the rotaxane like conformation. This conformation introduce more topological constrains into the polymer network. As the modulus $G=\upsilon kT$, where υ is the number of network strands per unit volume which is the inverse of the molecular weight of the structure included in the relaxation process. Introducing more threaded rings should introduce more entangled structure in the polymer matrix which should increase the modulus and lower the entanglement molecular weight of the polymer material.

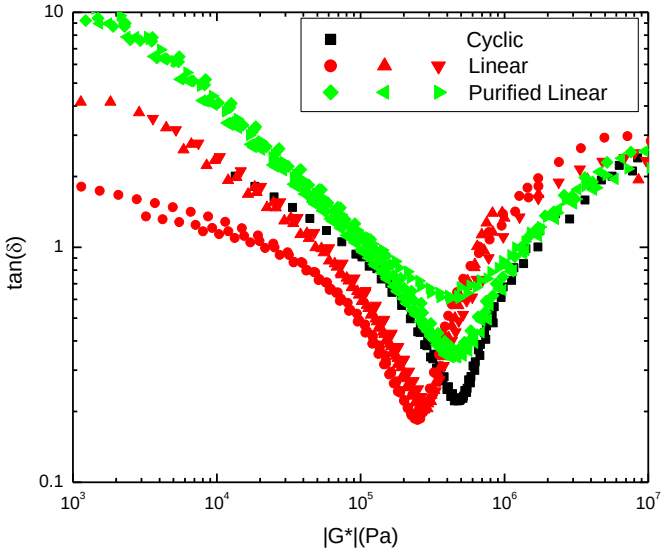

Figure 4.12 van Gurp-Palmen plot of the linear and cyclic poly(ammonium) at the reference temperature of 40^{o}C

4.4.3 Summary

In summary, both the reaction mechanism and rheological studies have proved that catalyst UC5 and UC6 cannot provide satisfied 100% pure macrocyclic polymers. For samples prepared by catalyst UC6, they contain around 40% linear chain contaminations. Because of the large amount of linear chain contamination, their properties have no differences from the linear chains. While for macrocyclic samples prepared by catalyst UC5, they have less linear chain contamination. Influenced by the "threading effect", their viscosity and plateau modulus are near or higher than their linear competitors. Changing the reaction condition and catalyst can't make further improvement to get better polymer rings. In the following work, we would like attack the problem by changing the monomer structures to see which kind of monomer structure can provide better pure rings.

4.3 Dendronized rings

In previous section, we discussed the possibility of getting pure macrocyclic polymers using the new metathesis polymerization catalyst from common cyclic monomers. Limited by different side reactions related with the catalyst, it is hard to get 100% pure macrocyclic polymer materials. Linear chain contamination greatly affects the properties of the viscoelastic properties of the final products. An alternative method is to solve the problem by changing the structure of monomers. Macromonomers (MM) are monomers or oligomer with complex structures and function groups which can be initiated for further polymerization. The complex structure can be linear or block chain, branched or hyperbranched and even dendronized structure. Polymers prepared by poly(macromonomer) (poly(MM)) method have a more regular and well control structure and widely used in functional polymer fields. [100, 128]

4.3.1 Synthesis of dendronized ring

As shown in Figure 3.2c, a new kind of dendronized macrocyclic polymer was synthesized via the REMP method using the dendronized macromonomer.[100] The structure of the macromonomer is shown in Figure 4.13.

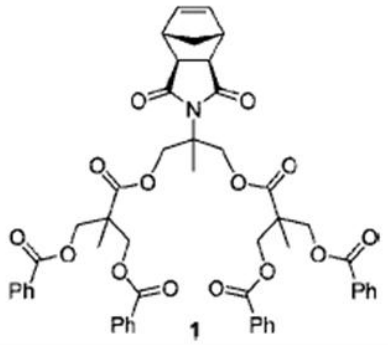

Figure 4.13 The structure of the dendronized macromonomer.

Due to the bulk side chain structure, the macrocyclic polymer chains are visible with atomic force microscope (AFM). Figure 4.14 is the AFM image of the dendronized polymer rings imaged by AJ Boydston.[100] The average diameter of the ring is around 35-40nm and the height of the ring is around 9nm. These new dendronized polymer rings looks very pure. No linear chain was found with the AFM image.

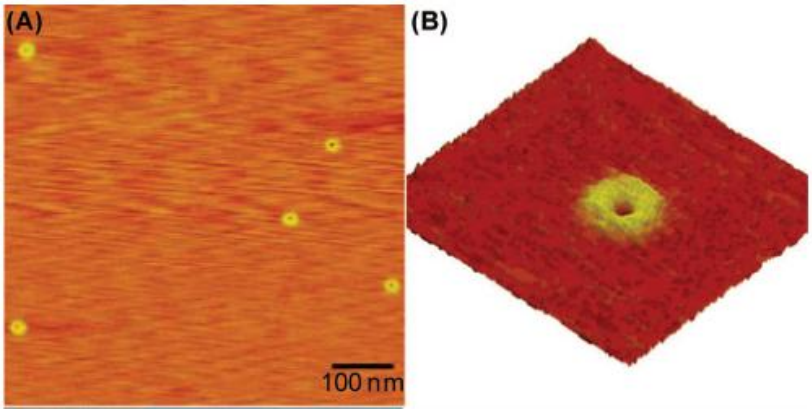

Figure 4.14 Visualized AFM image of the dendronized polymer rings (after Boydston et. al.[100])

Because of the difficulty in synthesis this complex macromonomer, only one dendronized polymer ring was prepared. The molecular weight of the dendronized polymer ring is 5.658 x 10^6 Da and the polydispersity index (PDI) is 1.16. If estimated from the molecular weight of the macromonomer, the DP is around 4740. To compare the viscoelastic properties of the dendronized macrocyclic polymer, we need to prepare the dendronized polymer with linear structure. However, limited by the steric hindrance, ring structure is more favorable for this kind of macromonomer. This could be the reason that we can get better rings with the same metathesis catalyst as used in previous study. With ring opening metathesis polymerization (ROMP) method, it is hard to get linear dendronized polymer with higher backbone degree of polymerization (DP). To prepared

linear dendronized polymers, ultrasonic was used to break the chain of the high DP dendronized rings into linear chains. This is not the best way to get the linear sample, because the large amounts of side chains have a higher possibility to get broken than the backbone of the polymer rings. The prepared linear chain may not bare the same structure as the dendronized macrocyclic polymer. The only linear sample prepared by the ultrasonic has the molecular weight of 3.23 x 10^6 Da , the PDI is 1.38 and the backbone DP is around 2230.

4.3.2 Viscoelastic properties of dendronized ring

The dynamic master curve of the dendronized polymer ring sample at the reference temperature of 80^{o}C was shown in Figure 4.15. The examined temperature range was between 45 to 200^{o}C.

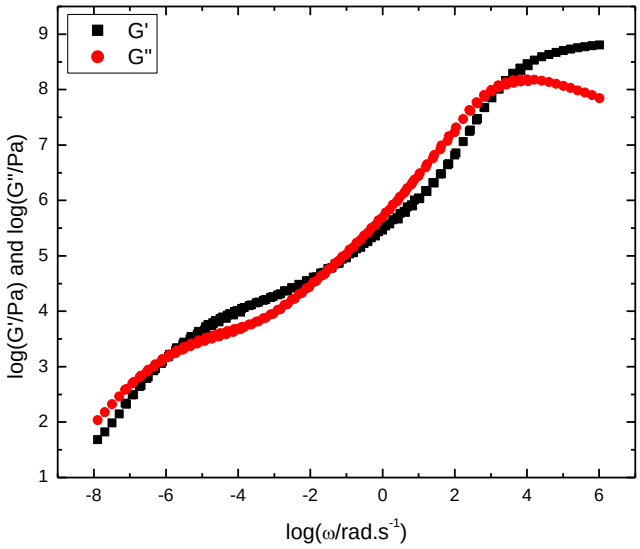

Figure 4.15 The dynamic master curve for the dendronized polymer ring sample at the reference temperature of 80^{o}C

Worried about the possible sample degradation or crosslinking at high temperature, we didn't perform the experiment at even higher temperature. Thus in the dynamic master curve, the sample didn't reach the terminal flow region. The long time viscoelastic behaviors of the ring samples can be estimated from the creep data. As shown in Figure 4.15, the dendronized polymer ring shows a clear glassy plateau with the modulus (G_g) around 10^9 Pa. The rubbery plateau modulus (G_e) is around $1.42*10^4$ Pa. Creep experiment performed at 120°C gives the plateau compliance (J_e) is equal to $7.69*10^{-5}$ Pa^{-1}, which gives the plateau modulus ($G_e=1/J_e$) around $1.3*10^4$ Pa. If the plateau found in the dynamic master curve is the entanglement plateau of the macrocyclic polymer, then the estimated number of entanglement for this macrocyclic polymer is around 27. The zero shear viscosity at 120°C for the ring polymer is $8.85*10^6$ Pa.s. The steady state recoverable compliance (J_s) can be estimated from the creep data with the equation $J_s= J(t)-t/\eta_0$. [1] Estimated from the recoverable compliance data at 120°C, the J_s value is $3*10^{-3}$ Pa^{-1} (Figure 4.16).

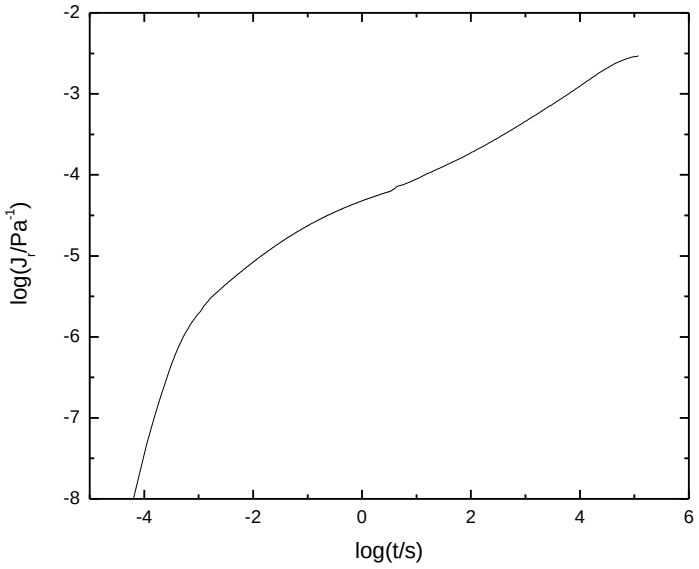

Figure 4.16 The recoverable compliance of dendronized polymer ring

In literature, if the rubbery plateau found in the dynamic master curve is the entanglement plateau, then the value of G_eJ_s is expected to be 2 and the experimental value is between 2 to 3. For our data, the G_eJ_s value is around 14. The value is much higher than what is reported for entangled linear polymer materials.

From above analysis, it can be found that the dendronized polymer ring shows quite different viscoelastic properties than normal entangled linear polymers. The dendronized polymer ring has a very complex molecular structure. Based on some model prediction,[57, 67, 70, 74] the ring structure should not get entangled. But in our data, we see a clear rubbery plateau. If estimated the volume fraction of the dendronized side chains by group contribution, [129, 130] the volume fraction of the side chain may account for over 75% of the total volume of the cyclic sample. As discussed in some paper, the side chains should act as solvent to dilute the backbone and lower the plateau modulus and increase the steady state recoverable compliance value. [11, 15, 19, 20, 38, 131] Thus the G_eJ_s value is expected to be higher.

4.3.3 Compare the viscoelastic responses of linear and cyclic dendronized polymer

Figure 4.17 compares the modulus of linear and cyclic dendronized polymer using the van Gurp-Palmen plot. As shown in the plot, the plateau modulus of the cyclic polymer is slight higher than that of the linear polymer. The plateau modulus found for the linear dendronzied sample is around $1.2*10^4$Pa. Estimated from the plateau modulus, the number of entanglement for the linear sample should be around 16. The glassy modulus values of the two samples are quite different. The differences between two samples could because of the possibility of breaking the molecular side chain structure of

the dendronized polymer during ultrasonic preparation of the linear dendronized polymer. The linear dendronized polymer could not be used to characterize the dendronized ring.

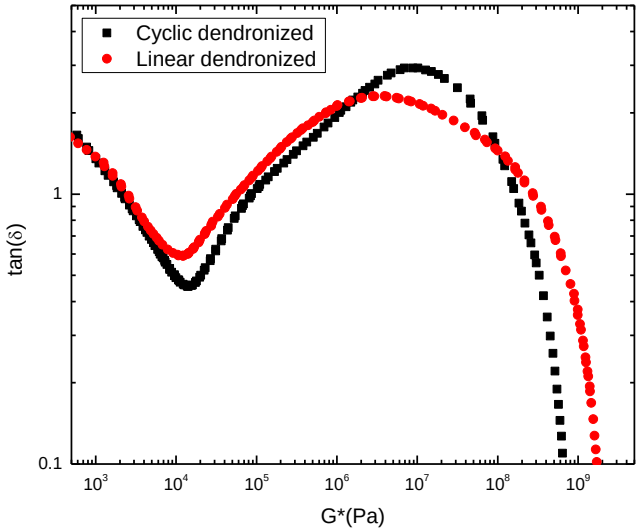

Figure 4.17 van Gurp-Palmen plot of the linear and cyclic dendronized polymer

The problem with the linear dendronized samples could be more clearly defined with their temperature dependent properties of the linear and cyclic samples. Figure 4.18 is the shift factor of the linear and cyclic sample with the same reference temperature of 80^{o}C. In literature,[48] the temperature dependence of the linear and cyclic samples is expected to be the same. However, for our linear and cyclic samples, they follow two different lines. From the dynamic master curve and the shift factors for the linear and cyclic samples, the WLF fitting parameter, the glass transition temperature (T_g), and the fragility (m) can be estimated and listed in Table 4.5.

Table 4.5 The parameters estimated from the dynamic master curve and shift factors of linear and cyclic dendronized polymers

sample	T_g	C^1_g	C^2_g	m	E_g (kJ)
linear	50.3	14.9	92.5	52.1	322.3
cyclic	61.5	13.8	74.9	61.6	394.6

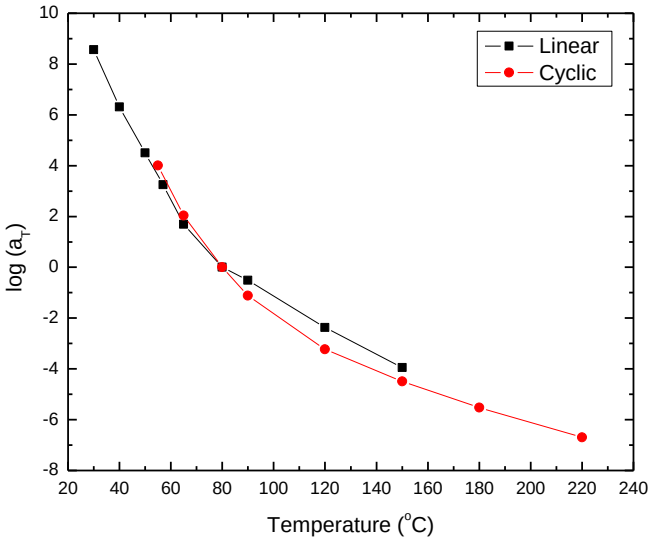

Figure 4.18 The shift factors of linear and cyclic dendronized polymer.

As shown in the table, the glass transition temperature (T_g) of the cyclic sample is much higher than that of the linear samples. In literature, the glass transition temperature (T_g) of cyclic polymer should be near to the value of linear polymers with high molecular weight. [64] Because of the chain ends effects,[63] only small molecular weight linear samples will show big deviation from the glass transition temperature (T_g) of the cyclic samples. However, for our linear samples, the molecular weight is high enough to make the sample get well entangled. The huge differences between the T_g of the linear samples and the cyclic samples should be because of the structure differences between the two samples. Comparing the fragility values, the cyclic chain is more rigid than the linear polymers, which could be because more side chains broke off from the dendronized linear samples.

4.3.4 Conclusion for dendronized polymers

In conclusion, due to the steric hindrance, polymer materials synthesized via the dendronized macromonomers prefer to take the cyclic architecture than linear. Preparation of dendronized macrocyclic polymer using the REMP method provides a promising way to get pure polymer rings. While due to similar reason, the preparation of linear dendronized sample become difficult. With the range of polymer chains imaged by the AFM, no linear chain contamination was found. The structure of the dendronized ring is very complex. Large amount of bulk side chain act as solvent, which lead to a very high G_eJ_s value from the creep experiment. The dendronized ring sample shows a clear rubbery plateau in both the dynamic master curve and creep data. The molecular weight of the cyclic sample is very high and the number of entanglement estimated is around 25. Preparing linear sample via ultrasonic breaking the ring sample has been proved to be failure. The prepare linear dendronized sample show quite different physical properties and temperature dependence from the macrocyclic sample. It is possible that during the ultrasonic breaking, it not only breaks the backbone but also break of the large side group.

4.4 The Wedge rings

4.4.1 Molecular information of wedge polymers

Synthesis of the dendronized rings provided an alternative way to get clean ring by changing the structure of monomer. However due to the great difficulty in preparing the pure linear dendronized polymers, we did not have a good reference to characterize the viscoelastic properties of our ring polymer materials. To solve this problem, another kind of macromonomer with similar structure but less steric hindrance than the dendronized macromonomer is prepared. Polymer materials prepared by this

macromonomer using the metathesis catalyst are named as wedge polymer. Detailed structure of the macromonomer and the synthesis route is shown in Figure 3.2d. Similar as in PCO system, in this work four wedge ring and four wedge linear samples are prepared. Their molecular information is determined by GPC-MALLS and the data is listed in table 4.6.

Table 4.6 The molecular weight of linear and cyclic wedge polymers

	M_w (g/mol)	DP	PDI
linear			
273-1	$2.82*10^6$	1001	3.3
273-2	$1.16*10^6$	699	1.9
221A	$1.35*10^6$	1406	1.5
221B	$5.71*10^6$	5314	1.1
cyclic			
276	$2.45*10^6$	2250	1.3
277	$4.70*10^6$	5137	1.1
278	$5.71*10^6$	5934	1.1
279	$5.56*10^6$	5708	1.1

The DP of each molecule is determined by dividing the number average molecular weight (M_n) with the molecular weight of macromonomer. To examine the purity of the macrocyclic sample, the most convenient way is to examine their radius of gyration (R_g) data. The R_g of macrocyclic samples should be only half of the linear sample with the same molecular weight. However, as shown in Figure 4.19, the radius of gyration value for the wedge rings are the near the value of the linear wedge samples. The slope is about 0.75, which indicate that at room temperature THF is a good solvent for the wedge polymers.

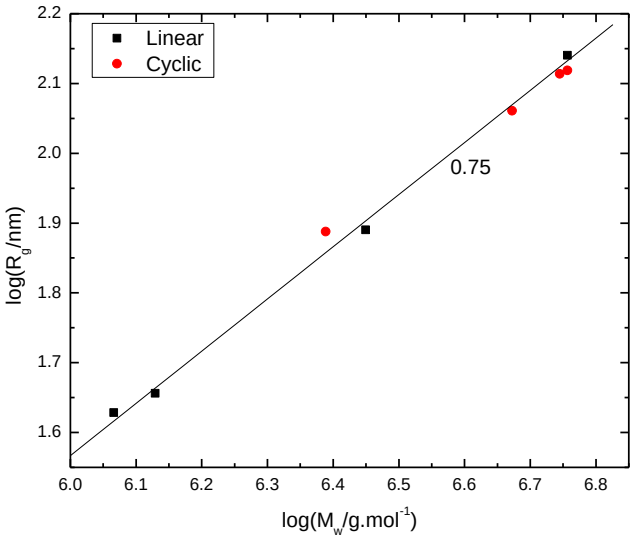

Figure 4.19 The radius of gyration of linear and cyclic wedge polymer in THF

4.4.2 Viscoelastic properties of linear and cyclic wedge polymer

Figure 4.20 compares the dynamic responses of cyclic wedge polymer with different molecular weight and the linear wedge polymer with the highest backbone DP. The master curve was constructed by shifting the dynamic responses at the temperature range of 30 to 180 ^{o}C. The terminal flow behaviors of the dynamic responses were calculated from the creep experiment at the 180^{o}C. From the dynamic data, it can be found that the glassy modulus of the linear and cyclic wedge polymer is very low. To the lowest temperature we examined, it is only around 10^{7}Pa. There is only one rubbery plateau region in the dynamic master curve and the plateau modulus value of the linear and cyclic samples are near.

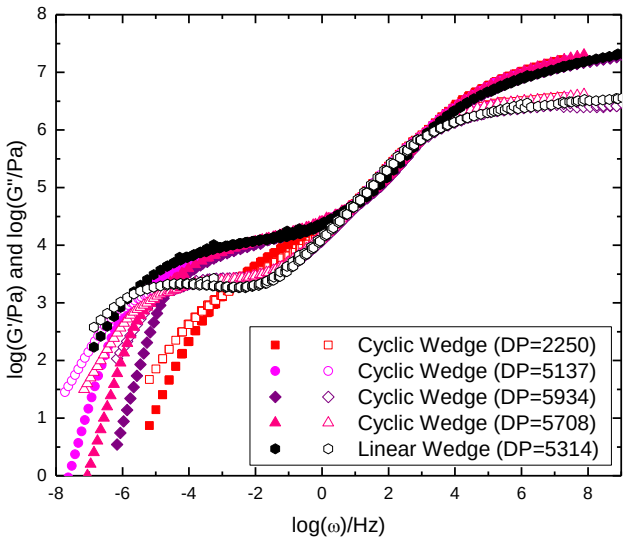

Figure 4.20 The dynamic mater curve of the linear and cyclic wedge polymer at the reference temperature of 80^{o}C

Figure 4.21 present the temperature dependence of the linear and cyclic wedge polymer. As discussed in other's work, the temperature dependence of the linear and cyclic samples is expected to the same. The shift factors for the linear and cyclic samples can well overlap with each other. The shift factor data can be fitted with the WLF equation, and the glass transition temperature of the linear and cyclic samples can be estimated from their dynamic master curve. The glass transition temperature for the linear and cyclic wedge polymers is near and the value is around 41.5^{o}C.

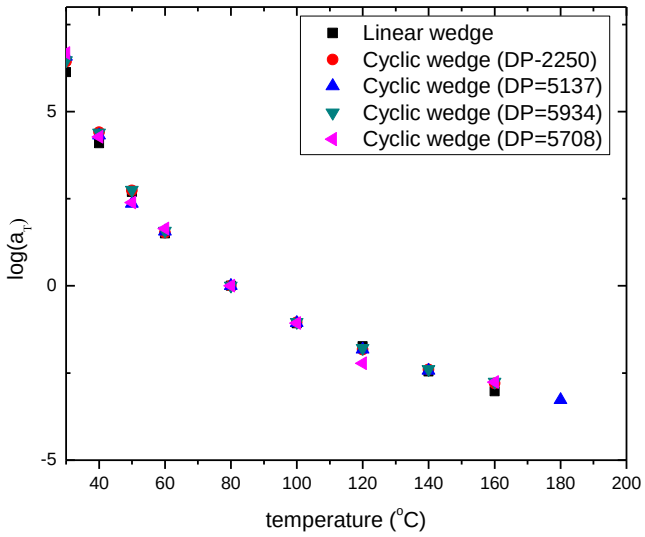

Figure 4.21 The shift factor for linear and cyclic wedge polymer

To estimated the accurate value of the plateau modulus for the linear and cyclic wedge polymer, their dynamic master curves were plotted following van Gurp-Palmen method (Figure 4.22). In the plot it can be found that the plateau moduli of the cyclic wedge polymer is around $1.17*10^4$Pa, which is near that of the linear wedge polymer ($G_N^0=1.28*10^4$Pa). Estimated from the plateau modulus value, the entanglement molecular weight (M_e) of cyclic wedge is about $2.51*10^5$g/mol. Then the number of entanglement for the cyclic wedge polymer investigated here is between 10 and 20. With such high number of entanglement, the cyclic wedge samples should get well entangled and we can find a clear rubbery plateau in the rubbery region.

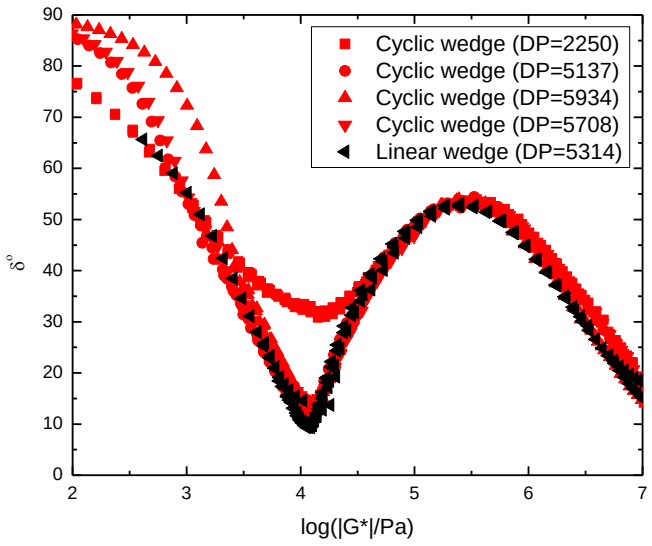

Figure 4.22 van Gurp-Palmen plot of linear and cyclic wedge polymer

If we compare the dynamic curve of linear and cyclic wedge polymer with near backbone DP (Figure 4.23), it can be found that the cyclic sample relax much faster than the linear ones. The plateau length of the cyclic sample is shorter than the linear samples with near molecular weight. If just compare the plateau length from the dynamic master curve, the cyclic sample should get less entangled. Thus the plateau modulus of the cyclic polymer should be lower than the linear ones. However in the dynamic maters curve, we found little differences between the plateau modulus of the linear and cyclic samples. The ring polymers relax faster than the linear samples, thus it is expected that the viscosity of the cyclic samples should be lower than the linear samples.

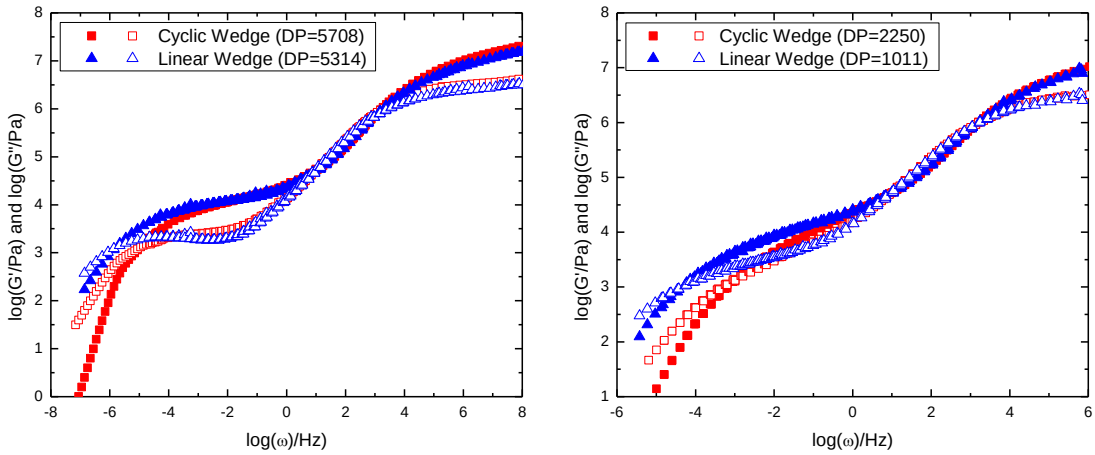

Figure 4.23 Compare the dynamic responses of linear and cyclic wedge polymer with near backbone DP

Figure 4.24 present the zero shear viscosity of linear and cyclic wedge polymer at the reference temperature of 80^{o}C. It is interesting to find except for one sample, the zero shear viscosity of the cyclic wedge samples are all lower than the linear samples with the same molecular weight. However as shown in previous data, there is little difference between the rubbery plateau and radius of gyration for the linear and cyclic samples. Thus it is high possible that our sample still get linear chain contaminated, but we got some better macrocyclic polymer material with less linear chain contamination than what we have before.

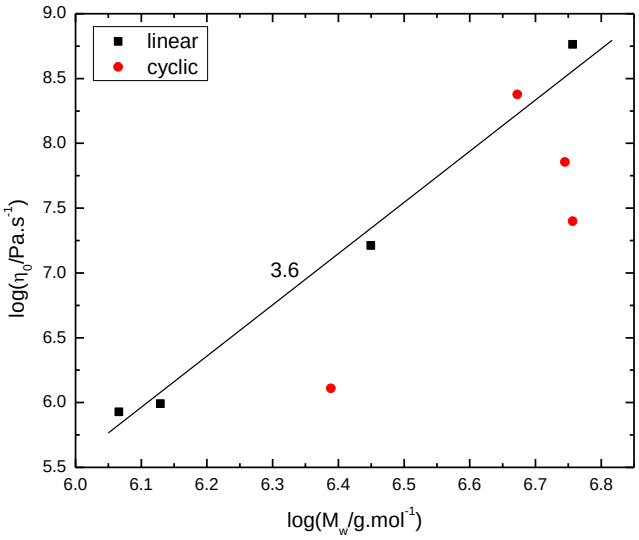

Figure 4.24 The zero shear viscosity of linear and cyclic wedge polymer vs molecular weight

4.4.3 Summary

In this section, we present the viscoelastic properties of a series of macrocyclic wedge polymers with different molecular weight. It is expected that due to the similar steric hindrance effect of the large side group, the wedge polymer should be a better candidate to pure ring polymers and compare with linear sample with same structure. However, even though the zero shear viscosity of the some ring samples were found to be lower than the linear samples with near molecular weight, the radius of gyration data shows that ring should get contaminated. Compare with the results for PCO and poly(ammonium) rings, the wedge rings show some signs of better ring quality.

4.5 Relaxation behavior of ring/linear mixture

For the four groups of macro cyclic samples examined in this work, most of them have been found to be the ring/linear mixture. Based on AJ Boydston's work of separating the linear from rings via the crown ether, there should be around 20% linear

chain contamination in rings prepared by catalyst UC5 and 40% linear chain in macrocyclic samples by catalyst UC6. [98] Recently Yan prepared some high DP ring polymers by more active catalyst SC5 and SC6 using similar macromonomer method. [132] In the AFM images, more linear chain contamination was found than what has been reported before for the UC5 and UC6 system. Since with current catalyst system, it is hard to totally avoid linear chain contamination in our ring samples. In the following part, we would like to do more studies of the influence of the linear chain to the relaxation behavior of the ring polymers.

4.5.1 Rheological polydispersity

The molecular weight of the ring samples are determined by the GPC-MALLS. It has been found that under normal condition, it is hard to separate the linear and cyclic samples with near molecular weight by GPC. [91, 92] Thus even if there is linear chain contaminations in the samples, from the GPC peak it is hard to find the differences. If the molecular weight of the samples is well controlled, the polydispersity of the samples still looks very narrow. However, due to the differences between their entanglement molecular weight, for linear and ring polymers with the same molecular weight, their relaxation time should be quite different. The ring/linear mixture should act as a polydispersed sample. If we can measure the polydispersity of samples from their rheological responses, the measured value should be higher than the value reported by the GPC.

van Gurp-Palmen plot is an very useful method to examine the rheological responses of polymer materials. [111, 112] It is sensitive to the composition change of the

samples. As shown by Trinkle,[111] the polydispersity of different polymer material can be estimated from the normalized modulus (G^*/G_N^0) at a fixed phase angle (Figure 4.25).

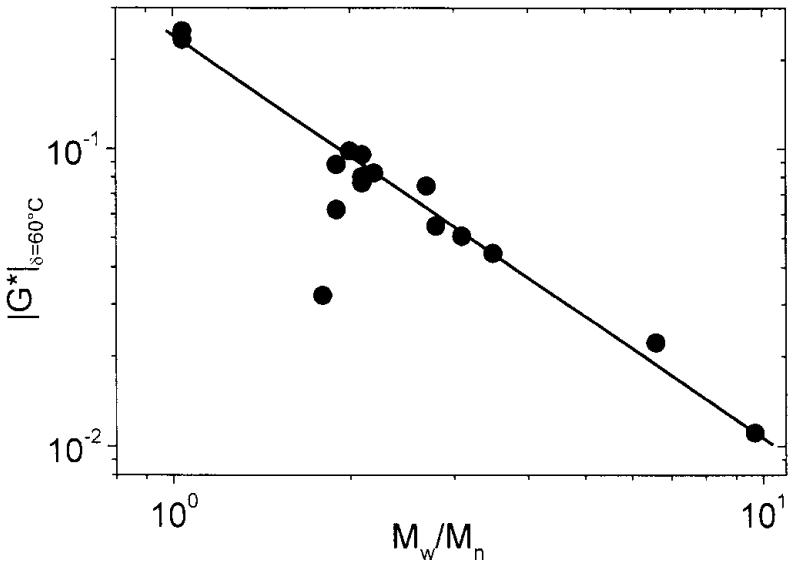

Figure 4.25 The relation between polydispersity (M_w/M_n) and normalized modulus at fixed phase angle ($\delta=60^o$) (After Trinkle et. al. [111])

We digitized the plot and got the equation,

$$\log\left(\frac{|G^*|_{\delta=60^o}}{G_N^0}\right) = -1.3558 * \log\left(\frac{M_w}{M_n}\right) - 0.6229 \qquad (4.1)$$

In this study we examine the viscoelastic properties of four kind of linear and cyclic polymers. For the PCO samples, limited by the experiment data range, the plateau modulus (G_N^0) estimated by the integration method may not be accurate enough. The linear dendronized polymer has been proved to lost some side chains and the unpurified poly(ammonium) linear samples have much lower plateau modulus than the cyclic samples. There should be some problem with the molecular structure of these samples, so we didn't put them into this discussion. In Table 4.7, the PDI value estimated by equation 4.1 is listed with the PDI value estimated by the GPC.

Table 4.7 Compare the polydispersity values estimated by van Gurp-Palmen plot for linear and cyclic samples with that estimated by GPC

sample			$\lvert G^* \rvert_{60^o}$ (Pa)	PDI $\lvert_{GPC}$	PDI $\lvert_{van\ Gurp}$
Wedge	Ring	276	650.3	1.3	3.4
		277	690.7	1.1	2.8
		278	1037	1.1	2.0
		279	690.7	1.1	2.9
	Linear	273-1	590	3.3	3.4
		273-2	1900	1.9	1.5
		221A	2130	1.1	1.4
		221B	768.8	1.2	2.5
Dendronized	Ring	2ab94	446.6	1.2	4.5
Poly(ammonium)	Ring	2ab112	20000	1.1	3.6
	Purified linear	2ab122a	43560	1.1	1.9
		2ab122b	40130	1.2	2.0
		2ab122c	48510	1.2	1.7
Roovers [56] PBD ring	$G_N^0{}_{ring}=0.2G_N^0{}_{linear}$		24530		1.5
	$G_N^0{}_{ring}=0.5G_N^0{}_{linear}$		24530		3.7
McKenna [48] PS ring (M_W=380k)	$G_N^0{}_{ring}=0.5G_N^0{}_{linear}$		19900	1.1	1.1
Kapnistos [57] PS ring (M_w=198k)	$G_N^0{}_{ring}=0.2G_N^0{}_{linear}$		7600	<1.1	1.1
	$G_N^0{}_{ring}=0.5G_N^0{}_{linear}$		7600	<1.1	2.1

In the table, it can be found that the PDI values for different polymer rings estimated by the van Gurp - Palmen plot are all much higher than what is estimated by the GPC. While for the linear samples, especially for the wedge linear, the differences are not that big. The method for estimating the sample PDI using the van Gurp - Palmen plot should be sensitive enough to determine the PDI change for the samples examined in our study. The obvious differences between the PDI value determined by the van Gurp – Palmen plot and the GPC should indicate the linear chain contamination nature of these samples.

We also digitize the plot data of some literature reported rings and examine the PDI of these samples. We use the literature reported plateau modulus (G_N^0) value of the linear samples as reference. Based on previous study the plateau modulus of cyclic

sample could be either 0.2 or 0.5 of plateau modulus value of linear samples. The results are also listed in Table 4.6. Based on this study it is very interesting to find that the estimated PDI for Roover's PBD ring sample and Kapnistos' PS ring sample are all higher than what they show from GPC. Moreover, the Kapnistos' PS ring samples are fractionated by the liquid chromatography at critical condition (LCCC). The results indicate that there should be some problem with Kapnistos samples even they use LCCC to fractionate their samples.

4.5.2 Retardation spectrum of ring/linear mixture

Based on the analysis in previous section, it can be determined that the ring samples studied in this work all contain some linear chains. In this part, we would like to further discuss the viscoelastic properties of these ring/linear mixture samples. The relaxation behavior of polymer materials can be modeled with different theoretical predictions. The simplest one is the Maxwell model, which gives,

$$G(t) = Gexp(-\frac{t}{\tau}) \quad (4.2)$$

As shown in the experimental section, the the retardation spectrum of a polymer material can be estimated from the relaxation modulus with equation 3.8 and 3.9. Estimated from the equations, the slope of log(L) vs log(τ) for the Maxwell model is zero.

For the Rouse model, the relaxation modulus is expressed with equation, [7]

$$G(t) \approx G(\frac{t}{\tau_0})^{-\frac{1}{2}}\exp(-\frac{t}{\tau_R}) \text{ for } t>\tau_0 \quad (4.3)$$

, where τ_R is the Rouse time. Figure 4.26 is the retardation spectrum of the Rouse model with τ_0=0.01s, G=10^6Pa and τ_R=10s,

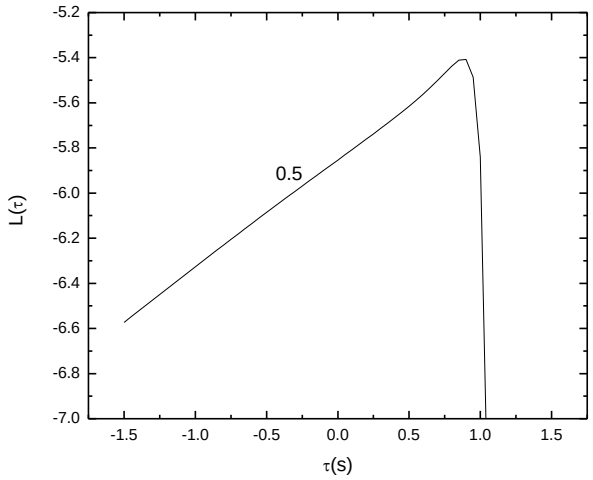

Figure 4.26 Retardation spectrum for Rouse model

As shown in Figure 4.26, the slope of log(L) vs log(τ) is 0.5. For Lattice animal model, the G(t) can be expressed as, [7]

$$G(t) \approx G_e(\frac{t}{\tau_e})^{-\frac{2}{5}}\exp\left(-\frac{t}{\tau_{ring}}\right) \qquad (4.4)$$

,where τ_{ring} is the relaxation time of the polymer ring. Figure 4.27 is the retardation spectrum predicted by the Lattice animal with $G_e=10^6$Pa and $\tau_e=0.01$s and $\tau_{ring}=10$ and 1000s.

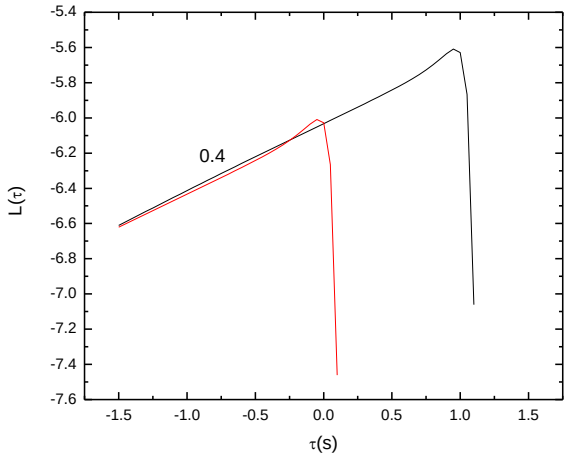

Figure 4.27 The retardation spectrum of Lattice animal model

For the lattice animal model, the slope of log(L) vs log(τ) is 0.4. Similarly, For the reptation model, the slope of log(L) vs log(τ) is expected to be 1/3.

The slope in the retardation spectrum can well represent the relaxation behavior of a polymer material under different condition. As shown in Figure 4.28, which is the retardation spectrum of 6% PS (M_w=5.48M g/mol) prepared by Roland.[133] In the Rouse region, the increase slope of log(L) vs log(τ) is around 0.5. While in the terminal region, the slope is around 1/3, which is so-called Andrade terminal region and defined as the onset of entanglement. [134, 135]

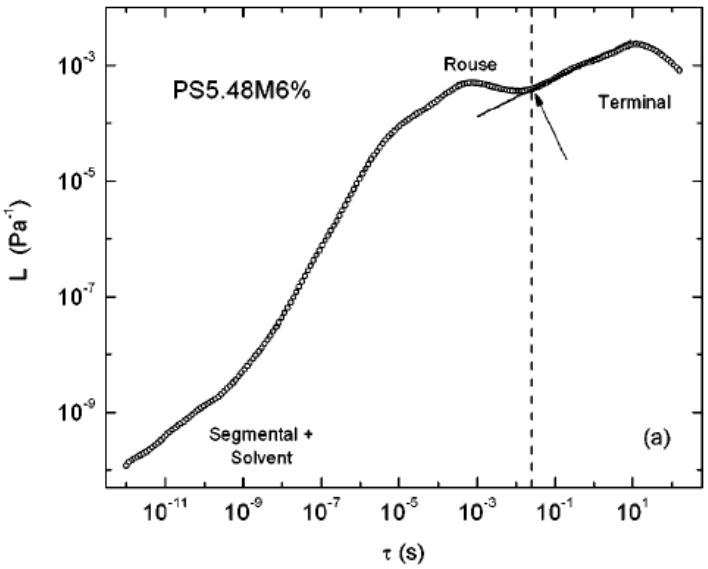

Figure 4.31The retardation spectrum of 6% PS solution (after Roland et. al.[133])

In Table 4.7, it is found that the measured sample PDI for the Roovers' PBD ring and Kapnistos' PS ring is higher than that estimated by GPC. Roovers' and Kapnistos' ring samples look like polydispersed samples. The molecular structures of these samples are simple without any branch or huge side chain structure. So it is high likely that these samples contain more than just macrocyclic structure. To compare with the retardation

spectrum of polydispered samples, we digitize the dynamic results of a known polydispersed sample and calculate its retardation spectrum (Figure 4.29). The molecular weight of the sample is high enough to get entangled, thus after the Rouse region, the sample should reptate and the slope is around 0.31. After that, the slope of logL vs logτ increase to around 1.

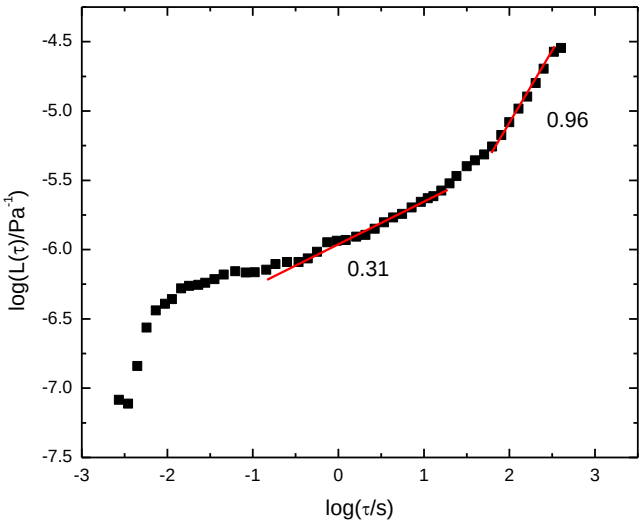

Figure 4.29 The retardation spectrum of polyisobutylene (PIB-15) with M_v=85 kg/mol and M_v/Mn=2, M_v is viscosity average molecular weight

Then, we digitize the data and analyze the retardation spectra of some literature reported polymer rings. Figure 4.30 is the retardation spectrum for McKenna's 380k PS ring, which sample shows similar PDI in both GPC and viscoelastic analysis. As shown in Figure 4.30, there are two peaks in the retardation spectrum. The first one is corresponding to the Rouse relaxation of the polymer chain and the second peak is the relaxation of the whole polymer. Allow the error in digitize the creep data from McKenna's paper, the data points are a little scattered. The slope of logL vs logτ after the Rouse region is about 0.32, which is near to 1/3 prediction of reptation model for

entangled polymer materials. This result indicates that with enough high molecular weight, the polymer ring can get entangled and should relax as what is predicted by the reptation model. In the retardation spectrum of entangled polymers, there are usually two peaks and the length between the two peak points scale with the molecular weight of the polymer.[1, 119, 120] According to McKenna, the plateau modulus of cyclic PS is 0.5 of the linear samples, thus for this 380k cyclic PS sample, the number of entanglement is around 11. In Figure 4.30, the distance between the two peaks is around 3.5. Thus the scale law between the number of entanglement and relaxation time is around 3.36, which is near what we see in the retardation spectrum and also near the value predicted by the reptation model.

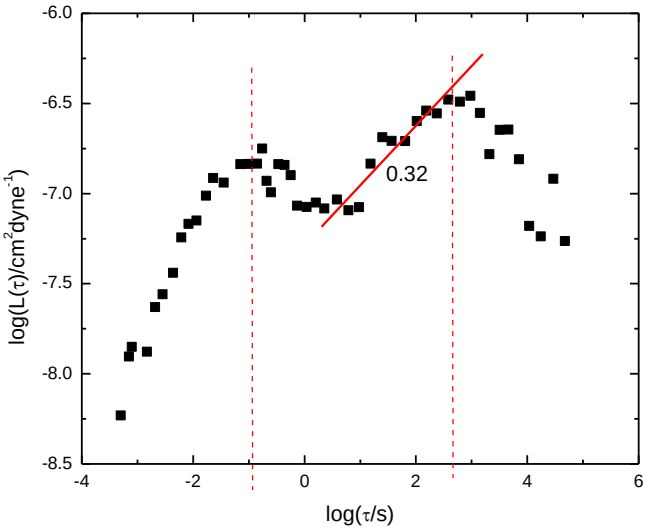

Figure 4.30 The retardation spectrum of McKenna's 380k PS ring

Figure 4.31 is the retardation spectrum of Roover's PBd rings. In this plot the Rouse region is not very obvious and looks like a shoulder in the retardation spectrum, but it can be determined from the slope of the logL vs logτ. After the Rouse region, the logL kept increase for some time and finally jump to another high peak before it get into

the terminal region. This phenomenon indicate that the sample contain a series of structures relax gradually and the whole chain will relax at a long time. The retardation spectrum of Roovers' ring looks like the retardation spectrum of a polydispersed linear samples. However, the sample should not be that polydispersed. In the Lattice animal model, the polymer ring should relax following the "leaves", "branches" and "trunk" sequence. If we regard the gradually relaxing part as the relaxation process of the "leaves" or "branches" as described in the "Lattice animal" model, then the slope of logL vs logτ should be 2/5. Or it could be 0.5 as predicted by the Rouse model. However, as shown in Figure 4.31, the slope is around 0.3, which is near the expectation of reptation model. While for the sudden increase part, the slope is around 1.4. We did similar estimation as did for McKenna's cyclic PS rings. The log time distance between the two peaks is around 3. The molecular weight of this cyclic PBd is 40kg/mol. If as in Roovers paper the plateau modulus of the ring is 0.2 of the linear, the number of entanglement is around 4. Thus the scale law of number of entanglement vs relaxation time is 5.0. If the the plateau modulus of the ring is 0.5 of the linear, the number of entanglement is around 10. Thus the scale law value is around 2.9, which is more near to what we found in the retardation spectrum.

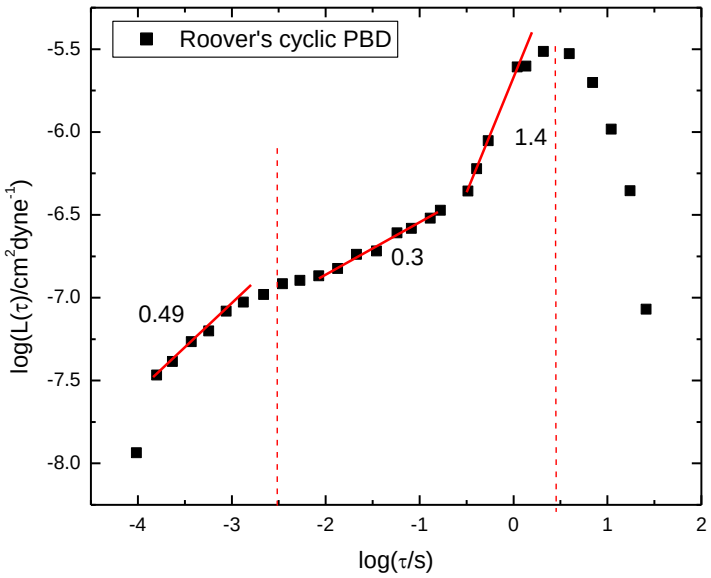

Figure 4.31 The retardation spectrum of Roovers' PBd ring

Figure 4.32 is the retardation spectrum of Kapnistos' ring. The retardation spectrum of this sample is quite different from the two samples discussed before. The time range covers about 7 decades, which is near the time ranges for previous two samples. In the plot, there is no sign of Rouse region, the first part of the curve can be fit with one line with the slope of 0.45. And the sample shows no sign of getting into the terminal region. Beyond the examined time range, there should be some relaxation need even longer time. In their paper, they claim their results fit the "lattice animal" model. However, if we didn't make great error in digitizing their data, their sample should relax faster than what is predicted by the "lattice animal" model. Takano [71] did some further study on their synthesis method and claim they may get knotted rings. Comparing with normal rings, knotted rings should have a more compact conformation. The faster relaxation than lattice animal model behavior of Kapnistos' ring should be the sign of forming knotted ring.

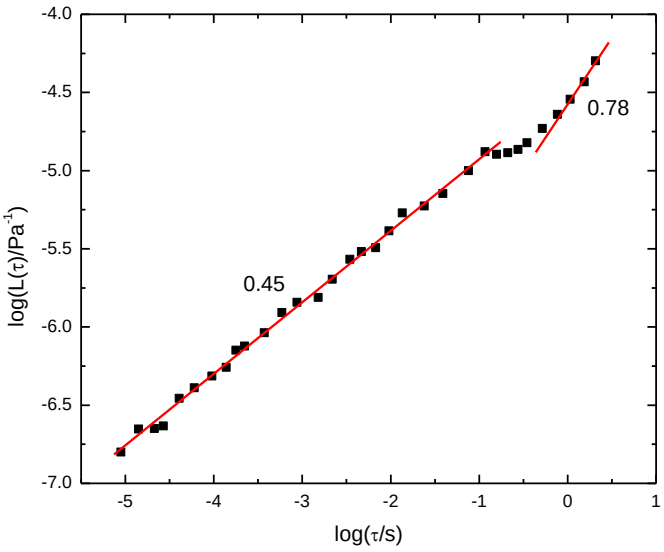

Figure 4.32 The retardation spectrum of Kapnistos' 198k PS ring

For our samples, we can't guarantee all samples are linear chain free. The PCO and polyammonium samples should have at least over 20% linear chain contamination. Figure 4.33 are the retardation spectrum for two near molecular weight cyclic PCO samples prepared by different catalyst.

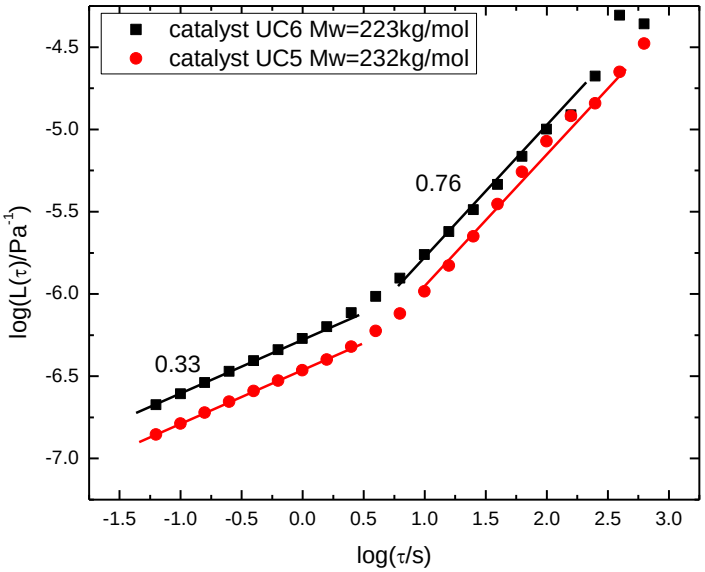

Figure 4.33 The retardation spectrum of cyclic PCO prepared by different catalyst

The two cyclic PCO sample have different amount of linear chain contamination with the sample prepared by UC5 have less linear chain in it. Limited by the experiment temperature range, we only have part of the data. However it is interesting to find that with near molecular weight, the cyclic sample contains less linear chain need more time to relax than the other one. Both samples show the same slope with the value of 0.33 which indicate the onset of entanglement. After that the slope of logL vs logτ for the two samples are still near with the value around 0.76.

Polyammonium ring is also a linear chain contaminated ring sample. Its retardation spectrum is shown in Figure 4.34. Similar as what we see in CPCO sample, the linear chain contaminated cyclic polyammonium sample contain some long time relaxation behavior. After the Rouse region, the initial logL vs logτ slope is around 0.3, than it will dramatically increase to the value about 0.76.

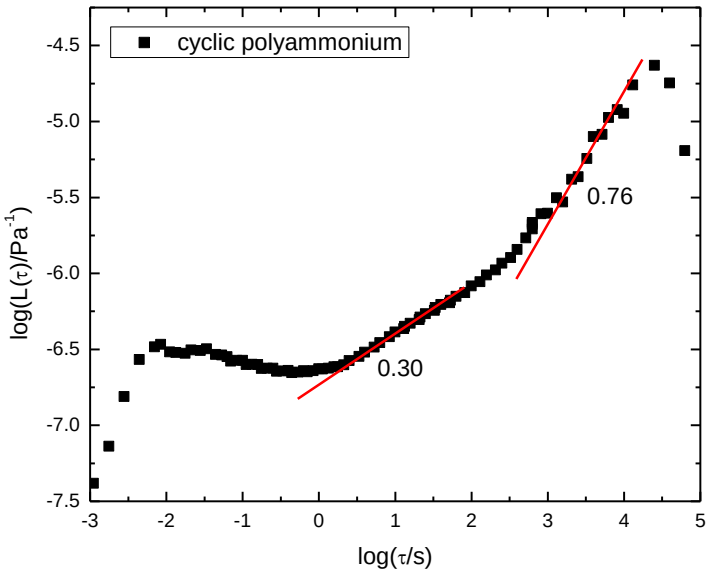

Figure 4.34 The retardation spectrum of the cyclic poly(ammonium) sample

For the dendronized ring sample, within the range examined there is no linear chain contamination found in the AFM images. However, in its retardation spectrum, we still see similar phenomenon as those cyclic samples with linear chain contamination (Figure 4.35). After the Rouse region, the power law dependence of L vs τ is only around 0.22. In previous discussion, this slope can represent the relaxation behavior of polymer chains. Thus for this samples, the relaxation time has a stronger dependence on the number of entanglement. This dendronized ring sample should relax follow some more complex mechanism. The dendronized samples contain over 70% of bulk side chains. These bulk structures should increase the spacing between polymer chains and act as solvent to dilute the polymer chain. As discussed in the brush polymer section, with this bulk side chain structure in the retardation spectrum we should expect a great increase of the logL value at longer relaxation time.

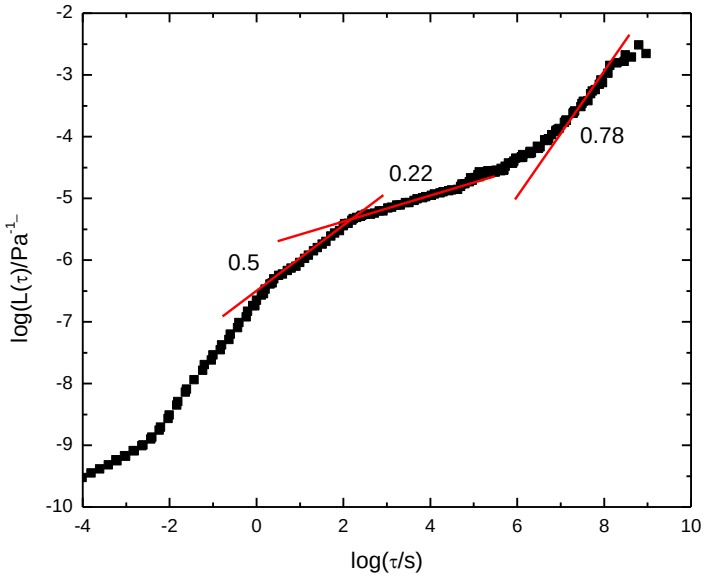

Figure 4.35 The retardation spectrum of dendronized ring

Wedge polymer show some sign of obtaining pure macrocyclic samples. Figure 4.36 shows the retardation spectrum of one wedge rings. Similar as the dendronized ring sample, after the Rouse region the sample relax slower than other linear samples. Also for the wedge polymer the bulk side chain occupy over 80% of the sample total volume, much stronger side chain effect is expected, and the slope of logL vs logτ near the terminal region is even higher than what we found for the dendronized polymer chains.

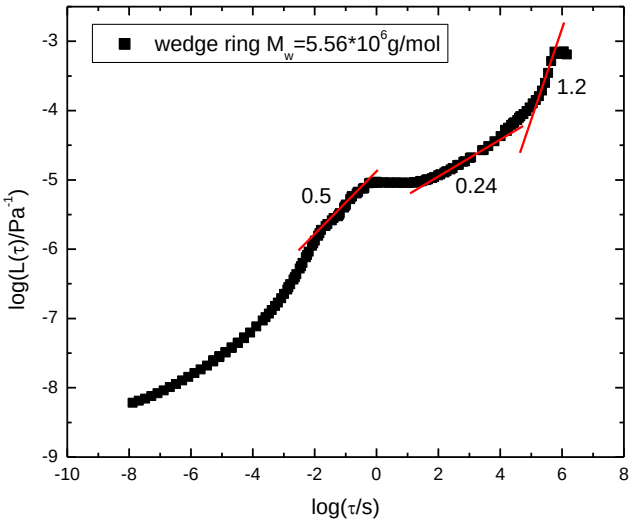

Figure 4.36 The retardation spectrum of wedge ring sample

The dendronized and wedge rings should have less linear chain contamination than the PCO and polyammonium rings. In the retardation spectrum, the only difference between the two samples is the slope after the Rouse region. The dendronized and wedge rings relax slower than the other two which relax more like the entangled linear chains. To further examine whether this is due to small amount of linear chain contamination, we digitize McKenna's recoverable compliance data on ring PS sample with known amount of linear chain contamination. Their retardation spectra are shown in Figure 4.37.

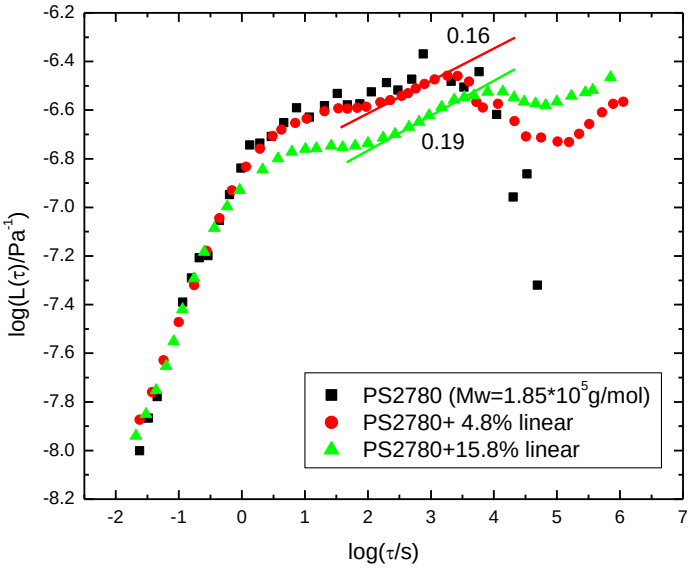

Figure 4.37 The retardation spectrum of cyclic PS and it mixture with known amount of linear chain.

In this plot it is interesting to find with linear chain contamination, the distance between the Rouse peak and the first relaxation peak increases, which means the sample need more time to relax. After the first relaxation peak there are more relaxations which need longer time. The slope values after the Rouse relaxation for the two linear chain contaminated samples are near. The values are also lower than what is predicted by any model and near to what we found for the dendronzied and wedge polymer. One possible explanation is the "threading effect" of the linear chain. Compare with the entangled chain, the threaded structure may need longer time to relax, thus the slope we found in the retardation spectrum should be lower than what is predicted than any model. However, with the increase of linear chain we may see a transition from the slower relaxation to the faster reptation relaxation. The slope should increase with increasing linear chain and finally we may only see the reptation like relaxation of the linear/ring mixture.

4.6 Conclusions and future work

In conclusion, in this section we tried every means to obtain pure macrocyclic polymer materials using the new REMP catalyst. Unfortunately, with our current study limited by the nature of the catalyst, we can't directly get pure macrocyclic polymer by reacting the cyclic monomer with the catalyst. Depend on the catalyst used, the macrocyclic material obtained by this method contain different amount of linear chain contamination. Some efforts have been applied to solve the problem by changing the structure of monomer. It is assumed that with strong steric hindrance the molecular chain should be more favorable of forming cyclic structure than linear structure. This tendency should help to get pure ring samples. Two series of samples were prepared by using the macromonomer with strong steric hindrance. For the dendronized ring sample, no linear chain contamination is found by the AFM. However, rheological analysis shows that the sample may still contain linear chains. Wedge structure is more flexible than the dendronized structure. The viscosities of wedge rings are lower than the linear samples. Further rheological study shows that the sample still get some linear chain contamination.

The slope of log L vs log τ in the retardation spectrum can represent the relaxation behavior of the polymer materials. By analyzing the retardation spectrum of our linear chain contaminated ring samples and some reported ring samples, it is found that it is high likely the polymer rings should relax following the reptation model. There is no sign the "lattice animal" or the Rouse model, which may fit for collapsed rings, can match the relaxation behavior of any literature reported rings. With linear chain contamination, the threaded structures relax slower than the chain reptation. The threading effects increase the number of entanglement and increase the relaxation time of the ring/linear mixture.

With large amount of linear chain contamination, the linear chain contaminated samples relax similar as the entangled polydispersed linear chains.

With the current REMP catalyst, it is hard to get pure macrocyclic polymer with simple polymerization reaction. But REMP is still a promising method to produce large amount of non-catenated ring. With current REMP reaction system, as there are large amount of linear chain contaminations, further purification is needed to get pure cyclic rings. Fractional precipitation or LCCC may work better to remove small amount of linear chain contamination. One way is to prepare a large amount of samples and fractionate several times. This may help to remove most of the linear chain contamination. From on our work on dendronized ring and wedge ring, changing the structure of monomer should be an alternative way to get better rings. However, this complex side chain structure makes the rheological responses of the ring polymer more complex. If we can find a more simple side chain structure but still have strong steric hindrance, it should be a better macromolecular structure to get pure rings and would be easier to distinguish different relaxation behaviors.

Chapter V:
Brush polymers with different side chain structures

Polymer architecture has long been known to greatly affect the rheological properties of polymer materials. Brush polymer is a unique type of graft polymers possessing a very high density of regularly spaced side chains along the backbone, and has become a subject of active research in the field of molecular rheology due to its interesting architecture [3, 11, 15, 18, 19, 25, 27, 31-33, 38, 136-144]. The grafting density and the molecular weight of the branches affect the movement of the backbone and the rheological responses of these complex macromolecules.

5.1 The rheological responses of densely branched brush polymer

The rheological responses of long chain branched polymers with relatively low grafting density have been well examined.[3, 11, 15, 18, 19, 25, 27, 31-33, 38, 136] In general, such polymers relax in a sequence with the grafted branches relaxing first, followed by the branching points, and the backbone subsequently reptates in a dilated tube. [15, 19] Side chains act as a solvent and decrease the rubbery modulus of the backbone. [11, 15] For polymers with shorter side chains and extremely high grafting density, similar to the long chain branched polymers, two rubbery plateaus are found in the dynamic master curves. [138-144] One corresponds to the relaxation of the side chains. A second, lower plateau with modulus value of approximately 1kPa is usually regarded as the rubbery plateau of the whole polymer. [137, 138, 140, 143] It is found that the modulus value of the lower plateau decreases with increasing side chain length and the entanglement molecular weights (M_e) of these densely branched brush polymers are extremely high. [140] The very low rubbery

modulus is attributed to the interactions between the densely packed side chains which causes the polymer backbones to be stiffened as the persistence length of the brush chain increases with increasing side chain density.[137, 139, 140, 145-147] A worm-like conformation is expected for this kind of brush polymer.[137, 148, 149] The stiffened chain conformation affects the inter chain interactions and increases the distance between entanglements. Prior studies were limited by the synthesis methods available to polymers with high backbone degree of polymerization (DP) but side chain length generally lower than 1/4 of the entanglement molecular weight of the corresponding linear polymer. [138, 140, 143] There are no prior systematic works investigating how the side chain length and backbone DP affect the rheological responses of the densely branched brush polymers. In the present investigation we take advantage of a new type of densely grafted brush polymer with narrow molecular weight distribution that is synthesized via ring opening metathesis polymerization (ROMP) of macromonomers (MMs). [150, 151] The resulting brush polymers possess low polydispersities (PDIs) in both backbones and side chains, and very high molecular weights (up to 6000 kDa). The MM synthetic approach ensures that each repeat unit in the backbone is grafted with a side chain, leading to very large branch to backbone ratios and a dense distribution of branching points. [128, 147, 148, 150, 151] We have synthesized polynorbornene-*g*-polylactide brush polymers with polylactide side chain length of 1/5, 1/2 and 1 entanglement distance of the corresponding linear polymer and the backbone degree of polymerization (DP) of 200, 400 and 800. In the following section, we first present our experimental methods and then show the results of dilute solution characterization of these densely branched brush polymers. This is followed by a presentation of the dynamic moduli of the materials and the temperature dependence of

the dynamics. We then discuss the sequential relaxation of these densely branched brush polymers covering the three ranges from the glassy relaxation through the Rouse-like relaxation regime of the side chains through the terminal regime which also shows the hallmark of unentangled Rouse-like behavior in spite of the high backbone DP of 800. Similar to what was originally shown by Plazek, [119, 120] the steady state recoverable compliance contributes to the long time dynamics of these unentangled or barely entangled materials.

5.1.1 Synthesis and molecular information of the densely branched brush sample

The polynorbornene-*g*- poly-(D, L)-lactide brush polymers used in this study were synthesized by previously described ring-opening metathesis polymerization (ROMP) of norbornenyl macromonomers (MMs) (Figure 5.1).[150] The molecular weights of the MMs and the brush polymers were controlled by the ratio of the monomer (or MM) to the initiator.

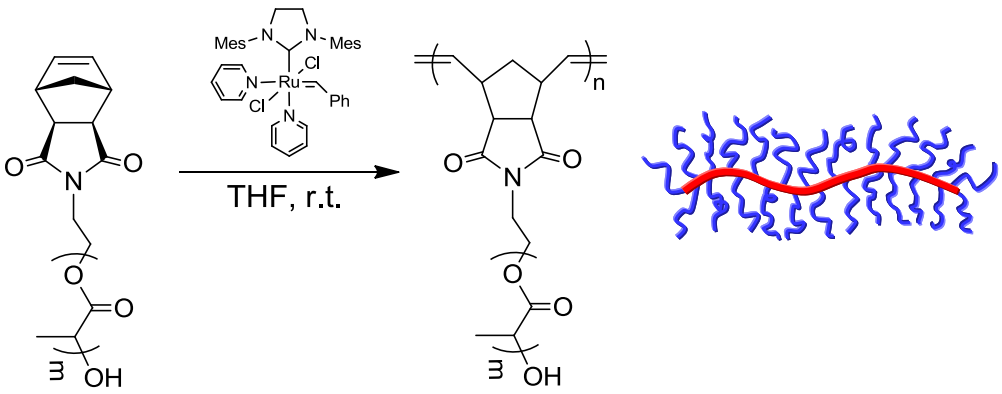

Figure 5.1. Scheme of the synthesis of polynorbornene-*g*- polylactide brush polymers and schematic of the resulting brush polymer.

The molecular weight of PLA brush polymers were determined by the GPC with the d*n*/d*c* values of 0.050 by assuming 100% mass elution from the columns. Detailed molecular weight information for the polymers are listed in Table 5.1.

Table 5.1 Sample molecular weight and characterization data

Sample number	M_{br} [a] (kDa)	DP [b]	M_w [c] (kDa)	PDI [d]	φ_{br} [e]
P(PLA1.4)-200	1.4	200	350	1.01	0.893
P(PLA1.4)-400		400	680	1.02	0.898
P(PLA1.4)-800		800	1510	1.04	0.900
P(PLA4.4)-200	4.4	200	840	1.02	0.951
P(PLA4.4)-400		400	2240	1.02	0.956
P(PLA4.4)-800		800	4880	1.03	0.958
P(PLA8.7)-200	8.7	200	1600	1.02	0.970
P(PLA8.7)-400		400	3660	1.08	0.975
P(PLA8.7)-800		800	6050	1.07	0.977

[a] M_{br} is the molecular weight of the side chains; [b] DP is the degree of polymerization of the backbone; [c] M_w is the molecular weight of the brush polymer determined by GPC-MALLS in THF; [d] Polydispersity index(PDI) of the brush polymer; [e] φ_{br} is the volume fraction of the side chain estimated by the group contribution method. [130]

5.1.2 Results and discussion.

5.1.2.1 Intrinsic viscosity.

The intrinsic viscosity ($|\eta|$) and molecular weight for these brush polymers with different side chain and backbone lengths were measured using GPC coupled with a light scattering detector and a viscometer. As shown in Figure 5.2, for the three groups of brush samples with fixed side chain molecular weight but increasing DP, the slope of $\log(|\eta|)$ vs $\log(M_w)$ decreases from 0.67 to 0.55 as the side chain molecular weight increases. Tsukahara [139] examined the intrinsic viscosity change for a series of poly(MM)s with different length polystyrene (PS) side chains. On the double logarithmic plot of intrinsic viscosity with the total polymer molecular weight, the intrinsic viscosity was found to be unchanged until a critical molecular weight value was reached. Then the

intrinsic viscosity was found to increase sharply and scale with the same Mark-Houwink parameter as that for PS in the same conditions. The critical molecular weight for the occurrence of this sudden viscosity change increased with side chain molecular weight. [139] In the present study, the slopes of log(|η|) vs log(Mw) are near and slightly lower than what is expected for PLA in good solvent, [126, 152] and the values decrease weakly with increasing side chain molecular weight. Though the data are limited, it appears likely that these polymers are above the region of their critical molecular weight.

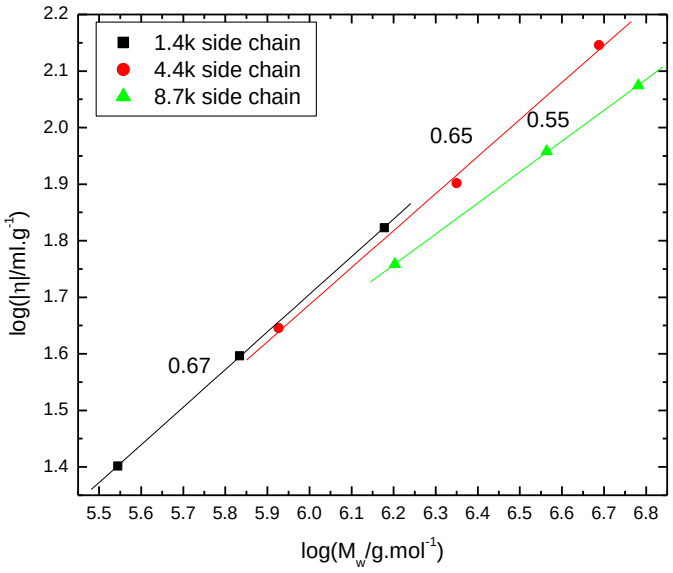

Figure 5.2. Intrinsic viscosity versus molecular weight for brush polymers with fixed side chain molecular weight but increasing DP (In THF at room temperature≈25°C).

The chain conformation of the densely grafted brush polymers can be estimated from their intrinsic viscosity data. The model proposed by Yamakawa[153-155] for the |η| and molecular weight of the bottle brush polymers was applied to analyze our data,

$$\left(\frac{M^2}{|\eta|_0}\right)^{1/3} = \Phi_{0,\infty}^{-1/3} A_0 M_L + \Phi_{0,\infty}^{-1/3} B_0 \left(\frac{\lambda^{-1}}{M_L}\right)^{-1/2} M^{1/2} \qquad (5.1)$$

M is the chain molecular weight; $|\eta|_0$ is the intrinsic viscosity for unperturbed conditions; $\Phi_{0,\infty}^{-1/3}$ is a constant; A_0 and B_0 are functions of the reduced hydrodynamic diameter; M_L is equal to M divided by the contour length (L) and λ^{-1} is the Kuhn length. For chains in good solvent, the expansion of the molecular dimension due to the excluded volume effect should be considered. The viscosity expansion factor is defined as $a_\eta^3 = |\eta|/|\eta|_0 = (1 + 3.8z + 1.9z^2)^{0.3}$, where z is the excluded volume parameter. As there is little knowledge about the values of the relevant parameters for the brush polymers used in the present study, we simply plotted the good solvent data of $(M^2/|\eta|)^{1/3}$ vs $M^{1/2}$ and from this plot estimated the change of M_L and λ^{-1} from the slope and the intercept (Figure 5.3).

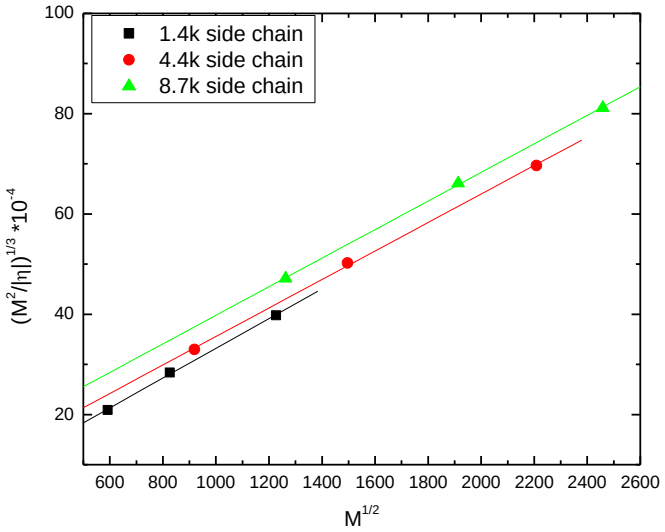

Figure 5.3. Plot of $(M^2/|\eta|)^{1/3}$ vs $M^{1/2}$ for the three groups of brush samples of different side chain length. (In THF at room temperature≈25°C).

In Figure 5.3, the three lines are nearly linear indicating that the influence of the viscosity expansion parameter is not very strong. The intercept ($\Phi_{0,\infty}^{-1/3} A_0 M_L$) values are 3.5×10^{-4}, 7.1×10^{-4} and 11.3×10^{-4}. Since in the equation $\Phi_{0,\infty}^{-1/3}$ and A_0 are a constant, this indicates that M_L increases with increasing side chain molecular weight ($M_{w,side}$ =1.4, 4.4

and 8.7kDa). As the molecular weight of the brush polymer is determined by the side chain molecular weight multiplied by the degree of polymerization (DP) of the macromonomers ($M_w \approx M_{w,side}$*DP), the contour length ($L=M/M_L= M_{w,side}/M_L$*DP) should be a constant value for brush polymers having the same DP. The slope values ($\Phi_{0,\infty}^{-1/3} B_0 (\frac{\lambda^{-1}}{M_L})^{-1/2}$) determined from Figure 3 for the three groups of samples are nearly constant, which implies that the Kuhn length (λ^{-1}) only increases with the side chain molecular weight and has a fixed value for brush polymers with the same side chain. If we assume the Kuhn length for the 1.4k side chain samples to be k_b, then the Kuhn length for the 4.4k and 8.7k side chain samples are $2.0k_b$ and $3.2k_b$, respectively. The results are similar to what has been well discussed in other work [139, 140, 145, 146, 156-158] for brush polymers with densely grafted branches and fixed side chain length. Due to the strong steric interactions between the side chains, the backbone becomes rigid and the Kuhn length of the branched polymer increases.

5.1.2.2 Dynamic responses of the brush polymers.

Figures 5.4a through 5.4c present dynamic master curves at 80^{o}C for the brush polymers having different DPs and side chain molecular weights over the full range from the glassy plateau to the terminal flow region. The master curves are presented as families of fixed backbone DP and varying side chain length. Within a given series of fixed backbone DP the curves are vertically shifted to separate the data for each different side chain length. The figures show clearly that from the glassy state to the terminal flow region, several different relaxation behaviors appear in sequence. In the following sections we plot the dynamic master curves in different ways and compare the influence

of side chain length and backbone DP to the sequential relaxation behaviors of these densely branched brush polymers.

In the terminal zone, most of the densely branched brush samples seem to behave in a Rouse-like manner. There is little evidence of entanglement. For linear polymer materials increasing the backbone length leads to a longer relaxation time and the terminal flow region will move to a lower frequency. [1] On the other hand, in Figure 5.4, if compare the brush samples with the same backbone DP, the terminal relaxation time not only depends on the DP of the polymer, but also increases with increasing side chain molecular weight. Similar phenomena have been observed for other brush or comb polymers with fixed backbone length and the influence of the side chains on the relaxation of the backbone was invoked to explain this phenomenon. [25]

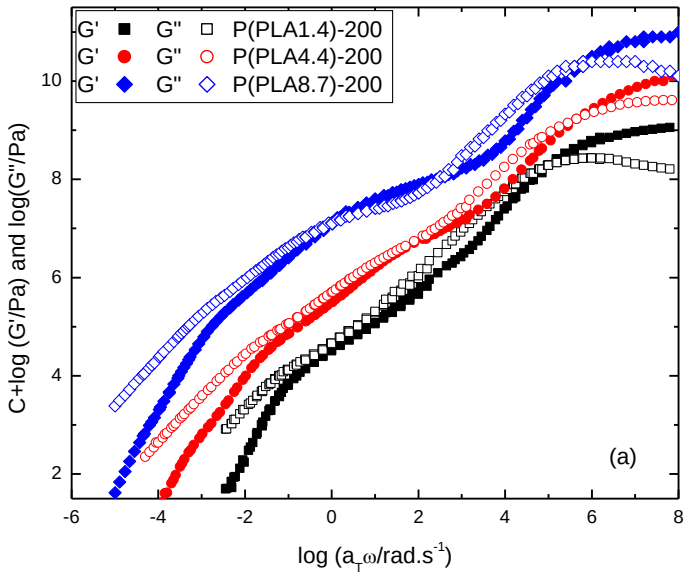

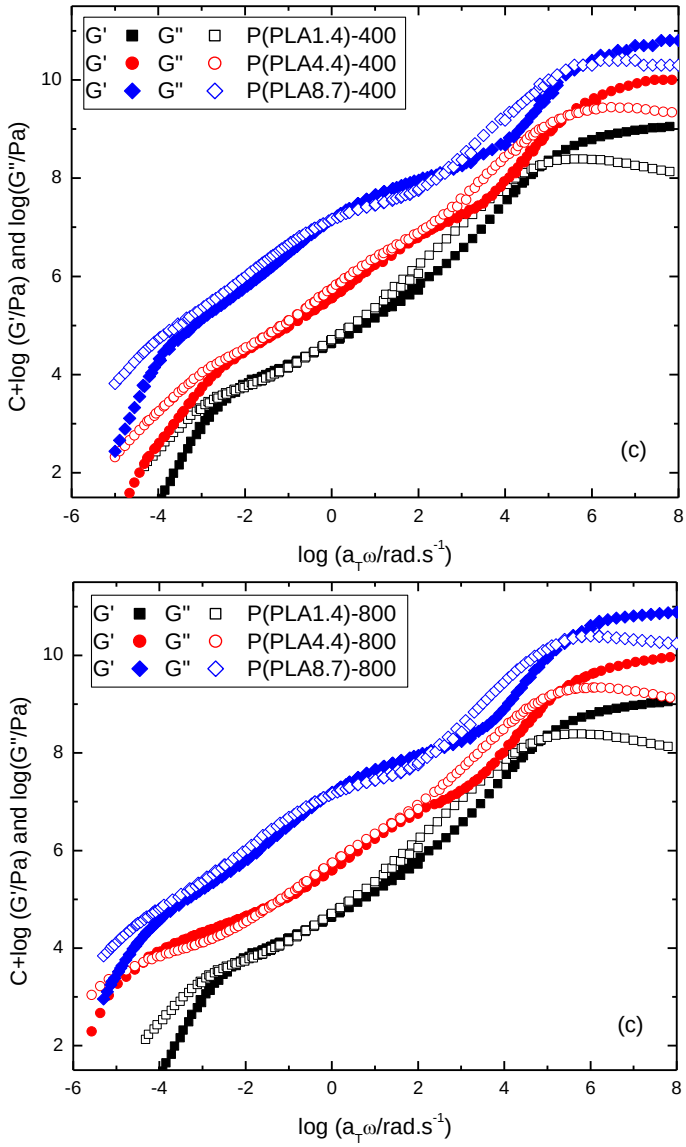

Figure 5.4. Comparison of the dynamic responses of the investigated brush polymers with fixed DP (200, 400 and 800). (Vertical shift of C=0, 1 and 2 used to separate the respective the curves)

For the samples with 4.4k and 8.7kDa side chains, two rubbery plateau regions can be observed in the dynamic master curve. Upon increasing side chain molecular weight, the first plateau from the glassy modulus region at intermediate frequencies becomes more obvious, while the second plateau gradually develops as the DP increases. The two plateau region phenomenon is referred to as a double relaxation mechanism

which is typical for brush, comb, or star polymers with long side chains. [3, 11, 15, 18, 19, 25, 27, 31-33, 38, 136]

To clarify the attribution of the two plateaus in the dynamic spectrum for the brush polymers with different side chain molecular weight, the dynamic master curves were plotted following the van Gurp-Palmen method [159] by plotting the phase angle (δ^o) vs the logarithm of the complex modulus |G*|. The van Gurp-Palmen plot is sensitive to the molecular weight and molecular architectures of the materials and provides an excellent tool to estimate the value of the plateau modulus [111]. The van Gurp-Palmen plots for the DP dependence and the side chain molecular weight dependence of several brush samples are shown in Figures 5.5a and 5.5b. Similar to the two plateau phenomenon discussed in relation to the dynamic curves, there are two minima in the phase angle (δ) vs log|G*|plot for most of the brush samples. As shown in Figure 5.5a, for the first minimum in the phase angle (δ) at higher modulus, the |G*| values and phase angle (δ) values are almost independence of the DP with fixed side chain molecular weight. While in Figure 5.5b, for fixed backbone DP and increasing side chain molecular weight, the |G*| values at the first minimum are almost fixed but the δ value decreases. In van Gurp-Palmen plots for linear polymers, as the molecular weight increases, the δ value will decrease and the |G*| values do not change [111]. Hence, Figures 5.5a and 5.5b suggest that the first minimum in the van Gurp-Palmen plot, which corresponds to the first plateau in the dynamic master curve, should be related with the relaxation of the side chains. The plateau modulus of the polylactide is reported to be approximately $5*10^5$Pa and the entanglement molecular weight is approximately 8.7kDa [160]. In Figures 5.5a and

5.5b the corresponding |G*|values for the first plateau is approximately $6.3*10^5$Pa, which is near to the plateau modulus value for the polylactide.

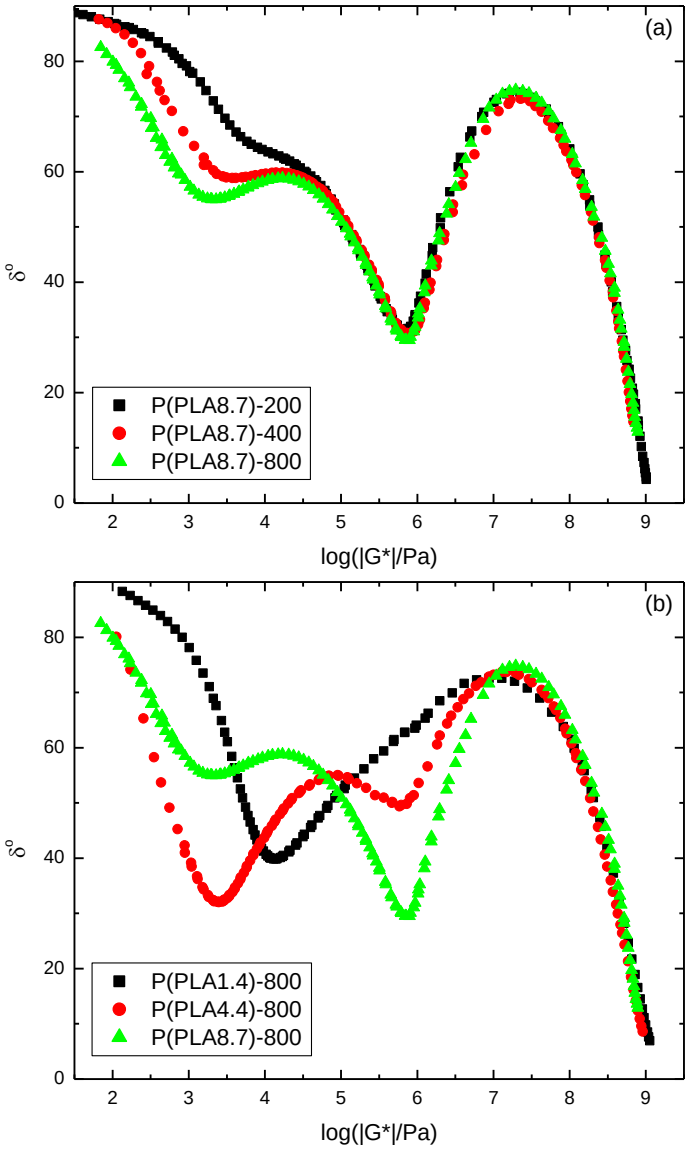

Figure 5.5. van Gurp-Palmen plot for brush polymers with (a) fixed side chain molecular weight and (b) fixed backbone DP

The second minimum in the van Gurp-Palmen plot gives a modulus value of approximately 2 to 5 kPa. For brush polymers with the same side chain molecular weight as shown in Figure 5.5a, the δ value at the second minimum decreases with increasing DP.

While for the polymers with the same DP but different side chain molecular weight (Figure 5.5b), the δ value increases with increasing side chain molecular weight. As discussed before, the side chains stiffen the backbone and increase the Kuhn length. We expect that the effect of the side chain on the conformation of the backbone also occurs in the melt [140] and these brush polymers of the same DP are unlikely to entangle as the side chain molecular weight increases. The second plateau should, thus, reflect the molecular weight and conformation change of the backbone and it should, consequently, correspond to the relaxation of the whole brush polymer. This lower plateau modulus phenomenon is similar to what has been reported for other poly(macromonomer) brushes [140, 143] with longer backbone but shorter side chain than our samples.

5.1.2.3 Sequential relaxation.

The branched polymers should relax sequentially. The chain segments should relax first, followed by the side chains, and the whole polymer should be the last to move.[15, 18, 19] To examine the sequential relaxation behaviors of the brush polymers, we plot the storage modulus (G') master curves of brush polymers having the same side chains shifted horizontally to match in the segmental regime. The slight horizontal shifting was applied to compensate for the modest differences in glass transition temperatures among the samples. As shown in Figure 5.6, the master curves can be divided into three regimes: the segmental regime, the arm regime and the terminal regime. For the brush polymers with the same side chains, when their glass transition regions are shifted together, the arm regimes overlap with each other very well. The length of the arm regime increases with increasing side chain length. In the terminal region, the curves

start to deviate from each other moving to lower frequency as the DP of the backbone increases.

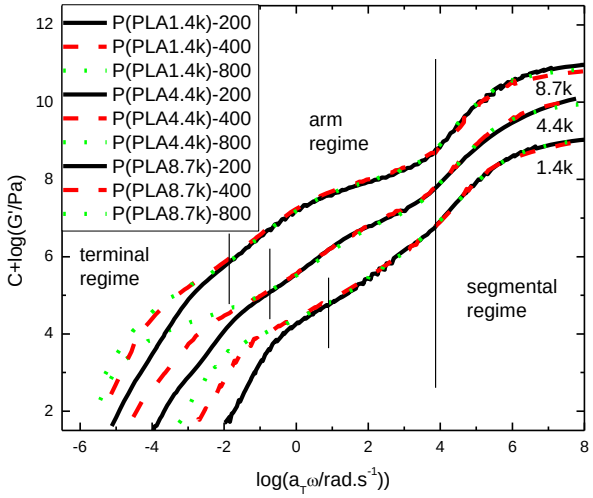

Figure 5.6. Sequential relaxation of the brush polymers. (Vertical shift of C=0, 1 and 2 used to separate the respective the curves)

5.1.2.4 Temperature dependence of the dynamic responses.

Figure 5.7 depicts the temperature shift factors for the three groups of brush polymers with the reference temperature T_{ref}= 80^{o}C. We fit the shift factors with the WLF equation [113] to obtain the fitting parameters C_1 and C_2 at the reference temperature of 80^{o}C.

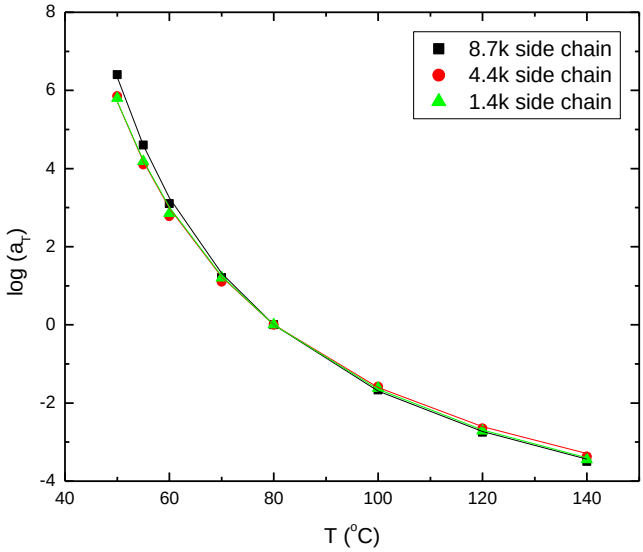

Figure 5.7. Temperature shift factors for brush polymers with different side chain molecular weight (1.4k, 4.4k and 8.7k Da) at the reference temperature of 80°C

Following the analysis method discussed before, the values for C_1^g, C_2^g, fragility index (m), apparent activation energy (E_g), and glass transition temperature (T_g) of the brush polymers are estimated and listed in Table 5.2.

Table 5.2 WLF fitting parameters, fragility, apparent activation energy and glass transition temperature determined from the dynamic modulus data for the brush polymers.

	C_1^g [a]	C_2^g [a] (K)	m [b]	E_g [c] (kJ/mol)	T_g [d] (K)
P(PLA1.4)-200	11.22	41.58	88.6	556.4	328.2
P(PLA1.4)-400			88.5	556.1	328.1
P(PLA1.4)-800			88.7	557.8	328.6
P(PLA4.4)-200	11.5	36.06	103.7	645.7	325.2
P(PLA4.4)-400			103.8	646.8	325.5
P(PLA4.4)-800			104.0	649.6	326.2
P(PLA8.7)-200	12.05	34.92	112.5	702.5	326.1
P(PLA8.7)-400			112.4	701.2	325.8
P(PLA8.7)-800			112.7	705.1	326.7

[a] C_1^g and C_1^g are the WLF fit parameters for the brush samples with reference temperature at the glass transition temperature; [b] m is estimated with equation 2; [c] E_g is estimated with equation 3; [d] T_g is the mechanical glass transition temperature at 100s relaxation time.

For these brush polymers the fragility values increase with increasing side chain molecular weight, which means the polymer molecules become less flexible as the side chain length increases.[117] As discussed in the section on intrinsic viscosity, the strong interactions among the side chains stiffen the backbone and increase the Kuhn length. [139, 140] Here in bulk, we see similar influence of the side chain to the conformation of the polymers. Unlike the work done by others on poly(macromonomers)[140] or comb polymers[161], the glass transition temperatures (T_g) of our samples are not greatly affected by the side chain length. The glass transition temperature (T_g) and fragility (m) for polylactide are reported to be 323K and 69.6, respectively. [162] The T_g values estimated for these brush polymers are close and within the glass transition temperature range expected for linear polylactide [126], which seems to confirm that the side chain properties determine the glass transition behaviors of these poly(macromonomers) [140]. However, it is worth remarking that there is a large difference in the fragility index m between the brushes and linear polylactide material, which remains an area for further investigation.

5.1.2.5 Segmental regime.

The segmental regime covers the glassy and glass transition region of the brush polymers. The glass transition behaviors of these brush polymers have been discussed in the previous section. If one compares the curves in Figure 5.6 and Figure 5.8, the side chain length and backbone DP have only minor effects on the glassy moduli (G_g). The glassy modulus value of the brush polymer is around 10^9 Pa which is much higher than that of polynorbornene and is closer to that of linear polylactide. [126]

5.1.2.6 Arm regime.

Figure 5.8 shows an expanded plot of the arm regime for the brush polymers with shifting the polymers with the same DP together. By shifting the samples with the same backbone DP together, the influence of arm length on the relaxation behavior of the brush polymer can be readily demonstrated. For each group of samples with the same backbone DP, a clear plateau is seen for samples with the 4.4kDa and 8.7kDa side chain. The plateau values are $6.3*10^5$ and $6.2*10^5$ Pa, which are independent of the arm length and backbone DP. This regime is missing or difficult to detect in the samples with the 1.4 kDa side chain molecular weight.

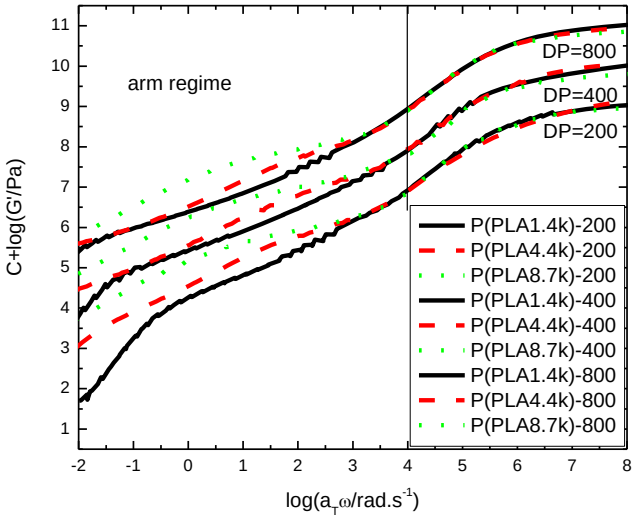

Figure 5.8. Expanded plot of the arm regime and segmental regime for the brush polymers with fixed DP. (Vertical shift of C=0, 1 and 2 used to separate the respective DP curves)

To further analyze the plateau found in the arm regime, the retardation spectra ($L(\tau)$) of the different brush polymers were calculated. The retardation spectra of the brush polymers with the same 200 backbone DP but different side chain molecular weight are plotted in Figure 5.9. Horizontal shifting was applied to overlap the glassy regions and eliminate the effects of the differences between the glass transition

temperatures. According to Plazek, [1, 119, 120] in the retardation spectra of entangled polymers, there are usually two peaks with equivalent height. The length between the two peak points corresponds to the length of the rubbery plateau.

In Figure 5.9, only one peak is found in the retardation spectra. With the increase of the side chain molecular weight, a shoulder plateau region and increases in length. If one integrates the retardation spectrum over the relaxation time (τ), the shoulder region in the spectrum corresponds to the side chain relaxation as seen in the dynamic curve. The length of the shoulder region can be estimated as the distance between the glass transition region and the transition region from arm relaxation to the terminal relaxation. If the side chains are entangled, then the length of the shoulder plateau should increase with the 3.4 power of molecular weight. [119] However in Figure 9, the relaxation time only scales approximately as the 2.3 power of the side chain molecular weight, which is consistent with the side chains being unentangled, Rouse-like chains. The unentangled nature and Rouse-like behaviors of side chains are similar to the treatment of the side chains in some current model predictions [11, 19, 34, 35].

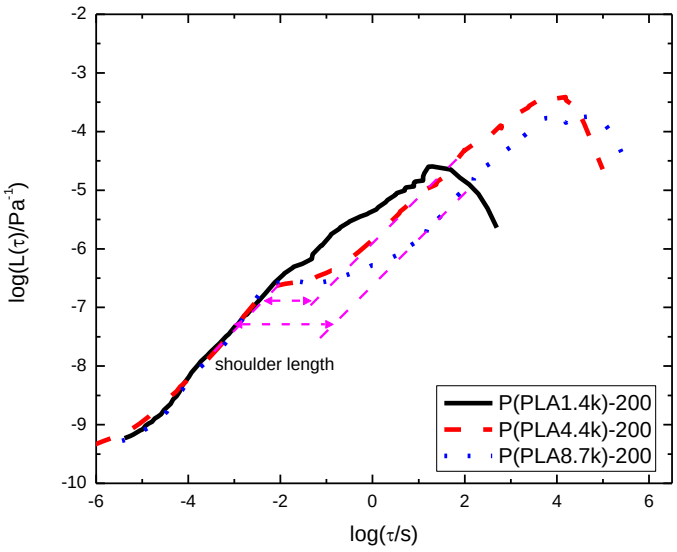

Figure 5.9. Double logarithmic representation of the retardation spectra (L(τ)) for brush polymers with fixed 200 DP backbone and different side chain molecular weights.

5.1.2.7 Terminal regime.

Figure 5.10 presents an expanded plot of the terminal regime and shows the relaxation behavior of the backbone. In the plot, a not very obvious plateau in the storage modulus curve can be found for each sample. This plateau corresponds to the second plateau found in the van Gurp-Palmen plot discussed previously. The modulus values for this plateau can be accurately estimated from the van Gurp-Palmen plot (Table 5.3). For a polymer network, the shear modulus can be expressed as, [7]

$$G = \upsilon kT = \frac{\rho RT}{M_s} \qquad (5.2)$$

υ is the number of network strands per unit volume which is the inverse of the molecular weight of the structure (M_s) included in the relaxation process. In the terminal regime, the whole polymer molecule relaxes. Thus the modulus value should decrease following the same ratio of the increasing DP. As shown in Table 5.3, the plateau modulus values decrease with increasing DP. If we take the modulus value of the 800DP samples as the reference and mark it as $G'_{1.4}$, $G'_{4.4}$ and $G'_{8.7}$, respectively for different side chains. Then

it can be found that, the storage modulus values decrease nearly linearly with increasing DP.

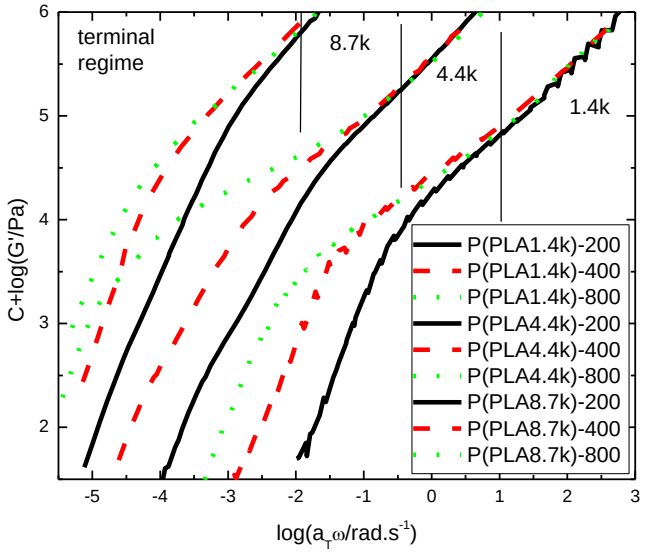

Figure 5.10. Expanded plot of the terminal regime for the relaxation of the brush polymer with fixed side chains. (Vertical shift of C=0, 1 and 2 used to separate the curves)

The plateau shown in Figure 5.10 looks like a rubbery plateau for the brush polymers. However, for an entangled polymer material, the rubbery plateau modulus should be a constant value and independent of the DP. [1] To further examine this, the steady state recoverable compliance (J_s) values for the brush polymers were estimated from the creep experiment data with the equation, $J(t)= J_R(t)+t/\eta$. The J(t) is the shear creep compliance and η is the steady shear viscosity. $J_R(t)$ is the recoverable compliance. According to Plazek [119, 120], for not well entangled polymers, the plateau or shoulder observed in the dynamic modulus data is not the rubbery plateau. It simply reflects the thermal entropy of the molecular orientation and is not the entropy due to the deformation of the chain entanglement network. The storage modulus value that appears to be a rubbery response in unentangled or lightly entangled linear polymers is indeed the

inverse value of the steady state recoverable compliance (J_s). The $G_b'J_s$ is expected to equal 1, and $\log(G_b')$ is equal to the negative $\log(J_s)$. The value of G_b' on this lower plateau is readily estimated from the van Gurp-Palmen plot. If it is the rubbery plateau, theoretically it should be twice the reciprocal of the steady state recoverable compliance ($G_N^0=2/J_s$). [1] Thus if the plateau associated with the backbone (G'_b) is not the rubbery plateau, then we expect $\log(J_s) = -\log(G'_b)$. The log values of plateau modulus (G'_b) in the terminal regime estimated from the van Gurp-Palmen plot and steady state recoverable compliance (J_s) obtained from the creep experiments are listed in Table 5.3.

Table 5.3 Estimated backbone plateau modulus (G_b') and steady state recoverable compliance (J_s) for the brush polymers at 80°C

	$\log(G_b')$ [a]	$\log(J_s)$ [b]	G'_bJ_s	G_b' ratio [c]
P(PLA1.4)-200	4.64	-4.55	1.2	$3.3G'_{1.4}$
P(PLA1.4)-400	4.38	-4.26	1.3	$1.8G'_{1.4}$
P(PLA1.4)-800	4.12	-3.96	1.4	$1.0G'_{1.4}$
P(PLA4.4)-200	4.11	-4.08	1.1	$5.2G'_{4.4}$
P(PLA4.4)-400	3.72	-3.62	1.3	$2.1G'_{4.4}$
P(PLA4.4)-800	3.39	-3.24	1.4	$1.0G'_{4.4}$
P(PLA8.7)-200	3.96	-3.94	1.0	$4.6G'_{8.7}$
P(PLA8.7)-400	3.62	-3.24	2.4	$2.1G'_{8.7}$
P(PLA8.7)-800	3.30	-3.07	1.7	$1.0G'_{8.7}$

[a] the plateau modulus in the terminal regime estimated using the van Gurp-Palmen plot, [b] steady state recoverable compliance estimated from the creep data, [c] the ratio of the plateau modulus with different DP.

As shown in Table 5.3, the value of G'_bJ_s is generally near to Plazek's prediction of 1 for unentangled polymer chains. Thus the backbone plateaus found in the dynamic curves reflect the thermal entropy of the chain orientation for these stiffened polymers and the plateaus observed are not due to the entanglement entropy.

From above discussion, we did not observe any sign of entanglement in both the arm regime and the terminal regime. Then for these brush polymers of very high molecular weight, are they all Rouse chains? Figure 5.11 shows the change of the steady state recoverable compliance with DP on a double logarithmic scale. It is assumed that side chains can act as a solvent to dilute the polymer backbone. [11, 15] While for linear polymers, solvent dilution effect will increase the J_s values. [163] From Figure 5.11, we see that for the brush polymers with the same backbone DP, the J_s values increase with side chain length. This shows the increasing dilution effect with side chain length. For the brushes with the same side chain molecular weight but different DP, the steady state recoverable compliance (J_s) increases with DP, and the J_s value is expected to approach a plateau at higher DP. This seems to be the case for the 1.7 kDa and 8.7 kDa side chain brushes, but is less clear for the 4.4 kDa samples. Such a trend is similar to what is expected for linear chains [48] and is consistent with these brushes being in the transition zone from the Rouse like chain to the fully entangled melt.

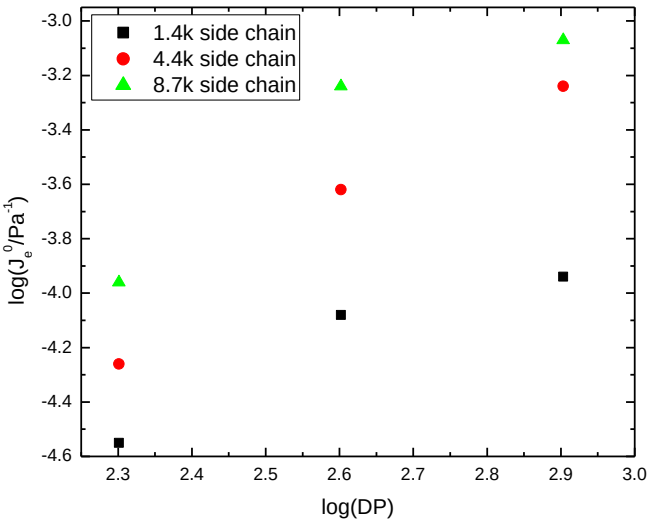

Figure 5.11. Double logarithmic representation of steady state recoverable compliance (J_s) vs. DP for the three groups of brush polymers studied.

To further clarify the entanglement conditions for the brushes in the melt, the zero shear viscosities (η_0) at Tg+30°C for the three series of samples were plotted against their weight average molecular weights (M_w) and this is shown in Figure 5.12. The viscosity data can be described with a line with a slope of approximately 1.7, which also indicates that these brush samples are in the transition zone from the unentangled near linear dependence on M_w towards but not reaching entangled behavior. [1]

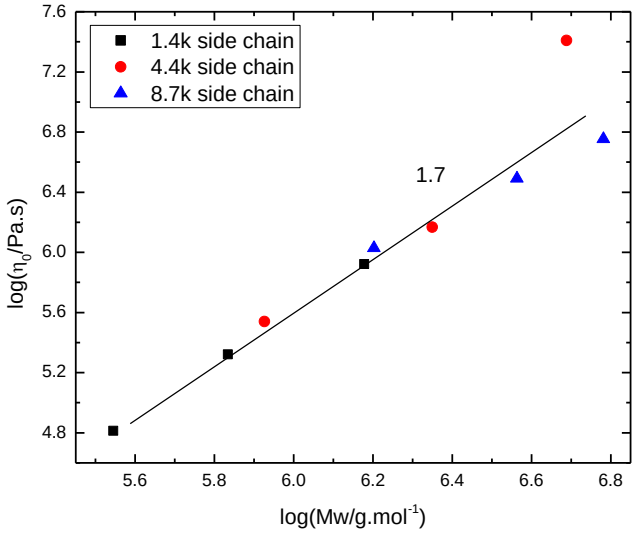

Figure 5.12. Double logarithmic representation of zero shear viscosity (η_0) at Tg+30°C vs. weight average molecular weight (M_w) for the three groups of brush polymer samples with different side chain lengths.

5.1.3 Summary and Conclusions

In this work, three series of densely branched polymers with uniform side chain length and uniform branching point distribution were synthesized via the polymerization of macromonomers using ROMP. Compared with other brush densely grafted polymers, these novel brush polymers have lower polydispersity and a complete grafting of side chains on every backbone repeat unit. The backbone DP of these special brush polymers is in the intermediate range, but the side chains are longer than what had been examined in others' work. Dilute solution characterization shows that the strong intermolecular

forces between the side chains cause the Kuhn length of the polymer backbone to increase as the side chains get longer. The densely branched brush polymers with the same backbone DP have the same contour lengths.

A sequential relaxation framework was applied to analyze the relaxation behaviors of these brush polymers. The dynamic modulus master curves of these dense brush polymers were divided into three regions, the segmental regime, arm regime and the terminal regime. Two plateaus were found in the dynamic master curves for the brush polymer with 4.4kDa and 8.7kDa side chain. One is in the arm regime and corresponds to the relaxation of the side chain. The other one is in the terminal regime and is related to the movement of the backbone. This double relaxation process phenomenon with one plateau being much lower than the other one is similar to what had been found in other brush polymers with similar structures.

Side chain properties affect the relaxation behavior of the whole brush polymer. For brush polymers with the same side chains but different backbone DP, their arm and segmental regimes are almost identical. The glassy modulus and glass transition temperature are near to the values for the polylactide side chains. The molecular weights of the brush polymers are huge and the side chains are long, however neither the side chains nor the whole polymer show evidence of entanglement. The Rouse-like behaviors of the side chain in the arm regime are confirmed by analyzing the retardation spectra.

A very low modulus plateau can be found in the terminal zone. Both the backbone DP and the arm length can affect the plateau value. Further analysis shows that the plateau is related to the relaxation of the backbone and is not the entanglement or rubbery plateau. It is the inverse value of the steady state recoverable compliance and only

reflects the thermal entropy of the molecular orientation. The unentangled nature of these brush polymers was further confirmed by the zero shear viscosity in the melt state. The slope of the zero shear viscosity vs weight average molecular weight is much smaller than 3.4, being 1.7, i.e., although having very large molar masses these brush polymer chains remain unentangled.

5.2 The rheological responses of linear wedge polymer

Polymer architecture has long been known to greatly affect the rheological properties of polymer materials. The brush polymer is a unique type of graft polymer possessing a very high density of regularly spaced side chains along the backbone, and has become a subject of active research in the field of molecular rheology due to its interesting architecture [19, 34, 140]. The number and the molecular weight of the branches affect the movement of the backbone and the rheological responses of these complex macromolecules.

Side chain structure has a complex effect to the viscoelastic properties of branched polymers. In the glassy state, with a huge side chain, the glass transition temperature of the branched polymer can be either increase of decrease depending on size, length, branching density or polarity of the side chain structure. [140, 161, 164, 165] The bulk side chain or pendent will make the backbone less flexible and increase the glass transition temperature, while longer side chain will introduce more free volume to the polymer material system and lower the glass transition temperature. In melt, the bulk side chain will affect the entanglement condition between polymers. It will act as a solvent to dilute the backbone and the lower the plateau modulus and viscosity of the

branched polymers. [2, 11, 15, 19, 25, 31, 33, 35, 37, 38] Side chain structure can affect other properties like melting point, density and mechanical modulus of branched polymer materials. [166] Recently, a new kind of brush polymer with densely branched side chains has been synthesized via ring opening metathesis polymerization (ROMP) of macromonomers (MMs)[100, 150, 151]. The MM approach to the synthesis ensures that each repeat unit in the backbone is grafted with a side chain structure, leading to very large branch to backbone ratios and a dense distribution of branching points. [100, 148, 150, 151] Due to the interactions between these dense packed side chains, the polymer backbones are stiffened and the persistence length of the brush chain increases with increasing side chain density.[139, 140, 145, 146, 167] A worm-like conformation is expected for this kind of brush polymers.[148, 149] The stiffened chain conformation also affects the inter chain interactions and increases the distance between entanglements. Rheological study of brush polymers has shown that the molecular chain relaxation is similar to other long chain branched polymers and the rubbery plateau of the polymer backbone is very low. [138, 141-144, 168-170]

In this work, a series of densely branch polymers with fixed branch structure but different backbone DP were synthesized via the ROMP method. These branched polymers were named as wedge polymer. The rheological responses of the wedge polymer from glassy to melt state were reported. The influences of side chain structure to the glassy and rubbery modulus were examined and compared with other branched polymers.

5.2.1 Polymer Synthesis

The wedge polymers used in this study were synthesized by previously described ring-opening metathesis polymerization (ROMP) of norbornenyl macromonomers (MMs) (Figure 5.13).[150] The molecular weights of the MMs and the wedge polymers were controlled by the ratio of the monomer (or MM) to the initiator. Side chain structures occupy for a large volume fraction of the monomer.

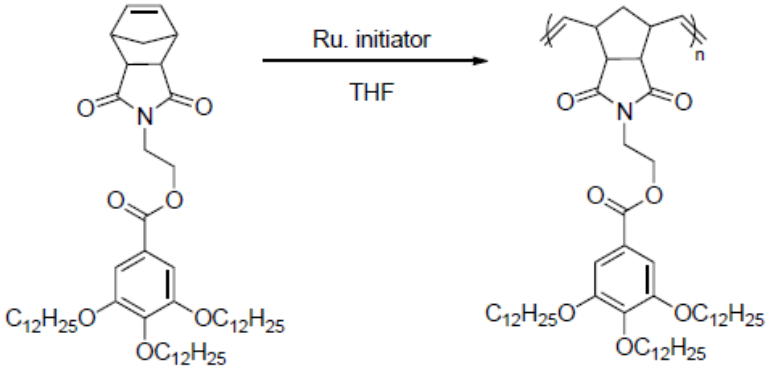

Figure 5.13. Scheme of the synthesis of wedge polymers.

The molecular weights of the wedge polymer were determined by the GPC with the d*n*/d*c* values of 0.110. Detailed molecular weight information is shown in Table 5.4.

Table 5.4 Molecular weight and characterization data for linear wedge sample

Sample number	DP [a]	M_w [b] (kDa)	PDI [c]	φ_{br} [d]	T_g [e] (^oC)
273-2	699	1164	1.93	0.876	42.2
221A	1406	1347	1.11	0.876	42.9
273-1	1001	2815	3.26	0.876	42.8
221B	5314	5713	1.25	0.877	43.4

[a] DP is the degree of polymerization of the macromonomers (MMs); [b] M_w is the molecular weight of the wedge polymer determined by GPC-MALLS in THF; [c] Polydispersity index(PDI) of the wedge polymer; [d] φ_{br} is the volume fraction of the side chain was estimated by the group contribution method [129, 130]. [e] The glass transition temperature (T_g) of the wedge polymer determined from the dynamic temperature ramp curve.

5.2.2 Result and discussion

5.2.2.1 Chain conformation in solution.

The radius of gyration (R_g) of the wedge polymer with different backbone DP was measured using GPC coupled with a light scattering detector. As shown in Figure 2, the size of the wedge polymer increase as the molecular weight get higher and the slope for the log(R_g) vs log(Mw) is 0.75, which indicate that the THF is a good solvent for the wedge polymer at room temperature.

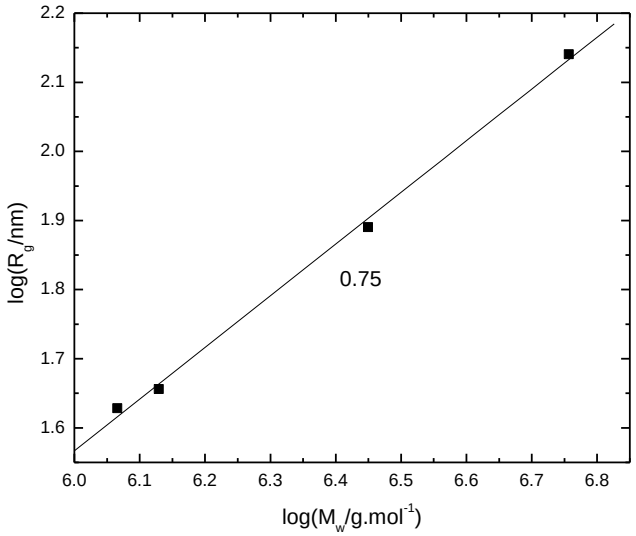

Figure 5.14. The radius of gyration (R_g) change for wedge polymer with different molecular weight in THF at room temperature (≈25°C)

5.2.2.2 Dynamic responses of wedge polymer.

Figure 5.15 shows the dynamic master curve for the four wedge polymer with different molecular weight at the reference temperature of 80°C. In the terminal zone, the relaxation time gets longer with increasing DP or molecular weight of the wedge polymer. A clear rubbery plateau can be well determined in the rubbery region and the value of the rubbery plateau (G_N^0) is around $1.3*10^5$ Pa. The entanglement molecular weight (M_e) can be estimated with the equation, [1]

$$G_N^0 = \upsilon kT = \frac{\rho RT}{M_e} \qquad (5.3)$$

, the estimated M_e is around $2.26*10^5$ g/mol. Thus the number of entanglement of the wedge polymer examine in this work is between 4 to 53.

The wedge polymer is a branched polymer with polynorbornene backbone and a unique branch structure. Within the experimental temperature range, the measured glassy modulus of the wedge polymer is near 10^8Pa. Mather et. al. [171] measure the tensile storage modulus (E') and loss modulus (E") of polynorbornene at different temperature. At the temperature of -20°C, which is the lowest temperature in our experiments, the E' is around $8*10^8$ Pa. If estimated the shear modulus from the tensile modulus using the passion ratio, the storage modulus (G') for linear polynorbornene is around $3*10^8$Pa. Influenced by the large side chain structure, the wedge polymer exhibit a much lower glassy modulus than the linear polynorbornene.

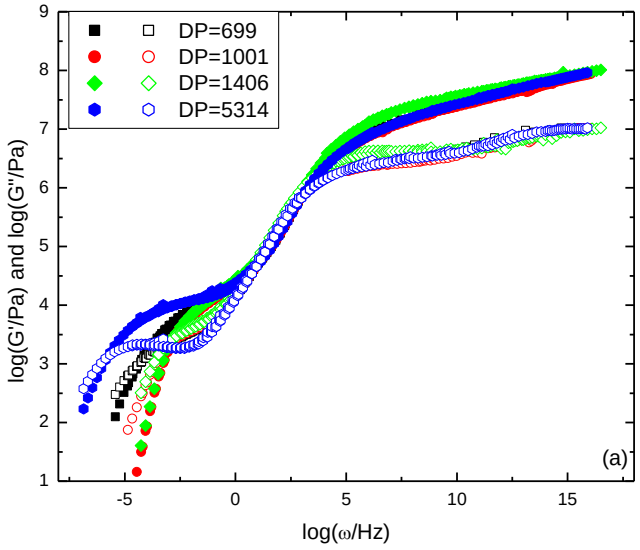

Figure 5.15 The dynamic master curve for wedge polymer with different backbone DP at the reference temperature of 80°C

Figure 5.16 is the shift factors to construct the dynamic master curve. The shift factors for the four samples are almost the same. The shift factor data at the temperature

above the glass transition temperature of the wedge polymer can be well fitted by the Williams-Landel-Ferry (WLF) [113] equation. The shift factor points begin to deviate from the WLF fitting curve when temperature is lower than their glass transition temperature and the materials are out of their equilibrium state.

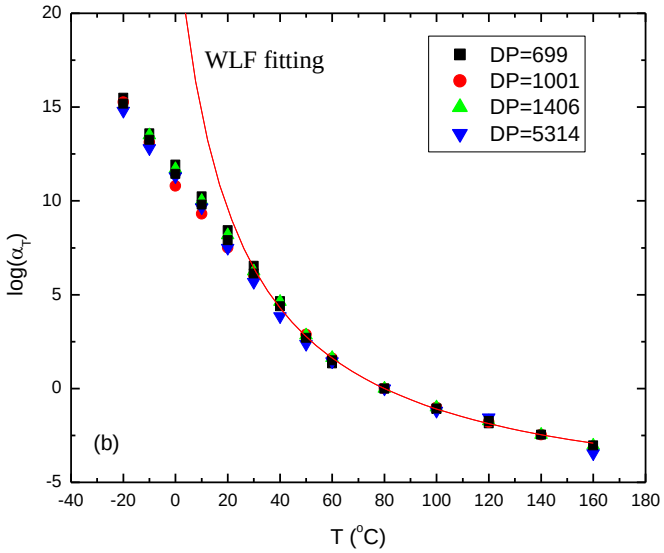

Figure 5.16. The shift factors for wedge polymer with different backbone DP at the reference temperature of 80°C

According to the principle of time (frequency)-temperature superposition, the temperature dependence of the G' (ω) and G"(ω) (G' (ω) and G"(ω) vs T) at the frequency of ω=0.01Hz (τ=1/ω) was converted from the dynamic master curve (G' (ω) and G"(ω) vs ω) with the WLF equation and used to determine the glass transition temperature (T_g) for the relaxation time of 100 seconds. T_g was estimated from the peak of the tan(δ) curve in the dynamic modulus thermal spectrum (Table 5.4). As shown in Table 5.4, the T_g for the wedge polymer is around 42°C and the T_g for polymer with the highest DP is higher than those of polymers with lower DP. In literature the glass

transition temperature for the polynorbornene is around 35°C. [126, 172] The wedge polymers are branched polynorbornene with bulk side chain. Influenced by the bulk side chain, the glass transition temperature of the wedge polymer is higher than linear polynorbornene. We fit the shift factors with the WLF equation at the reference temperature set to T_g to estimate the C_1^g and C_2^g. The fragility (m) of the wedge sample can be estimated with equation, [1, 117]

$$m = \frac{C_1^g T_g}{C_2^g} \qquad (2)$$

The fragility of the wedge polymer is around 45, which means the backbone of the samples is flexible.

5.2.2.3 Zero shear viscosity of the wedge polymer.

Figure 5.17 shows the increase of zero shear viscosity for the wedge polymer with different molecular weight. The scaling parameter of the molecular weight with zero shear viscosity is around 3.4, which is similar as what is expected for entangled linear polymers.

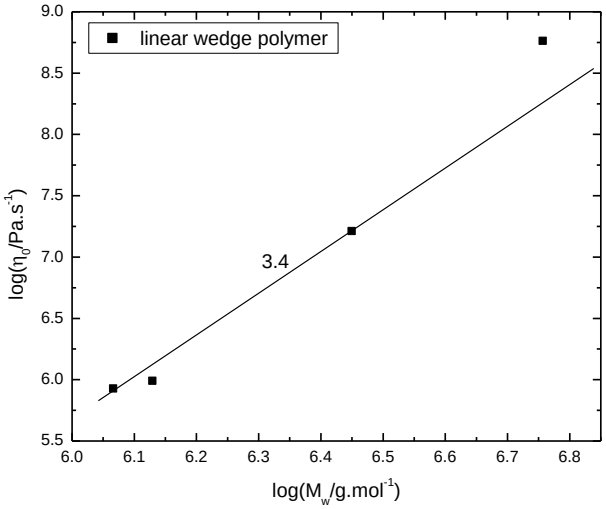

Figure 5.17. The zero shear viscosity for the wedge polymer at the reference temperature of 80^{o}C

Figure 5.18 shows the retardation spectrum for the linear wedge polymers with different backbone DP. Influence by the huge side group or side chain, similar as the PLA brush polymer, we see a sharp increase in the L value before the sample get into the terminal zone. From the slope of the logL vs logτ, the linear wedge reptate following what is predicted by the reptation model.

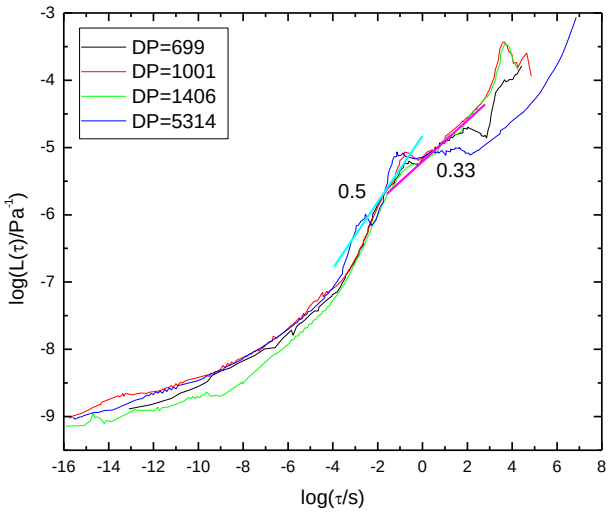

Figure 5.18 The retardation spectrum of Linear wedge polymer

5.2.3 Conclusion

In conclusion, a series of wedge polymer with bulk side chain and polynorbornene backbone were synthesized via the poly(macromolecules) method. The fragility value indicates the wedge polymer is a flexible polymer. Affected by the bulk side chain structure, the glass transition temperature of the wedge polymer is higher than the linear polynorbornene. The wedge polymer shows a much lower glassy modulus around 10^{8}Pa.

5.3 The influence of side chain structure to the viscoelastic properties of brush polymer

In this work, three kinds of brush polymers (PLA brush, wedge, dendronized) with the same backbone structure were synthesized via the macromonomer method. Even thought for the structure of linear dendronized polymer is not perfect and some side chain structures were break off from the backbone. It still can be very useful to compare with other linear brush polymer with the same backbone structure. For PLA grafted linear polymers, with increasing of the side chain molecular weight, the large portion of side chain gradually determine the viscoelastic properties of this complex molecule. To simply study the influence of side chain structure to the viscoelastic properties of brush polymers, we choose the sample with the highest backbone DP and shortest side chain length, which should get slightly entangled and the side chain should still influence not determine the viscoelastic properties of the polymer. Considering the differences in their glass transition temperature, we normalized the three samples in one van Gurp-Palmen plot (Figure 5.19). As shown in the plot, the plateau modulus values of the three samples are near, but the glass transition behavior and the glassy modulus of them are quite different.

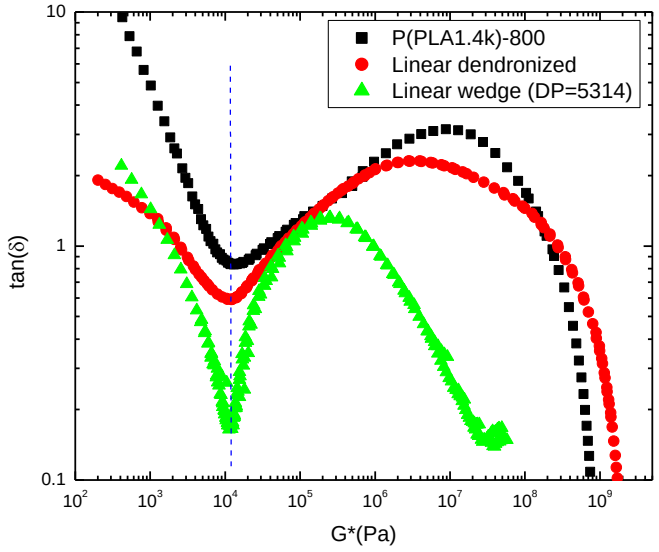

Figure 5.19 The van Gurp-Palmen plot of linear brush polymer with different side chain structure.

Figure 5.20 is the temperature dependence of the three samples with shifted to the same reference temperature. The three samples show quite different temperature dependence. The shift factors can be fitted with the WLF equation and the glass transition temperature and fragility values can be estimated and listed in Table 5.5. From the fragility value it can be found that the wedge sample is more flexible than the linear dendronized sample and PLA brush sample. This trend is similar as the steric hindrance differences between the three samples. Influenced by the differences in flexibility of the side chain structures, the glass transition temperature of the brush samples increased as the chain flexibility decreased.

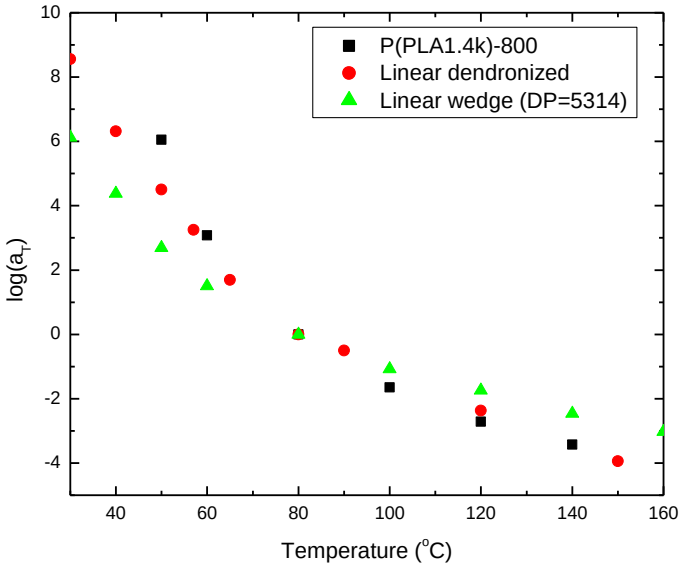

Figure 5.20 The shift factors for linear polymers with different side chain structures with the same reference temperature 80°C

Table 5.5 Compare the glass transition temperature and fragility of linear polymer with different side chain structure

Sample	T_g (K)	C^1_g	C^2_g (K)	m	E_g (kJ/mol)
P(PLA1.4k)-800	55.6	11.22	41.58	88.7	557.8
Linear dendronized	45.5	15.25	79.46	61.1	227.16
Linear wedge (DP=5314)	43.4	11.57	79.78	45.5	275.37

5.4 Summary and Future work

Polymerization of brush or branched polymer with uniform side chain/group structure via the ROMP of macromonomer provides a promising way to fabricate the structure of novel polymers. In this work, we studied the viscoelastic properties of PLA brush, wedge and dendronized polymer with regular side chain structure. Side chains play

an important role in the relaxation of this complex polymer, they can either increase the space between polymer chains and dilute the polymer backbone or make the polymer backbone more rigid and lower their plateau modulus. The large volume fraction of side chain will also influence the glassy behavior of these linear polymers. It is found that the flexibility of the side chain will influence the glass transition temperature of the brush polymer and determine their glassy modulus.

For the PLA brush polymer, due to the difficulty to get even higher backbone DP, the samples didn't get quite entangled. In future, if we can use some more active catalyst to get PLA brush with higher backbone DP, the work on the PLA brush sample would be more complete. Usually, the side chains are treated as Rouse chains in the relaxation of brush polymers. Only for star polymer, the side chains are treated to be entangled chain. The architecture of the densely branched brush polymer looks like an extended star polymer. For the PLA brush, the molecular weight of the side chain is high, but it is not high enough to get entangled. If we can get some brush polymer with both side chain and backbone can get entanglement, it will help us to further understand the relaxation of this complex molecule. By comparing the glassy behavior of PLA brush, wedge and dendronized polymer, we see the influence of side chain flexibility or side chain chemical nature to the glassy modulus or glass transition temperature. In future, if we can get a series of bulk side chain structure with near chemical composition but different flexibility or near flexibility but different chemical composition (polarity), it should help to determine that whether it is the chain flexibility (inter chain interaction) or the chemical structure (intra chain interaction) will determine the glassy modulus.

Chapter VI:
Future work

In this work, we studied the viscoelastic properties of two kinds of polymer materials, macrocyclic polymer and densely grafted polymer. The macrocyclic polymer or polymer rings are prepared by the new catalyst using the REMP methods. However, the rheological studies show that the polymer rings are not pure rings. They all get some linear chain contamination. We and our collaborator in Caltech tried to get pure polymer rings by studying the reaction mechanism and changing the monomer structure. The purity of the polymer rings get improved by still not 100% pure and the "threading effect" introduced by the linear chain contamination still great affect the property of the polymers rings. Fractionated precipitation has been found to be not capable enough to purify the polymer ring samples prepared by the REMP method. And the separation process of using crown ether to remove linear chain from the polyammonium rings is hard to get large amount of pure samples. The LCCC methods seems to be very effective to separate linear and ring polymers, but based on current reported data, its efficiency and validity is still questionable. Based on our knowledge on the REMP method, future work should focus on finding new method to purify the polymer ring samples. We can alter the structure of the polymer rings and use the possible physical property differences, like crystallinity, to separate the samples.

The structure of densely grafted polymer material makes it find a wide application as bio-materials. Current work on the densely grafted polymer materials is not complete. The ROMP and norbornate based macromonomer provide a good basis to expand this study. Limited by the experimental conditions, our current work on the PLA grafted

densely grafted polymers only worked with barely entangled polymer backbone and side chains. In future if a more active catalyst can be found, work on higher DP backbone polymers would help to get the work more complete. Also we only worked with the linear PLA side chain. The limited molecular weight of the side chains makes the side chains barely entangled chains. So whether the Rouse-like behavior of the side chain is because of the grafted nature or due to the property of the side chain is still a question. Future work should try to find replacement of the side chain with more flexible chains to get them more entangled, and then the entanglement nature of the side chain could be studied more completely. By comparing the viscoelastic responses of the PLA brush polymers and wedge polymers, we see some sign of the influence to side chain structure to the glassy behavior of these densely grafted polymers. In future if we can change the side structure and alter the interaction and flexibility of the polymer materials. We can do more systematically study of the influence of inter and intra molecular interactions to the viscoelastic properties of this interesting polymer materials.

Reference:

1. Ferry, J. D., *Viscoelastic Properties of Polymers*. Wiley: New York, 1980.
2. McLeish, T. C. B., Tube theory of entangled polymer dynamics. *Advances in Physics* **2002,** 51, (6), 1379-1527.
3. McLeish, T. C. B., Polymer architecture influence on rheology. *Current Opinion in Solid State & Materials Science* **1997,** 2, (6), 678-682.
4. de Gennes, P.G., *Scaling Concepts in Polymer Physics*. Cornell University Press: Ithaca, NY, 1979; p 324.
5. M. Doi; Edwards, S. F., *The Theory of Polymer Dynamics*. Oxford University Press, USA: 1988; p 408.
6. Likhtman, A. E.; McLeish, T. C. B., Quantitative Theory for Linear Dynamics of Linear Entangled Polymers. *Macromolecules* **2002,** 35, (16), 6332-6343.
7. Rubinstein, M.; Colby, R. H., *Polymer Physics*. Oxford University Press, USA: 2003; p 454.
8. Rubinstein, M.; Colby, R. H., Self-consistent theory of polydisperse entangled polymers: Linear viscoelasticity of binary blends. *The Journal of Chemical Physics* **1988,** 89, (8), 5291-5306.
9. Milner, S. T.; McLeish, T. C. B., Reptation and Contour-Length Fluctuations in Melts of Linear Polymers. *Physical Review Letters* **1998,** 81, (3), 725.
10. Colby, R. H.; Fetters, L. J.; Graessley, W. W., The melt viscosity-molecular weight relationship for linear polymers. *Macromolecules* **1987,** 20, (9), 2226-2237.
11. Wang, Z. W.; Chen, X.; Larson, R. G., Comparing tube models for predicting the linear rheology of branched polymer melts. *Journal of Rheology* **2010,** 54, (2), 223-260.
12. Berry, G.; Fox, T. G., The viscosity of polymers and their concentrated solutions. *Advances in Polymer Science*, **1968**; 5, 261-357.
13. Klein, J., Dynamics of entangled linear, branched, and cyclic polymers. *Macromolecules* **1986,** 19, (1), 105-118.
14. Graessley, W. W.; Roovers, J., Melt Rheology of Four-Arm and Six-Arm Star Polystyrenes. *Macromolecules* **1979,** 12, (5), 959-965.
15. Ball, R. C.; McLeish, T. C. B., Dynamic dilution and the viscosity of star-polymer melts. *Macromolecules* **1989,** 22, (4), 1911-1913.
16. Lee, J. H.; Archer, L. A., Stress Relaxation of Star/Linear Polymer Blends. *Macromolecules* **2002,** 35, (17), 6687-6696.
17. Lee, J. H.; Fetters, L. J.; Archer, L. A., Branch-point motion in asymmetric star polymers. *Macromolecules* **2005,** 38, (10), 4484-4494.
18. Lee, J. H.; Orfanou, K.; Driva, P.; Iatrou, H.; Hadjichristidis, N.; Lohse, D. J., Linear and Nonlinear Rheology of Dendritic Star Polymers: Experiment. *Macromolecules* **2008,** 41, (23), 9165-9178.
19. Milner, S. T.; McLeish, T. C. B., Parameter-free theory for stress relaxation in star polymer melts. *Macromolecules* **1997,** 30, (7), 2159-2166.
20. Milner, S. T.; McLeish, T. C. B.; Young, R. N.; Hakiki, A.; Johnson, J. M., Dynamic dilution, constraint-release, and star-linear blends. *Macromolecules* **1998,** 31, (26), 9345-9353.
21. Newkome, G. R.; Moorefield, C. N.; Vögtle, F., *Dendritic Molecules : concepts, synthesis, perspectives*. VCH: Weinheim; New York, 1996.
22. Sendijarevic, I.; McHugh, A. J., Effects of Molecular Variables and Architecture on the Rheological Behavior of Dendritic Polymers. *Macromolecules* **2000,** 33, (2), 590-596.
23. Jahromi, S.; Palmen, J. H. M.; Steeman, P. A. M., Rheology of Side Chain Dendritic Polymers. *Macromolecules* **2000,** 33, (2), 577-581.

24. Wooley, K. L.; Hawker, C. J.; Pochan, J. M.; Frechet, J. M. J., Physical properties of dendritic macromolecules: a study of glass transition temperature. *Macromolecules* **1993,** 26, (7), 1514-1519.
25. Kapnistos, M.; Vlassopoulos, D.; Roovers, J.; Leal, L. G., Linear rheology of architecturally complex macromolecules: Comb polymers with linear backbones. *Macromolecules* **2005,** 38, (18), 7852-7862.
26. Kapnistos, M.; Koutalas, G.; Hadjichristidis, N.; Roovers, J.; Lohse, D. J.; Vlassopoulos, D., Linear rheology of comb polymers with star-like backbones: melts and solutions. *Rheologica Acta* **2006,** 46, (2), 273-286.
27. Daniels, D. R.; McLeish, T. C. B.; Kant, R.; Crosby, B. J.; Young, R. N.; Pryke, A.; Allgaier, J.; Groves, D. J.; Hawkins, R. J., Linear rheology of diluted linear, star and model long chain branched polymer melts. *Rheologica Acta* **2001,** 40, (5), 403-415.
28. Daniels, D. R.; McLeish, T. C. B.; Crosby, B. J.; Young, R. N.; Fernyhough, C. M., Molecular rheology of comb polymer melts. 1. Linear viscoelastic response. *Macromolecules* **2001,** 34, (20), 7025-7033.
29. Das, C.; Inkson, N. J.; Read, D. J.; Kelmanson, M. A.; McLeish, T. C. B., Computational linear rheology of general branch-on-branch polymers. *Journal of Rheology* **2006,** 50, (2), 207-234.
30. Inkson, N. J.; Graham, R. S.; McLeish, T. C. B.; Groves, D. J.; Fernyhough, C. M., Viscoelasticity of monodisperse comb polymer melts. *Macromolecules* **2006,** 39, (12), 4217-4227.
31. McLeish, T. C. B.; Larson, R. G., Molecular constitutive equations for a class of branched polymers: The pom-pom polymer. *Journal of Rheology* **1998,** 42, (1), 81-110.
32. McLeish, T. C. B.; Allgaier, J.; Bick, D. K.; Bishko, G.; Biswas, P.; Blackwell, R.; Blottiere, B.; Clarke, N.; Gibbs, B.; Groves, D. J.; Hakiki, A.; Heenan, R. K.; Johnson, J. M.; Kant, R.; Read, D. J.; Young, R. N., Dynamics of entangled H-polymers: Theory, rheology, and neutron-scattering. *Macromolecules* **1999,** 32, (20), 6734-6758.
33. McLeish, T. C. B.; Milner, S. T., Entangled dynamics and melt flow of branched polymers. *Advances in Polymer Science*, **1999**, 143, 195-256.
34. van Ruymbeke, E.; Bailly, C.; Keunings, R.; Vlassopoulos, D., A general methodology to predict the linear rheology of branched polymers. *Macromolecules* **2006,** 39, (18), 6248-6259.
35. Larson, R. G., Combinatorial rheology of branched polymer melts. *Macromolecules* **2001,** 34, (13), 4556-4571.
36. Lee, J. H.; Driva, P.; Hadjichristidis, N.; Wright, P. J.; Rucker, S. P.; Lohse, D. J., Damping Behavior of Entangled Comb Polymers: Experiment. *Macromolecules* **2009,** 42, (4), 1392-1399.
37. Park, S. J.; Larson, R. G., Modeling the linear viscoelastic properties of metallocene-catalyzed high density polyethylenes with long-chain branching. *Journal of Rheology* **2005,** 49, (2), 523-536.
38. Park, S. J.; Larson, R. G., Dilution exponent in the dynamic dilution theory for polymer melts. *Journal of Rheology* **2003,** 47, (1), 199-211.
39. Park, S. J.; Larson, R. G., Tube Dilation and Reptation in Binary Blends of Monodisperse Linear Polymers. *Macromolecules* **2004,** 37, (2), 597-604.
40. Semlyen, J. A., *Cyclic polymers*. Kluwer Academic Publishers: Dordrecht; Boston, 2000.
41. Endo, K., Synthesis and Properties of Cyclic Polymers. *Advances in Polymer Science* **2008,** 217, 121-183.
42. McLeish, T., Polymers Without Beginning or End. *Science* **2002,** 297, (5589), 2005-2006.

43. Muller, M.; Wittmer, J. P.; Cates, M. E., Topological effects in ring polymers: A computer simulation study. *Physical Review E* **1996,** 53, (5), 5063.
44. Tsolou, G.; Stratikis, N.; Baig, C.; Stephanou, P. S.; Mavrantzas, V. G., Melt Structure and Dynamics of Unentangled Polyethylene Rings: Rouse Theory, Atomistic Molecular Dynamics Simulation, and Comparison with the Linear Analogues. *Macromolecules* **2010,** 43, (24), 10692-10713.
45. Brown, S.; Lenczycki, T.; Szamel, G., Influence of topological constraints on the statics and dynamics of ring polymers. *Physical Review E* **2001,** 63, (5), 052801.
46. Mckenna, G. B.; Plazek, D. J., The Viscosity of Blends of Linear and Cyclic Molecules of Similar Molecular Mass. *Polymer Communications* **1986,** 27, (10), 304-306.
47. McKenna, G. B.; Hadziioannou, G.; Lutz, P.; Hild, G.; Strazielle, C.; Straupe, C.; Rempp, P.; Kovacs, A. J., Dilute solution characterization of cyclic polystyrene molecules and their zero-shear viscosity in the melt. *Macromolecules* **1987,** 20, (3), 498-512.
48. McKenna, G. B.; Hostetter, B. J.; Hadjichristidis, N.; Fetters, L. J.; Plazek, D. J., A study of the linear viscoelastic properties of cyclic polystyrenes using creep and recovery measurements. *Macromolecules* **1989,** 22, (4), 1834-1852.
49. Roovers, J., Dilute-solution properties of ring polystyrenes. *Journal of Polymer Science: Polymer Physics Edition* **1985,** 23, (6), 1117-1126.
50. Edwards, C. J. C.; Stepto, R. F. T.; Semlyen, J. A., Studies of cyclic and linear poly(dimethyl siloxanes): 8. Light scattering measurements in good and poor solvents. *Polymer* **1982,** 23, (6), 869-872.
51. Higgins, J. S.; Dodgson, K.; Semlyen, J. A., Studies of cyclic and linear poly(dimethyl siloxanes): 3. Neutron scattering measurements of the dimensions of ring and chain polymers. *Polymer* **1979,** 20, (5), 553-558.
52. Clarson, S. J.; Dodgson, K.; Semlyen, J. A., Cyclic polysiloxanes: 2. Neutron scattering from poly(phenylmethylsiloxane). *Polymer* **1987,** 28, (2), 189-192.
53. Edwards, C. J. C.; Rigby, D.; Stepto, R. F. T.; Dodgson, K.; Semlyen, J. A., Studies of cyclic and linear poly(dimethyl siloxanes): 10. Calculations of radii of gyration. *Polymer* **1983,** 24, (4), 391-394.
54. Clarson, S. J.; Semlyen, J. A., Cyclic polysiloxanes: 1. Preparation and characterization of poly(phenylmethylsiloxane). *Polymer* **1986,** 27, (10), 1633-1636.
55. Roovers, J., The melt properties of ring polystyrenes. *Macromolecules* **1985,** 18, (6), 1359-1361.
56. Roovers, J., Viscoelastic properties of polybutadiene rings. *Macromolecules* **1988,** 21, (5), 1517-1521.
57. Kapnistos, M.; Lang, M.; Vlassopoulos, D.; Pyckhout-Hintzen, W.; Richter, D.; Cho, D.; Chang, T.; Rubinstein, M., Unexpected power-law stress relaxation of entangled ring polymers. *Nature Material* **2008,** 7, (12), 997-1002.
58. Dodgson, K.; Bannister, D. J.; Semlyen, J. A., Studies of cyclic and linear poly(dimethyl siloxanes). 4. Bulk viscosities. *Polymer* **1980,** 21, (6), 663-667.
59. Hadziioannou, G.; Cotts, P. M.; ten Brinke, G.; Han, C. C.; Lutz, P.; Strazielle, C.; Rempp, P.; Kovacs, A. J., Thermodynamic and hydrodynamic properties of dilute solutions of cyclic and linear polystyrenes. *Macromolecules* **1987,** 20, (3), 493-497.
60. Bloomfield, V.; Zimm, B. H., Viscosity, Sedimentation, et Cetera, of Ring- and Straight-Chain Polymers in Dilute Solution. *The Journal of Chemical Physics* **1966,** 44, (1), 315-323.
61. Fukatsu, M.; Kurata, M., Hydrodynamic Properties of Flexible-Ring Macromolecules. *The Journal of Chemical Physics* **1966,** 44, (12), 4539-4545.

62. Geiser, D.; Höcker, H., Synthesis and Investigation of Macrocyclic Polystyrene. *Macromolecules* **1980,** 13, (3), 653-656.
63. Ueberreiter, K.; Kanig, G., Self-plasticization of polymers. *Journal of Colloid Science* **1952,** 7, (6), 569-583.
64. Santangelo, P. G.; Roland, C. M.; Chang, T.; Cho, D.; Roovers, J., Dynamics near the Glass Temperature of Low Molecular Weight Cyclic Polystyrene. *Macromolecules* **2001,** 34, (26), 9002-9005.
65. Clarson, S. J.; Dodgson, K.; Semlyen, J. A., Studies of cyclic and linear poly(dimethylsiloxanes): 19. Glass transition temperatures and crystallization behaviour. *Polymer* **1985,** 26, (6), 930-934.
66. Di Marzio, E. A.; Guttman, C. M., The glass temperature of polymer rings. *Macromolecules* **1987,** 20, (6), 1403-1407.
67. Rubinstein, M., Dynamics of Ring Polymers in the Presence of Fixed Obstacles. *Physical Review Letters* **1986,** 57, (24), 3023.
68. de Gennes, P. G., Reptation of a Polymer Chain in the Presence of Fixed Obstacles. *The Journal of Chemical Physics* **1971,** 55, (2), 572-579.
69. Khokhlov, A. R.; Nechaev, S. K., Polymer chain in an array of obstacles. *Physics Letters A* **1985,** 112, (3-4), 156-160.
70. Obukhov, S. P.; Rubinstein, M.; Duke, T., Dynamics of a ring polymer in a gel. *Physical Review Letters* **1994,** 73, (9), 1263-1266.
71. Ohta, Y.; Kushida, Y.; Matsushita, Y.; Takano, A., SEC-MALS characterization of cyclization reaction products: Formation of knotted ring polymer. *Polymer* **2009,** 50, (5), 1297-1299.
72. Viovy, J. L.; Rubinstein, M.; Colby, R. H., Constraint release in polymer melts: tube reorganization versus tube dilation. *Macromolecules* **1991,** 24, (12), 3587-3596.
73. Vettorel, T.; Reigh, S. Y.; Yoon, D. Y.; Kremer, K., Monte-Carlo Method for Simulations of Ring Polymers in the Melt. *Macromolecular Rapid Communications* **2009,** 30, (4-5), 345-351.
74. Thomas, V.; Grosberg, A. Y.; Kremer, K., Statistics of polymer rings in the melt: a numerical simulation study. *Physical Biology* **2009,** 6, (2), 025013.
75. Everaers, R.; Sukumaran, S. K.; Grest, G. S.; Svaneborg, C.; Sivasubramanian, A.; Kremer, K., Rheology and Microscopic Topology of Entangled Polymeric Liquids. *Science* **2004,** 303, (5659), 823-826.
76. Uchida, N.; Grest, G. S.; Everaers, R., Viscoelasticity and primitive path analysis of entangled polymer liquids: From F-actin to polyethylene. *The Journal of Chemical Physics* **2008,** 128, (4), 044902-6.
77. Beaucage, G.; Kulkarni, A. S., Dimensional Description of Cyclic Macromolecules. *Macromolecules* **2009,** 43, (1), 532-537.
78. Scott, D. W., Equilibria between Linear and Cyclic Polymers in Methylpolysiloxanes. *Journal of the American Chemical Society* **1946,** 68, (11), 2294-2298.
79. Brown, J. F.; Slusarczuk, G. M. J., Macrocyclic Polydimethylsiloxanes. *Journal of the American Chemical Society* **1965,** 87, (4), 931-932.
80. Dagger, A. C.; Semlyen, J. A., Studies of cyclic and linear poly(dimethylsiloxanes): 34: Preparation, fractionation and characterisation of the first per-deuterated macrocyclic poly(dimethylsiloxanes). *Polymer* **1999,** 40, (11), 3243-3245.
81. Roovers, J.; Toporowski, P. M., Synthesis of high molecular weight ring polystyrenes. *Macromolecules* **1983,** 16, (6), 843-849.
82. Roovers, J.; Toporowski, P. M., Synthesis and characterization of ring polybutadienes. *Journal of Polymer Science Part B: Polymer Physics* **1988,** 26, (6), 1251-1259.

83. Madani, A. E.; Favier, J.-C.; Hémery, P.; Sigwalt, P., Synthesis of ring-shaped polyisoprene. *Polymer International* **1992,** 27, (4), 353-357.
84. Cho, D. Y.; Masuoka, K.; Koguchi, K.; Asari, T.; Kawaguchi, D.; Takano, A.; Matsushita, Y., Preparation and characterization of cyclic polystyrenes. *Polymer Journal* **2005,** 37, (7), 506-511.
85. Kawaguchi, D.; Nishu, T.; Takano, A.; Matsushita, Y., Direct Observation of an Isolated Cyclic Sodium Poly(styrenesulfonate) Molecule by Atomic Force Microscopy. *Polym. J* **2007,** 39, (3), 271-275.
86. Iyer, B. V. S.; Lele, A. K.; Shanbhag, S., What is the size of a ring polymer in a ring-linear blend? *Macromolecules* **2007,** 40, (16), 5995-6000.
87. Subramanian, G.; Shanbhag, S., Conformational properties of blends of cyclic and linear polymer melts. *Physical Review E* **2008,** 77, (1), 9.
88. Subramanian, G.; Shanbhag, S., Conformational free energy of melts of ring-linear polymer blends. *Physical Review E* **2009,** 80, (4), 041806.
89. Joyce, S. J.; Hubbard, R. E.; Semlyen, J. A., Modelling of polymeric threading processes. *European Polymer Journal* **1993,** 29, (2-3), 305-312.
90. Yu, G.E.; Sun, T.; Yan, Z.-G.; Price, C.; Booth, C.; Cook, J.; Ryan, A. J.; Viras, K., Low-molar-mass cyclic poly(oxyethylene)s studied by Raman spectroscopy, X-ray scattering and differential scanning calorimetry. *Polymer* **1997,** 38, (1), 35-42.
91. Lee, W.; Lee, H.; Lee, H. C.; Cho, D.; Chang, T.; Gorbunov, A. A.; Roovers, J., Retention Behavior of linear and ring polystyrene at the chromatographic critical condition. *Macromolecules* **2002,** 35, (2), 529-538.
92. Lee, H. C.; Lee, H.; Lee, W.; Chang, T.; Roovers, J., Fractionation of Cyclic Polystyrene from Linear Precursor by HPLC at the Chromatographic Critical Condition. *Macromolecules* **2000,** 33, (22), 8119-8121.
93. Gorbunov, A. A.; Skvortsov, A. M., Patterns of the behaviour of ring macromolecules in pores. *Polymer Science U.S.S.R.* **1984,** 26, (10), 2305-2314.
94. Ten Brinke, G.; Hadziioannou, G., Topological constraints and their influence on the properties of synthetic macromolecular systems. 1. Cyclic macromolecules. *Macromolecules* **1987,** 20, (3), 480-485.
95. Koniaris, K.; Muthukumar, M., Knottedness in ring polymers. *Physical Review Letters* **1991,** 66, (17), 2211.
96. Bielawski, C. W.; Benitez, D.; Grubbs, R. H., An "Endless" Route to Cyclic Polymers. *Science* **2002,** 297, (5589), 2041-2044.
97. Bielawski, C. W.; Benitez, D.; Grubbs, R. H., Synthesis of Cyclic Polybutadiene via Ring-Opening Metathesis Polymerization: The Importance of Removing Trace Linear Contaminants. *Journal of the American Chemical Society* **2003,** 125, (28), 8424-8425.
98. Boydston, A. J.; Xia, Y.; Kornfield, J. A.; Gorodetskaya, I. A.; Grubbs, R. H., Cyclic Ruthenium-Alkylidene Catalysts for Ring-Expansion Metathesis Polymerization. *Journal of the American Chemical Society* **2008,** 130, (38), 12775-12782.
99. Xia, Y.; Boydston, A. J.; Yao, Y.; Kornfield, J. A.; Gorodetskaya, I. A.; Spiess, H. W.; Grubbs, R. H., Ring-Expansion Metathesis Polymerization: Catalyst-Dependent Polymerization Profiles. *Journal of the American Chemical Society* **2009,** 131, (7), 2670-2677.
100. Boydston, A. J.; Holcombe, T. W.; Unruh, D. A.; Fréchet, J. M. J.; Grubbs, R. H., A Direct Route to Cyclic Organic Nanostructures via Ring-Expansion Metathesis Polymerization of a Dendronized Macromonomer. *Journal of the American Chemical Society* **2009,** 131, (15), 5388-5389.
101. Grubbs, R. H., *Handbook of Metathesis*. John Wiley & sons, 2003

102. Candau, F.; François, J.; Benoit, H., Effect of molecular weight on the refractive index increment of polystyrenes in solution. *Polymer* **1974,** 15, (10), 626-630.
103. François, J.; Candau, F.; Benoit, H., Effect of molecular weight on the partial specific volume of polystyrenes in solution. *Polymer* **1974,** 15, (10), 618-625.
104. Hutcheson, S. A.; McKenna, G. B., The measurement of mechanical properties of glycerol, m-toluidine, and sucrose benzoate under consideration of corrected rheometer compliance: An in-depth study and review. *The Journal of Chemical Physics* **2008,** 129, (7), 074502-14.
105. Liu, C.; He, J.; Ruymbeke, E. v.; Keunings, R.; Bailly, C., Evaluation of different methods for the determination of the plateau modulus and the entanglement molecular weight. *Polymer* **2006,** 47, (13), 4461-4479.
106. Wang, S.; Wang, S.Q.; Halasa, A.; Hsu, W. L., Relaxation Dynamics in Mixtures of Long and Short Chains: Tube Dilation and Impeded Curvilinear Diffusion. *Macromolecules* **2003,** 36, (14), 5355-5371.
107. Sanders, J. F.; Ferry, J. D., Polymer Entanglement Spacings Estimated from Integration of the Loss Compliance. *Macromolecules* **1969,** 2, (4), 440-442.
108. Wu, S., Dynamic rheology and molecular weight distribution of insoluble polymers: tetrafluoroethylene-hexafluoropropylene copolymers. *Macromolecules* **1985,** 18, (10), 2023-2030.
109. Onogi, S.; Masuda, T.; Kitagawa, K., Rheological Properties of Anionic Polystyrenes. I. Dynamic Viscoelasticity of Narrow-Distribution Polystyrenes. *Macromolecules* **1970,** 3, (2), 109-116.
110. Wu, S., Chain structure and entanglement. *Journal of Polymer Science Part B: Polymer Physics* **1989,** 27, (4), 723-741.
111. Trinkle, S.; Friedrich, C., Van Gurp-Palmen-plot: a way to characterize polydispersity of linear polymers. *Rheologica Acta* **2001,** 40, (4), 322-328.
112. van Gurp, M.; Palmen, J., Time-Temperature Superposition for Polymer Blends. *Rheology Bulletin* **1998,** 67, (1), 5-8.
113. Williams, M. L.; Landel, R. F.; Ferry, J. D., The Temperature Dependence of Relaxation Mechanisms in Amorphous Polymers and Other Glass-forming Liquids. *Journal of the American Chemical Society* **1955,** 77, (14), 3701-3707.
114. Angell, C. A., Spectroscopy simulation and scattering, and the medium range order problem in glass. *Journal of Non-Crystalline Solids* **1985,** 73, (1-3), 1-17.
115. Plazek, D. J.; Ngai, K. L., Correlation of polymer segmental chain dynamics with temperature-dependent time-scale shifts. *Macromolecules* **1991,** 24, (5), 1222-1224.
116. Wang, L.M.; Angell, C. A.; Richert, R., Fragility and thermodynamics in nonpolymeric glass-forming liquids. *The Journal of Chemical Physics* **2006,** 125, (7), 074505-8.
117. Qin, Q.; McKenna, G. B., Correlation between dynamic fragility and glass transition temperature for different classes of glass forming liquids. *Journal of Non-Crystalline Solids* **2006,** 352, (28-29), 2977-2985.
118. Simon, S. L.; Plazek, D. J.; Sobieski, J. W.; McGregor, E. T., Physical aging of a polyetherimide: Volume recovery and its comparison to creep and enthalpy measurements. *Journal of Polymer Science Part B: Polymer Physics* **1997,** 35, (6), 929-936.
119. Plazek, D. J., Whats wrong with the moduli Brown, Charley - or get the H out and go to L. *Journal of Rheology* **1992,** 36, (8), 1671-1690.
120. Plazek, D. J.; Echeverria, I., Don't cry for me Charlie Brown, or with compliance comes comprehension. *Journal of Rheology* **2000,** 44, (4), 831-841.

121. Rylander, P. N., *Catalytic Hydrogenation Over Platinum Metals*. Academic Press: 1967.
122. Grubbs, R.; Tumas, W., Polymer synthesis and organotransition metal chemistry. *Science* **1989,** 243, (4893), 907-915.
123. Walker, R.; Conrad, R. M.; Grubbs, R. H., The Living ROMP of trans-Cyclooctene. *Macromolecules* **2009,** 42, (3), 599-605.
124. Wu, Z.; Grubbs, R. H., Synthesis of Narrow Dispersed Linear Polyethylene and Block Copolymers from Polycyclobutene. *Macromolecules* **1994,** 27, (23), 6700-6703.
125. Odian, G., *Principles of Polymerization*. Wiley-Interscience: 2004.
126. Mark, J. E., *Polymer Data Handbook*. Oxford University Press, USA: 1999.
127. Guidry, E. N.; Cantrill, S. J.; Stoddart, J. F.; Grubbs, R. H., Magic Ring Catenation by Olefin Metathesis. *Organic Letters* **2005,** 7, (11), 2129-2132.
128. Ito, K.; Kawaguchi, S., Poly(macromonomers): Homo- and copolymerization. *Advances in Polymer Science*, **1999**; 142, 129-178.
129. Jia, Q.; Wang, Q.; Ma, P., Position Group Contribution Method for the Prediction of Critical Volume of Organic Compounds. *Journal of Chemical & Engineering Data* **2008,** 53, (11), 2606-2612.
130. Marrero, J.; Gani, R., Group contribution based estimation of pure component properties. *Fluid Phase Equilibria* **2001,** 183, 183-208.
131. Ngai, K. L.; Plazek, D. J.; O'Rourke, V. M., Viscoelastic properties of amorphous polymers .7. Changes of the anomalous behavior of low molecular weight polystyrene with the addition of a diluent. *Macromolecules* **1997,** 30, (18), 5450-5456.
132. Xia, Y.; Boydston, A. J.; Grubbs, R. H., Synthesis and Direct Imaging of Ultrahigh Molecular Weight Cyclic Brush Polymers. *Angewandte Chemie International Edition* **2011**.
133. Roland, C. M.; Archer, L. A.; Mott, P. H.; Sanchez-Reyes, J., Determining Rouse relaxation times from the dynamic modulus of entangled polymers. *Journal of Rheology* **2004,** 48, (2), 395-403.
134. da C. Andrade, E. N., On the Viscous Flow in Metals, and Allied Phenomena. *Proceedings of the Royal Society of London. Series A* **1910,** 84, (567), 1-12.
135. Plazek, D. J., Dynamic mechanical and creep properties of a 23% cellulose nitrate solution; Andrade creep in polymeric systems. *Journal of Colloid Science* **1960,** 15, (1), 50-75.
136. van Ruymbeke, E.; Kapnistos, M.; Vlassopoulos, D.; Huang, T. Z.; Knauss, D. M., Linear melt rheology of pom-pom polystyrenes with unentangled branches. *Macromolecules* **2007,** 40, (5), 1713-1719.
137. Sheiko, S. S.; Sumerlin, B. S.; Matyjaszewski, K., Cylindrical molecular brushes: Synthesis, characterization, and properties. *Progress in Polymer Science* **2008,** 33, (7), 759-785.
138. Namba, S.; Tsukahara, Y.; Kaeriyama, K.; Okamoto, K.; Takahashi, M., Bulk properties of multibranched polystyrenes from polystyrene macromonomers: rheological behavior I. *Polymer* **2000,** 41, (14), 5165-5171.
139. Tsukahara, Y.; Kohjiya, S.; Tsutsumi, K.; Okamoto, Y., On the Intrinsic Viscosity of Poly(macromonomer)s. *Macromolecules* **1994,** 27, (6), 1662-1664.
140. Tsukahara, Y.; Namba, S.; Iwasa, J.; Nakano, Y.; Kaeriyama, K.; Takahashi, M., Bulk Properties of Poly(macromonomer)s of Increased Backbone and Branch Lengths. *Macromolecules* **2001,** 34, (8), 2624-2629.
141. Berry, G. C.; Kahle, S.; Ohno, S.; Matyjaszewski, K.; Pakula, T., Viscoelastic and dielectric studies on comb- and brush-shaped poly(n-butyl acrylate). *Polymer* **2008,** 49, (16), 3533-3540.

142. Neugebauer, D.; Zhang, Y.; Pakula, T.; Sheiko, S. S.; Matyjaszewski, K., Densely-grafted and double-grafted PEO brushes via ATRP. A route to soft elastomers. *Macromolecules* **2003,** 36, (18), 6746-6755.
143. Pakula, T.; Zhang, Y.; Matyjaszewski, K.; Lee, H. I.; Boerner, H.; Qin, S. H.; Berry, G. C., Molecular brushes as super-soft elastomers. *Polymer* **2006,** 47, (20), 7198-7206.
144. Ying, Z.; Costantini, N.; Mierzwa, M.; Pakula, T.; Neugebauer, D.; Matyjaszewski, K., Super soft elastomers as ionic conductors. *Polymer* **2004,** 45, (18), 6333-6339.
145. Nakamura, Y.; Wan, Y.; Mays, J. W.; Iatrou, H.; Hadjichristidis, N., Radius of gyration of polystyrene combs and centipedes in solution. *Macromolecules* **2000,** 33, (22), 8323-8328.
146. Terao, K.; Farmer, B. S.; Nakamura, Y.; Iatrou, H.; Hong, K.; Mays, J. W., Radius of Gyration of Polystyrene Combs and Centipedes in a Ï‘ Solvent. *Macromolecules* **2005,** 38, (4), 1447-1450.
147. Wintermantel, M.; Gerle, M.; Fischer, K.; Schmidt, M.; Wataoka, I.; Urakawa, H.; Kajiwara, K.; Tsukahara, Y., Molecular Bottlebrushes†. *Macromolecules* **1996,** 29, (3), 978-983.
148. Zhang, M.; Müller, A. H. E., Cylindrical polymer brushes. *Journal of Polymer Science Part A: Polymer Chemistry* **2005,** 43, (16), 3461-3481.
149. Sheiko, S. S.; Möller, M., Visualization of Macromolecules: A First Step to Manipulation and Controlled Response. *Chemical Reviews* **2001,** 101, (12), 4099-4124.
150. Xia, Y.; Olsen, B. D.; Kornfield, J. A.; Grubbs, R. H., Efficient Synthesis of Narrowly Dispersed Brush Copolymers and Study of Their Assemblies: The Importance of Side Chain Arrangement. *Journal of the American Chemical Society* **2009,** 131, (51), 18525-18532.
151. Xia, Y.; Kornfield, J. A.; Grubbs, R. H., Efficient Synthesis of Narrowly Dispersed Brush Polymers via Living Ring-Opening Metathesis Polymerization of Macromonomers. *Macromolecules* **2009,** 42, (11), 3761-3766.
152. Garlotta, D., A literature review of poly(lactic acid). *Journal of Polymers and the Environment* **2001,** 9, (2), 63-84.
153. Yamakawa, H., *Modern Theory of Polymer Solutions*. Harper & Row: New York, 1971.
154. Yamakawa, H.; Yoshizaki, T., Dynamics of helical wormlike chains. I. Dynamic model and diffusion equation. *The Journal of Chemical Physics* **1981,** 75, (2), 1016-1030.
155. Yamakawa, H.; Yoshizaki, T., Transport Coefficients of Helical Wormlike Chains. 3. Intrinsic Viscosity. *Macromolecules* **1980,** 13, (3), 633-643.
156. Terao, K.; Nakamura, Y.; Norisuye, T., Solution Properties of Polymacromonomers Consisting of Polystyrene. 2. Chain Dimensions and Stiffness in Cyclohexane and Toluene. *Macromolecules* **1999,** 32, (3), 711-716.
157. Terao, K.; Hokajo, T.; Nakamura, Y.; Norisuye, T., Solution Properties of Polymacromonomers Consisting of Polystyrene. 3. Viscosity Behavior in Cyclohexane and Toluene. *Macromolecules* **1999,** 32, (11), 3690-3694.
158. Nemoto, N.; Nagai, M.; Koike, A.; Okada, S., Diffusion and Sedimentation Studies on Poly(macromonomer) in Dilute Solution. *Macromolecules* **1995,** 28, (11), 3854-3859.
159. van Gurp, M. Palmen, J., Time-Temperature Superposition for Polymer Blends. *Rheology Bulletin* **1998,** 67, (1), 5-8.
160. Dorgan, J. R.; Williams, J. S.; Lewis, D. N., Melt rheology of poly(lactic acid): Entanglement and chain architecture effects. *Journal of Rheology* **1999,** 43, (5), 1141-1155.

161. Reimschuessel, H. K., On the glass transition temperature of comblike polymers: Effects of side chain length and backbone chain structure. *Journal of Polymer Science: Polymer Chemistry Edition* **1979,** 17, (8), 2447-2457.
162. Zuza, E.; Ugartemendia, J. M.; Lopez, A.; Meaurio, E.; Lejardi, A.; Sarasua, J.-R., Glass transition behavior and dynamic fragility in polylactides containing mobile and rigid amorphous fractions. *Polymer* **2008,** 49, (20), 4427-4432.
163. Ngai, K. L.; Plazek, D. J.; O'Rourke, V. M., Viscoelastic properties of amorphous polymers .7. Changes of the anomalous behavior of low molecular weight polystyrene with the addition of a diluent. *Macromolecules* **1997,** 30, (18), 5450-5456.
164. Singh, A.; Krogman, N. R.; Sethuraman, S.; Nair, L. S.; Sturgeon, J. L.; Brown, P. W.; Laurencin, C. T.; Allcock, H. R., Effect of Side Group Chemistry on the Properties of Biodegradable l-Alanine Cosubstituted Polyphosphazenes. *Biomacromolecules* **2006,** 7, (3), 914-918.
165. Yazdani-Pedram, M.; Soto, E.; Tagle, L. H.; Diaz, F. R.; Gargallo, L.; Radic, D., Effect of the side chain structure on the glass transition temperatures of some poly(thiocarbonate)S. *Thermochimica Acta* **1986,** 105, 149-160.
166. Rodriguez, F., *Principles of Polymer Systems*. Taylor & Francis: 1996.
167. Rousseau, D.; Marty, J.D.; Mauzac, M.; Martinoty, P.; Brandt, A.; Guenet, J.-M., Conformation in solution of side-chain liquid crystal polymers as a function of the mesogen-graft amount. *Polymer* **2003,** 44, (7), 2049-2055.
168. Mendil, H.; Baroni, P.; Noirez, L., Unexpected giant elasticity in side-chain liquid-crystal polymer melts: A new approach for the understanding of shear-induced phase transitions. *Europhysics Letters* **2005,** 72, (6), 983-989.
169. Auad, M. L.; Kempe, M. D.; Kornfield, J. A.; Rendon, S.; Burghardt, W. R.; Yoon, K., Effect of Mesophase Order on the Dynamics of Side Group Liquid Crystalline Polymers. *Macromolecules* **2005,** 38, (16), 6946-6953.
170. Rubin, S. F.; Kannan, R. M.; Kornfield, J. A.; Boeffel, C., Effect of Mesophase Order and Molecular Weight on the Dynamics of Nematic and Smectic Side-Group Liquid-Crystalline Polymers. *Macromolecules* **1995,** 28, (10), 3521-3530.
171. Mather, P. T.; Jeon, H. G.; Romo-Uribe, A.; Haddad, T. S.; Lichtenhan, J. D., Mechanical Relaxation and Microstructure of Poly(norbornyl-POSS) Copolymers. *Macromolecules* **1999,** 32, (4), 1194-1203.
172. Esteruelas, M. A.; Gonzalez, F.; Herrero, J.; Lucio, P.; Olivan, M.; Ruiz-Labrador, B., Thermal properties of polynorbornene (cis- and trans-) and hydrogenated polynorbornene. *Polymer Bulletin* **2007,** 58, (5-6), 923-931.